DEVELOPMENT OF A HARDWARE-IN-THE-LOOP WIND ENERGY CONVERSION SYSTEM EMULATOR

A THESIS SUBMITTED TO
THE GRADUATE SCHOOL OF NATURAL AND APPLIED SCIENCES
OF
MIDDLE EAST TECHNICAL UNIVERSITY

BY

GÖKMEN CENGİZ

IN PARTIAL FULFILLMENT OF THE REQUIREMENTS
FOR
THE DEGREE OF MASTER OF SCIENCE
IN
ELECTRICAL AND ELECTRONICS ENGINEERING

FEBRUARY 2015

Approval of the thesis:

DEVELOPMENT OF A HARDWARE-IN-THE-LOOP WIND ENERGY CONVERSION SYSTEM EMULATOR

submitted by **GÖKMEN CENGİZ** in partial fulfillment of the requirements for the degree of **Master of Science in Electrical and Electronics Engineering Department, Middle East Technical University** by,

Prof. Dr. Gülbin Dural Ünver _____
Dean, Graduate School of **Natural and Applied Sciences**

Prof. Dr. Gönül Turhan Sayan _____
Head of Department, **Electrical and Electronics Engineering**

Prof. Dr. H. Bülent Ertan _____
Supervisor, **Electrical and Electronics Engineering Dept, METU**

Examining Committee Members:

Prof. Dr. Muammer Ermiş _____
Electrical and Electronics Engineering Dept., METU

Prof. Dr. H. Bülent Ertan _____
Electrical and Electronics Engineering Dept., METU

Prof. Dr. A. Nezih Güven _____
Electrical and Electronics Engineering Dept., METU

Assoc. Prof. Oğuz Uzol _____
Aerospace Engineering Dept., METU

İbrahim Kaya, M. S. _____
ASELSAN Inc.

Date: 12.02.2015

I hereby declare that all information in this document has been obtained and presented in accordance with academic rules and ethical conduct. I also declare that, as required by these rules and conduct, I have fully cited and referenced all material and results that are not original to this work.

Name, Last name: Gökmen Cengiz

Signature:

ABSTRACT

DEVELOPMENT OF A HARDWARE-IN-THE-LOOP WIND ENERGY CONVERSION SYSTEM EMULATOR

Cengiz, Gökmen

M.S., Department of Electrical and Electronics Engineering

Supervisor: Prof. Dr. H. Bülent Ertan

February 2015, 183 pages

This thesis focuses on developing a hardware-in-the-loop wind energy conversion system emulator. In addition, software for simulating the hardware-in-the-loop system is developed. The thesis describes how a wind turbine model is developed by controlling an induction motor to emulate wind turbine shaft. Control of the overall hardware-in-the-loop system for achieving an accurate medium for wind energy conversion system emulation is explained. The software uses the same model for the wind turbine as the HIL system. Modelling of the generator and gearbox is fairly straightforward. However, back-to-back converters which facilitate connection of the system to the grid are highly nonlinear elements. A novel neural network based model is developed for these converters by performing experiments on them and the accuracy of the model is investigated. Finally, the software developed is used to investigate problems of islanding operation so that energy quality of the local loads can be maintained in this operation.

Keywords: Wind Energy Conversion Systems, Hardware-in-the-Loop Emulation, Wind Generator Test, Control, Control of Wind Turbine, Islanding Operation

ÖZ

YAZILIM İÇİNDE DONANIM RÜZGAR ENERJİSİ DÖNÜŞÜM SİSTEMİ EMÜLATÖRÜ GELİŞTİRİLMESİ

Cengiz, Gökmen

Yüksek Lisans, Elektrik ve Elektronik Mühendisliği

Tez Yöneticisi: Prof. Dr. H. Bülent Ertan

Şubat 2015, 183 sayfa

Bu tez çalışmasında, yazılım içinde donanım rüzgar enerjisi dönüşüm sistemi emülatörü geliştirilmesine odaklanılmıştır. Buna ek olarak yazılım içinde donanım sistemini benzeten bir yazılım geliştirilmiştir. Tez, rüzgar türbini milinin taklit edilmesi için indüksiyon motoru kullanarak nasıl bir türbin modeli geliştirildiğini açıklar. Rüzgar enerjisi dönüşüm sistemi benzetimi yapabilen doğru bir ortam elde etmek için yazılım içinde donanım sisteminin genel kontrolü açıklanmıştır. Yazılım, yazılım içinde donanım sisteminde kullanılan rüzgar türbini modelinin aynısını kullanmaktadır. Jeneratör ve dişli kutusunun modellenmesi oldukça basittir. Bununla birlikte sistemin şebekeye bağlantısını kolaylaştıran arka arkaya dönüştürücüler son derece doğrusal olmayan elemanlardır. Bu dönüştürücüler için üzerlerinde deneyler yaparak yeni bir sinir ağı tabanlı model geliştirilmiştir ve modelin doğruluğu incelenmiştir. Son olarak, geliştirilen yazılım ada operasyonunda yerel yüklerin enerji kalitesinin korunması için çıkan problemleri incelemek amacıyla kullanılmıştır.

Anahtar Kelimeler: Rüzgar Enerjisi Dönüşüm Sistemleri, Yazılım İçinde Donanım Benzetimi, Rüzgar Jeneratörü Testi, Kontrol, Rüzgar Türbini Kontrolü, Ada Operasyonu

To my precious family…

ACKNOWLEDGEMENTS

I would like to enounce my deep gratitude to my supervisor Prof. Dr. H. Bülent Ertan for her valuable supervision, advice, useful critics and discussions throughout this study.

I am also grateful to my thesis committee members Prof. Dr. Muammer Ermiş, Prof. Dr. A. Nezih Güven, Assoc. Prof. Oğuz Uzol and İbrahim Kaya for their criticism and advices.

Special thanks should be given to Murat Kayhan, İbrahim Erseçgin, Baki Er and Bünyamin Bostancı for their involvements in the tests of this study. Their support during this study helped me complete it in an easy way.

My warmest thanks to Gözde Özel for her endless love, patience, care, motivation and most importantly morale support at every stage of this study.

I wish to express my endless thanks to every member of my family, Bahar Cengiz and Erol Cengiz, for their unconditional love.

I am deeply grateful to Can Görür, Ahmet Ada, Ömer Cem Ayaz, Volkan Çağlayan, Kaan Çetinkaya, Veysel Çakır, Barış Çiftçi, Anıl Civil, Kübra Mutlu, Burak Çetinkaya, Gizem Akar, Nehir Utku, Yasin Çevik, Nadir Usluer, Aycan Aydoğdu, İsmail Tugay Güzel, Hilal Irmak Güzel, Mustafa Karagöz, Burak Latifoğlu, Yunus Gündüz, Durmuş Cengiz, Hülya Cengiz and Kaan Cengiz for their friendships, encouragement and support.

TABLE OF CONTENTS

LIST OF TABLES

TABLES

LIST OF FIGURES

FIGURES

LIST OF ABBREVATIONS

HIL	(Hardware-In-The-Loop)
MPPT	(Maximum Power Point Tracking)
WECS	(Wind Energy Conversion System)
PMSG	(Permanent Magnet Synchronous Generator)
DFIG	(Doubly Fed Induction Generator)
MPP	(Maximum Power Point)
HCS	(Hill Climb Search)
P&O	(Perturbation and Observation)
PWM	(Pulse Width Modulation)
EMF	(Electromotive Force)
PCC	(Point of Common Coupling)

CHAPTER 1

INTRODUCTION

1.1. Motivation

In Turkey, investment of wind energy continues to increase. At present installed wind plant capacity is about 3762 MW and an additional 1170 MW wind plant investment is under construction [58]. Although there is an increasing demand for the renewable energy sources, there is no available test environment to certificate wind energy systems and test available technology at realistic conditions in Turkey yet. A test environment could be needed to evaluate performance of purchased systems at certain local operating conditions. Such an environment also provides an opportunity for users to assess the systems they plan to purchase and make a correct choice.

A test environment is also needed to conduct realistic tests at the development stage of new technologies. However, establishing such platforms can be costly for the investors. Since a wind turbine is a massive construction, testing and development of such a component needs broad facilities and costly investments. To develop a wind turbine at the facility also requires a wind tunnel and grid connection, which are the main cost of the test system.

Furthermore, the increased penetration of renewable energy sources created a new topic: “Smart Grid”. Since renewable energy sources are free to use, it is expected that there will be a new type generation of the power, which is named as “Distributed Generation”. Distributed generation can be simply stated as the power generation at the point of consumption. Accelerating the integration of renewable energy sources is thought to increase utilization of distributed generation systems. As a result, there is a need of “smart” grid instead of centralized grid to direct many distributed energy

sources. However, leading of many small energy sources (microgrids) may turn out many problems such as grid faults, islanding etc. Thus, there is also a need for a test platform to study fault conditions under realistic but controlled conditions.

Our main motivation on this study is to develop a hardware-in-the-loop (HIL) emulation platform to conduct tests and develop new control techniques for the wind energy conversion systems. Using HIL setup, it is aimed to shorten validation process of components used in wind turbines and control techniques, conduct different tests repetitively and easily, prevent damage from highly dangerous grid tests (grid interruption or grid recovery) and minimize cost of failure and cost to test.

1.2. Problem Definition and Our Approach

In this study, one of the goals is to establish a realistic environment to test hardware, which will be used to convert the turbine output to electricity and connect to the grid. For this purpose, a model that calculates the speed and torque of the turbine shaft, using the wind data recorded (or artificially created) on a realistic model is intended to be used. A motor that is controlled by these data will be replicating the mechanical behavior of turbine shaft on its shaft. The shaft will be driving the gear box (or directly driven) and the generator to be used in the real system. The generator output will be connected to the grid via actual converters of the system. Thus, desired tests can be made on the system, in a controlled but realistic environment.

The user interface will be prepared for input of system data (wind data and others). Also a turbine model library will be created which will allow users to enter turbine model parameters and study behavior of their hardware operating with different turbines. Moreover, a software will be prepared which will process torque, velocity, current and voltage data coming from system sensors and present to users. A software and hardware running on a computer or on a separate processor will perform system protection functions. Energy produced by a permanent magnet generator will be fed to mains supply.

A MATLAB-based model will be also developed of this “hardware-in-the-loop” (HIL) test system that can simulate the scenarios that can be studied in the “HIL” test system with acceptable accuracy. Once the accuracy of this system is verified with tests, a tool will be available to study operation of a given wind energy conversion system, which allows study of various operating scenarios and protection methods with different turbines, generators, gearbox and control methods. Such software simulates global behavior correctly; however, the effect of various operations on the electronic hardware can be realistically studied using HIL. From this perspective, these two simulation medium complement each other.

Using the software developed, the possibility of feeding local loads connected to the generator bus from wind generator will be investigated when the mains supply to the generator feeder is interrupted. For this purpose, measures that can be taken to avoid harming the loads and preserving energy quality, such as;

- Control of the converters at the generator output
- The type of control that should be used on the turbine side
- And preservation of energy quality after interruption

1.3. Contribution

The contributions of this thesis are given as:

- Developing a modular hardware-in-the-loop emulator,
- Preparing an interface at the Labview platform to gather all the data for tested equipment,
- Establishing a software simulator that can imitate the behavior of the HIL setup,
- Detecting differences between the results of HIL setup and software simulator, and so creating artificial neural networks,
- Investigating islanding operation and microgrid stability,

- Evaluating efficiency of the used techniques,
- Proposing new control strategies for stand-alone operation.

1.4. Outline of Thesis

This chapter is aimed to give a brief description about this study, problem definition and our approach and contribution of the study.

Chapter 2 details the wind energy conversion system components. All the components have been modeled in MATLAB/Simulink environment by taking into consideration dynamical conditions. The control techniques of the wind turbine power control have been examined in detail and control models have been developed at the simulation environment.

Chapter 3 starts with the literature survey of the HIL setup. Then, HIL setup configuration and its logic of operation have been explained. Every physical model has been detailed and the measurements taken from them have been shared. Differences of the HIL setup and software simulator have been analyzed and the artificial neural networks have been established accordingly. For the last, tests conducted on the HIL setup and the software simulators have been compared and the differences are explained.

Chapter 4 provides a brief introduction to the concepts of smart grid, distributed generation and islanding. Grid codes applied in Turkey have been clarified and the software simulator has been explained. Grid side converter is investigated particularly and intentional islanding operation is analyzed. Islanding detection algorithms and control strategies have been proposed and their efficiency has been discussed.

Finally in Chapter 5, the thesis is concluded by stating what have been studied and investigated through in this study. Future works that can be done to improve this study have been outlined.

CHAPTER 2

SOFTWARE SIMULATOR OF WIND ENERGY CONVERSION SYSTEM

2.1. Introduction

The milestones of this thesis work are: 1) developing a software simulator that imitates a wind energy conversion system (WECS); 2) building a hardware-in-the-loop (HIL) emulator to test components of WECS; 3) conducting experiments related to the grid connection of WECS and improving control techniques. Developing the idea without damaging the hardware and experimenting with different control parameters and possible operation modes has driven us to improve a software simulator. Furthermore, software simulator is thought to accelerate development process for different strategies. In the simulator different wind characteristics can be tested without having a wind tunnel, reactions of the wind turbines can be observed by not having the turbine actually or efficiencies of the power electronics components can be analyzed by not connecting them actually to the system. It is known that a software simulator cannot replace the actual system, but it can present us the idea to be tested is applicable or not or the components/controllers are compatible with the WECS that is studied instantly. With the knowledge that a software simulator is only not adequate to imitate a WECS, a HIL emulator is established in the laboratory as well. This emulator will be explained in Chapter 3 in detail. One more thing that can be expressed about the software simulator is that it can reduce the cost of experiments. Conducting experiments about the developed idea or the component at an actual system is not only hard to implement but also an expensive process if it is considered that an average wind turbine is about 1-3 MW and of 100-140 meter in length.

The software simulator is established with the intent of giving flexibility to the user. That is, simulator is designed modular to allow the user change the desired part as before starting testing and observe the results accordingly. In this section a wind energy conversion system consisting of a wind turbine, generator and back-to-back (AC/DC/AC) drivers has been modeled and simulated in the environment of MATLAB/Simulink. Moreover, controllers used in the WECS have been discussed by comparing advantages/disadvantages and these have been designed in the simulation environment.

2.2. Block Diagram of the Software Simulator System

Software simulation has been developed to simulate a wind turbine-generator system which is connected to the grid via a bidirectional power converter. In other words, the purpose of this system is to model the behavior of the shaft of the wind turbine closely to a real system considering changes of wind speed by taking into consideration mechanical inertia. In the simulation, hardware-in-the-loop system is desired to be imitated as well. To sum up, software simulation shows the characteristics of a wind energy conversion system, which also covers HIL system.

Simulator is initiated with entering the wind data. Wind data can be sourced either from a measurement at an actual turbine or random generation. In the simulation, wind data is modeled; however, modeled wind data can be ignored and the measured one can be set at the simulator, too. The modeled wind data can be seen in Figure 2.1 with block number ‘1’. Block 1 is sourced from the user. The user can set desired wind profile by setting ramp, gust, random noise and constant parameters. By doing that, any wind profile can be created and the behavior of the wind turbine against different wind conditions can be observed. The parameters of ramp, gust, random noise and constant wind models are given at the ‘Wind Data Model’ section in detail.

Wind turbine which is modeled in the software is a variable speed, variable pitch turbine which is numbered as block ‘2’ in Figure 2.1. That is, power of the turbine can be controlled via either pitching the blades or changing the shaft speed through

generator side controller. By this way, wind turbine will be able to capture maximum power from the wind. Why this type of turbine is selected will be detailed at section 2.2. The wind turbine is selected as a power of 11kW. The wind turbine is operated at 80% efficiency due to losses occurred during operation of the wind energy conversion system. The inertia of the system is 0.2 kg*m^2. In the simulation, shaft stiffness and damping factor is also considered to get closer look from the perspective of dynamic model. The shaft stiffness is selected as 0.3, which is in the range of low-speed forged alloy steel. Damping factor is set as 0.01 since the modeled system is relatively small and there is slight effect of damping factor. The pitch angle, which is shown with the symbol of β, is limited to be changed within the range of -2^0 to 30^0, which is typically range for variable pitch turbines. The time constant of the pitching blade, which comes from the response of the hydraulic systems used to pitch the blades, is set as 0.25 s. The rate of change of blades is also set to a limit of 10^0 not to distort stabilization of the tower during pitching period.

The generator in the simulator is selected as a permanent magnet synchronous generator. The generator is modeled in two parts: electrical and mechanical model. The parameters of the modeled generator are asked from the user according to the generator that he/she desires to test. The generator used in the software simulation is the one used at the HIL setup as well. Thus, parameters of the generator have been measured from that generator, which is already set up in the laboratory. To characterize the generator, stator resistance, q-axis inductance, d-axis inductance, open circuit characteristics, torque constant, flux linkage, inertia and losses (core, copper and shaft) should be taken out. These parameters have been extracted with the experiments conducted on the generator which is installed at the HIL setup. Both the values of the parameters of the generator and the formulations can be seen in Chapter 3, 'Generator Model and AC/DC Converter Model' section.

In the simulator, power electronics of the system has been established with two converters: AC/DC (generator side) converter and DC/AC (grid side) converter. While AC/DC converter controls the DC link voltage, DC/AC converter stabilizes the output three-phase AC voltage to grid voltage and supplies active and reactive

power to the central grid. The converters can be seen in Figure 2.1 with block number '5'. The converters are operated at 6 kHz switching frequency. There is also DC link capacitors and braking chopper for the sake of the power electronics. DC link capacitors, with block number of '5.2', stores the DC voltage to be used by the DC/AC converter. These capacitors supply the isolation between the turbine and the grid. In addition, DC link capacitors are used to control of active power at the DC/AC converter. Thus, these are also critical components for the full-scale power electronics used by variable-speed variable-pitch wind turbines. The DC link capacitors used in the software simulation is set as 2000 μF, which is the value at the HIL setup. The last equipment in the power electronics section is the braking chopper, which is numbered as '5.3'. Braking chopper consists of a resistor and IGBT switch which is triggered beyond a DC voltage set by the user. This voltage is named as activation voltage, which is 750VDC for the software simulation and HIL setup. The resistor should be in the range of 2-5 Ω for proper operation in the HIL setup. Thus, braking resistor is set as 2 Ω in the simulation as well.

The simulator also includes a 'Controllers' block numbered as '4': maximum power point tracking (MPPT) control with the number of '4.2' and pitch control with the number of '4.1'. These controllers are used either to operate the wind turbine at the optimum point or to limit extracted power not to damage to the system. The MPPT controller traces the shaft speed and output power of the system. The controller generates a speed reference for the next time step by considering turbine torque, generator torque and inertia of the whole system as in Equation (2.1),

$$T_{wt} - T_{shaft} = J\frac{\Delta w_t}{\Delta t} \tag{2.1}$$

Since the turbine torque, shaft torque and step time of the controller is known, it is easy to define next time step for the MPPT controller reference. By increasing or decreasing the shaft speed for the specified wind speed, maximum operating point of the turbine is found and the maximum power is attained. The time step of the controller is set to 50ms for this simulation. During time step, the wind speed is assumed to be constant until next time step and the next speed reference is calculated

accordingly. By doing that, operating point is attained. Detailed explanation is also conducted in 'MPPT Controller' section as well. Another controller is the pitch control that can be seen in Figure 2.1 as block '4.1'. This block traces the output power and activates if the maximum allowed power for the specified wind is exceeded. Pitch controller gets turbine torque and shaft speed as input and results in pitch angle reference for the turbine. Pitch angle is set to 0^0 for the below rated power operation. For above rated power, pitch controller is activated.

The software simulator also includes filters numbered as '6' in Figure 2.1. Filter block '6' consists of grid side inductance, inverter side inductance and capacitances, which is the configuration of LCL filter. This filter is used in the simulation due to presenting in the HIL setup as well. LCL filter is used to filter out harmonics formed at the PWM frequency of 6 kHz. Grid side inductance is set to 1.2 mH, inverter side inductance is set to 2 mH and capacitors are set to 8 μF for the simulation.

The loads which are used especially to observe islanding operation in the next chapters consist of resistive elements. In the simulation, 2 kW resistive loads have been used. Loads can be seen in Figure 2.1 with numbered block of '7' as well.

For the last, grid connection block which is numbered as '8' can be seen in Figure 2.1. Grid connection consists of low voltage/medium voltage transformer, transmission lines and three-phase breakers. This connection is not detailed here. At Chapter 4, the islanding operation is considered out and the grid connection is explained in detail at that section.

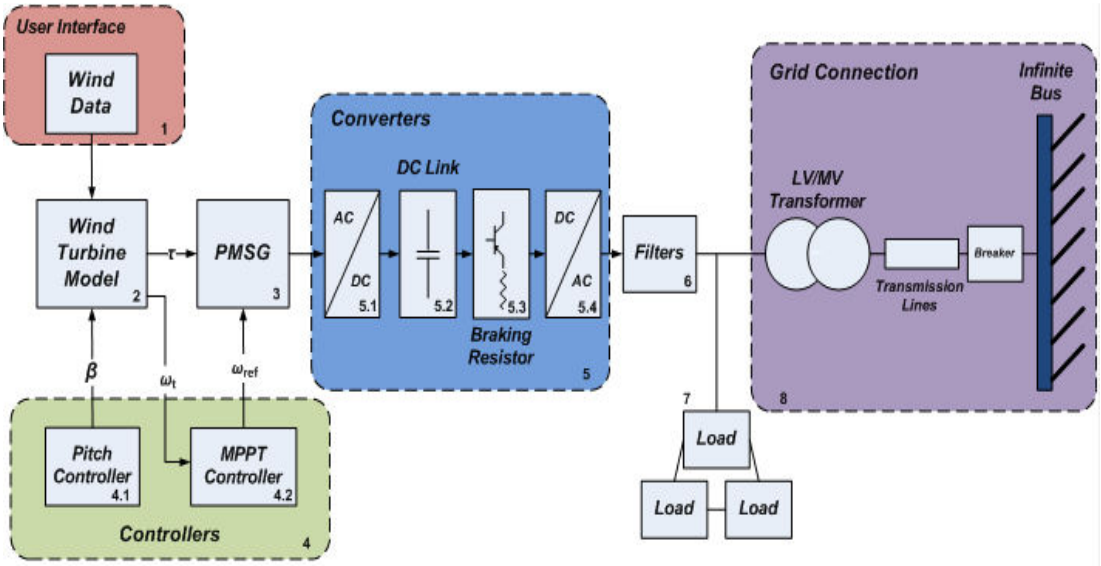

Figure 2.1 Block diagrams of the software simulator

2.3. Wind Data Model

The simulator is designed to allow different wind characteristics to see the effect of it on the components of the system. Thus, the wind data (block '1') is modeled in the simulator in two different configurations:

- User can enter a wind profile which is measured from a wind turbine site,
- User can generate manually arranged wind profile.

Loading a wind profile to the simulator is efficient to see the actual characteristics of the turbine at the specified geography. However, user can also desire to arrange different wind profiles to observe the performance of the components at the extreme conditions. In other words, user can demand to force the turbine or its components to challenging test such as HALT (highly accelerated life test) test. Hence, wind model has been divided into components. Wind speed is modeled as consisting of constant

(base) and non-constant components. Non-constant wind speeds can be modeled in three subparts: ramp, gust and random noise components [1].

$$v_w(t) = v_b(t) + v_r(t) + v_g(t) + v_n(t) \tag{2.2}$$

where v_b is the constant (base) wind component, v_r is the ramp wind component, v_g is the gust wind component, v_n is the random noise component. These wind components are visualized in Figure 2.2. The components of the wind speed have been modeled in Simulink. Constant wind speed is speed set with a constant number such as 6 m/s for all the period. Ramp wind component is adjusted with three parameters: start time (T_{sr}), initial output (which is 0 for Figure 2.2), maximum duration of ramp signal (T_{max}) and final output value. These values can be set in Simulink 'Ramp' model as seen in Figure 2.3. Gust wind component is regulated with entering gust start time (T_{sg}), finish time (T_{eg}) and amplitude (V_g) in the Simulink model. Random noise component is started with the operation of wind model from the start. In random noise model, minimum and maximum values of the wind speed are defined and random wind speed is generated with either uniform or Gaussian normal distribution. Distribution and repeatability of the values can be set in the model as well.

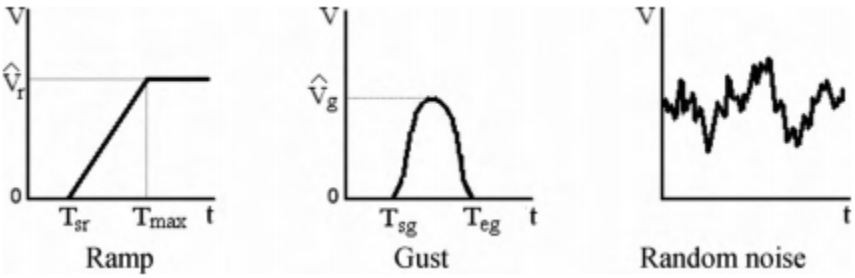

Figure 2.2 Non-constant wind speed components [1]

As seen in Figure 2.3, the user can either select to enter wind profile or generate its own profile. By setting the switch at the desired position, user can initiate the simulation.

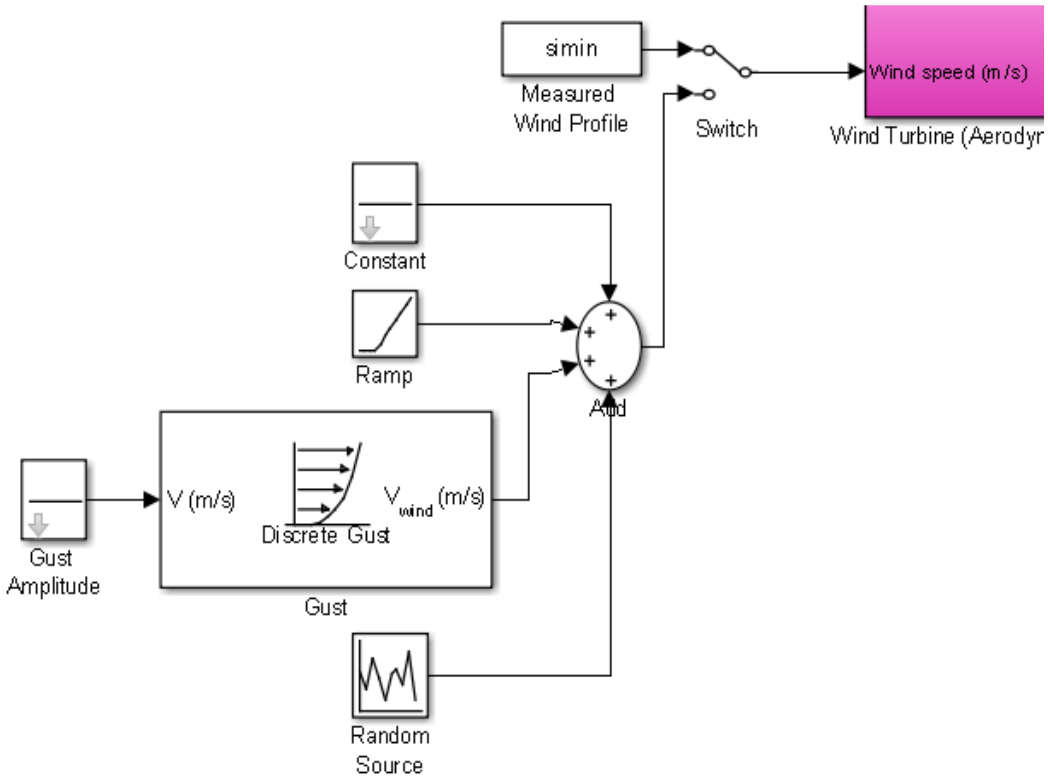

Figure 2.3 Wind model at Simulink

2.4. Wind Turbine Model

2.4.1. Wind Energy Conversion System Configurations

Control of wind turbines applied in the industry is divided into two sections: speed control and power control. Speed control is denoted as fixed speed and variable speed wind turbines in the literature. Power control means limitation of the power

extracted from the turbine in case of winds blowing higher than the cut-out speed. Power control is mainly divided into two sections: stall control and pitch control.

Fixed speed turbines use induction generators, of which rotor speed is controlled by the frequency of the national grid. That is, if the slip on the generator is neglected it can be said that the rotor speed is controlled by the frequency of central grid, gearbox and generator.

The induction generators used in fixed speed turbines can be classified into two main groups: squirrel cage induction generator and wound rotor induction generator. In fixed speed wind turbines, reactive power cannot be controlled by the power electronics. Thus, soft starters and capacitor banks are used to reduce reactive power at the grid side as seen in Figure 2.4, Type A connection. Fixed speed wind turbines generate maximum power at only one speed. Fixed speed wind turbines do not use power electronics components, so they present low cost design for the wind turbines. In addition, their design is simpler and more reliable due to having no complex electronic control components. However, its uncontrollability results in poor power quality and being subjected to high mechanical stresses [2]. In fixed speed turbines, only small variations at the shaft speed are tolerated. Thus, fluctuations in wind speed are directly converted to mechanical torque fluctuations -and since these fluctuations cannot be controlled- they are transmitted to the electrical power grid, resulting in a poor power quality [3].

Variable speed wind turbines (VSWT) are connected to the grid with an induction or synchronous generator and through power converters. Utilizing power converters gives the flexibility of control of aerodynamic efficiency of the wind turbines. In other words, shaft speed can be controlled at VSWTs by the rotor side converter. Rotor side converter is controlled via maximum power point controller. The controller supplies the reference speed which achieves to reach maximum power coefficient by changing shaft speed of the turbine [2].

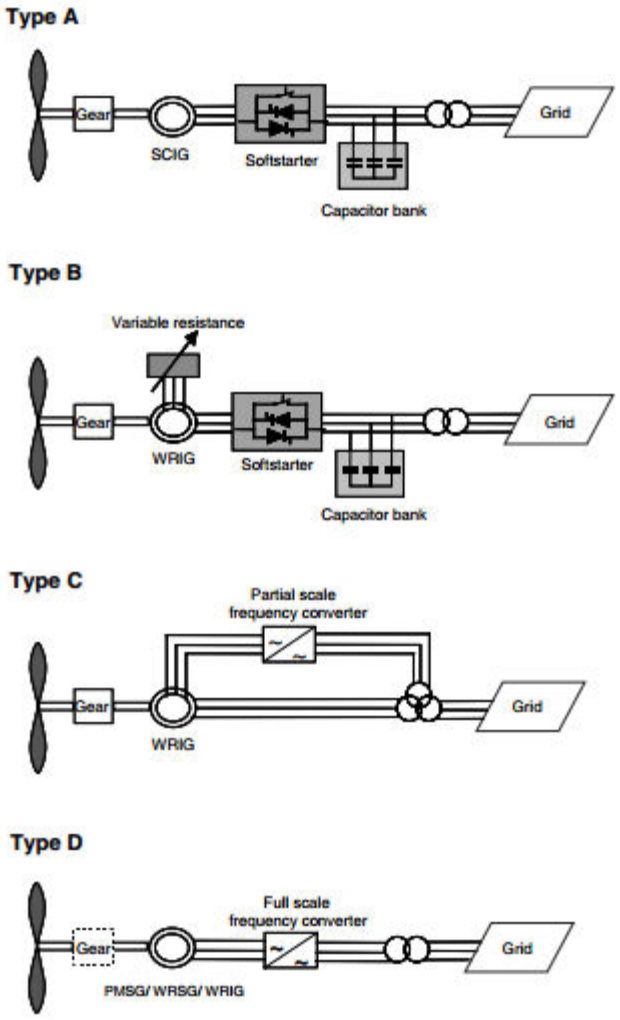

Figure 2.4 Typical wind turbine concepts [2]

Variable speed wind turbines provide many advantages when compared to the fixed one. Advantages of these turbines are [2]:

- decreased stresses on the shaft – VSWTs constitute high inertia due to having PMSGs and DFIGs. Thus, gust wind components are less effective compared to fixed speed turbines. Moreover, variable speed operation is possible during gusts, which cuts the fluctuations at the output power and mechanical shaft.

- extraction more power from same wind speed – utilizing MPPT techniques, speed of the shaft of the turbine can be brought to maximum power point
- decreased noise – PMSGs and DFIGs present lower speed operations and so reduced noise
- control of the power by the grid side power converter – both reactive and active power can be controlled upon request from SCADA (or smart grid operators)
- adaptability to changing conditions on the power system – detection of fault conditions at the grid side and low voltage fault-ride through capability of the power converters increases the ability to stabilize the conversion system
- influence on network stability – power converters provide isolation between turbine and the grid and the distortions on the turbine side can be absorbed within the generator torque

The disadvantages of the VSWTs can be sequenced as:

- additional losses – power electronics creates additional losses due to having semiconductors (IGBT etc.) in the converter design
- more components – back-to-back converters and DC link capacitors increases the number of components
- increased capital cost – power electronics adds an additional cost to initial investment expenditure

Type B, C and D wind turbines are classified into variable speed wind turbines. These turbines differ from each other due to their either power control strategy (pitch or stall control) or types of generators and power converters (DFIG or PMSG, partial scale or full-scale converters).

Although the variable speed wind turbines have many advantages upon fixed speed wind turbines, the cost required to achieve variable speed was initially quite high, as power electronics (IGBT) in the early 1990s were expensive; however, as converter

costs fell precipitously, variable speed variable pitch turbines could be priced at near-parity to fixed speed stall controlled (FSSC) turbines. Then, FSSC turbines themselves had to adapt via two-speed generators (occupying two windings; one winding for low speed and the other one is for medium and high speed operation) and active-stall techniques just to survive. By 2010, FSSC turbines had essentially disappeared from the global market [4]. Furthermore, in 1990's, the main concern was to stabilize voltage at the distribution grid by not harming local power quality. However, for now, large wind farms scaled with the capacity of MWs connected directly to the transmission system and wind power integration problems such as power system control and stability issues are addressed, i.e. global power quality issue [5]. With the updated grid codes of the countries, fault-ride though capability and power control capabilities of the turbines is dictated to the turbine producers. Fixed-speed wind turbines (Type A) would disconnect from the grid even if there is a quite small disturbances due to absence of power electronics. Utilizing power electronics, however, eases to satisfy grid codes. Reasons expressed at the above leaded the producers to the variable speed variable pitch wind turbines (why pitch control is selected will be detailed in the upcoming chapters). In the simulation software, wind turbine is so designed to be variable speed variable pitch one. Wind turbine model has been divided into two sections: aerodynamic model and kinetic model.

2.4.2. Aerodynamic Model of the Wind Turbine Used in the Simulation

Wind turbines have been modeled according to blade element theory for years. This model considers air flow and forces on a rotor blade segment, blade pitch angle, lift and drag coefficients and the turbine mechanical characteristics. Power extracted from a turbine can be expressed with a relation,

$$P_w = \frac{1}{2}\rho C_p(\lambda,\beta)A_r\vartheta_\omega^3 \tag{2.3}$$

where ρ is air density, C_p is the power coefficient, A is the area covered by the rotor blades, β is the pitch angle and ϑ is the wind speed upstream of the rotor (turbine model is numbered as '2' in Figure 2.1).

Power coefficient can be defined as ratio of the power P_w absorbed by the turbine to that of the moving air mass under smooth flow conditions at the turbine. It is a dimensionless coefficient. This coefficient mainly depends on two factors: tip-speed ratio and pitch angle. Pitch angle can be defined as the angle of attack of the blades of a turbine into or out of the wind to control the absorption of the power. Tip-speed ratio can be defined as the ratio between the tangential speed of the tip of a blade and actual wind velocity. It can be expressed with a relation,

$$\lambda = \frac{\omega_R R}{\vartheta} \tag{2.4}$$

Power coefficient of a turbine can be numerically approximated by using these two factors. According to data fields derived from measurements of the turbine, power coefficient can be expressed as a function. In the simulation, power coefficient has been declared with a generic equation,

$$C_p(\lambda, \beta) = c_1 \left(\frac{c_2}{\lambda_i} - c_3 \beta - c_4 \right) e^{\frac{-c_5}{\lambda_i}} + c_6 \lambda \tag{2.5}$$

where c_1=0.5176, c_2=116, c_3=0.4, c_4=5, c_5=21, c_6=0.0068 and

$$\left(\frac{1}{\lambda_i} = \frac{1}{\lambda + 0.08\beta} - \frac{0.035}{\beta^3 + 1} \right) \tag{2.6}$$

Equation (2.5) and (2.6) with the specified coefficients give us a C_p-λ curve at different pitch angles as in Figure 2.5.

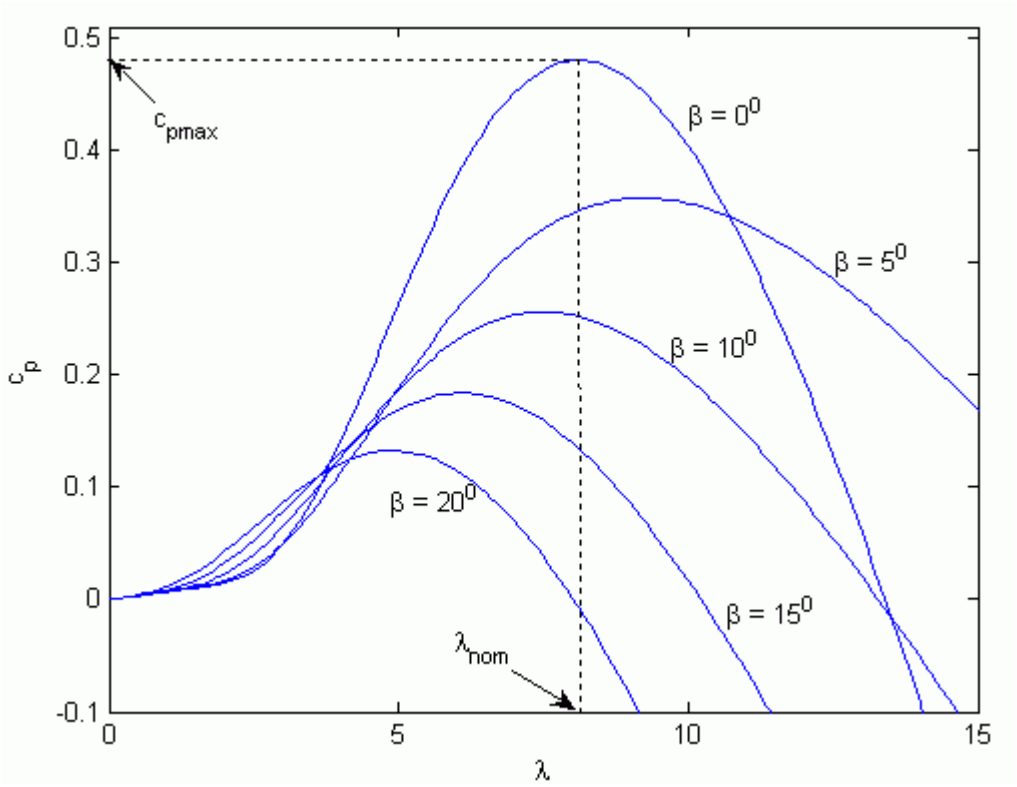

Figure 2.5 Cp- λ curve of the wind turbine model in Simulink

Figure 2.5 implies that power extracted from a turbine decreases with the increasing pitch angle (C_p is lowered when β is increased!). Thus, pitching the blade is not used while extracting maximum power from the turbine. It is, however, used at the extreme conditions such as wind speed's exceeding rated speed or at grid faults. By applying pitch control, power that can damage the system or components has been suppressed. In the simulation, pitch angle is set to 0 during steady state tests. When grid-side experiments have been conducted as in Chapter 4, it is activated. The configuration of the pitch controller and how this is activated is detailed in the upcoming chapters.

SimPowerSytems block in Matlab/Simulink includes a wind turbine model that is set up according to Equation (2.3) as seen in Figure 2.6. In this model, wind turbine is characterized in per unit (pu) system. The model requires three input variables: wind

speed, shaft speed (generator speed) and pitch angle. Wind speed is entered to the model in “m/s”, shaft speed is set with per unit system (base speed is the rated speed of the generator) and pitch angle is set by degrees. Base speed of the generator is taken as the rated speed in the simulation (e.g. in the HIL system nominal voltage is generated when PMSG is rotated with 750rpm, which is the rated speed of an 8 pole machine). Pitch angle is set to 0^0 degree for maximum power extraction until pitch controller is needed. Wind speed should be inserted in m/s to this block, too. It is converted in the blockset to per unit system using base wind speed. Blockset needs some parameters to evaluate the system as per unit. Thus, parameters are inserted with an interface, named as “Mask” in Simulink as seen in Figure 2.7. As seen in Figure 2.7, maximum power extracted from turbine is set to 80% of total available power due to losses of the whole system.

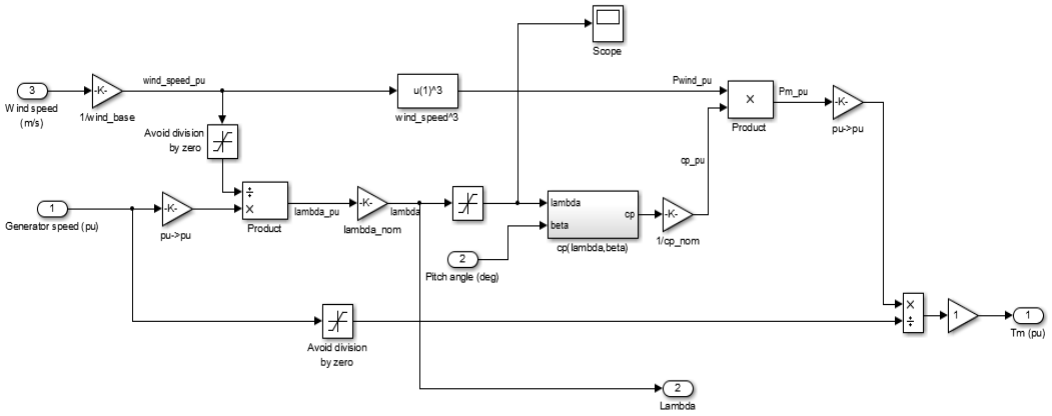

Figure 2.6 Wind turbine blockset in Simulink

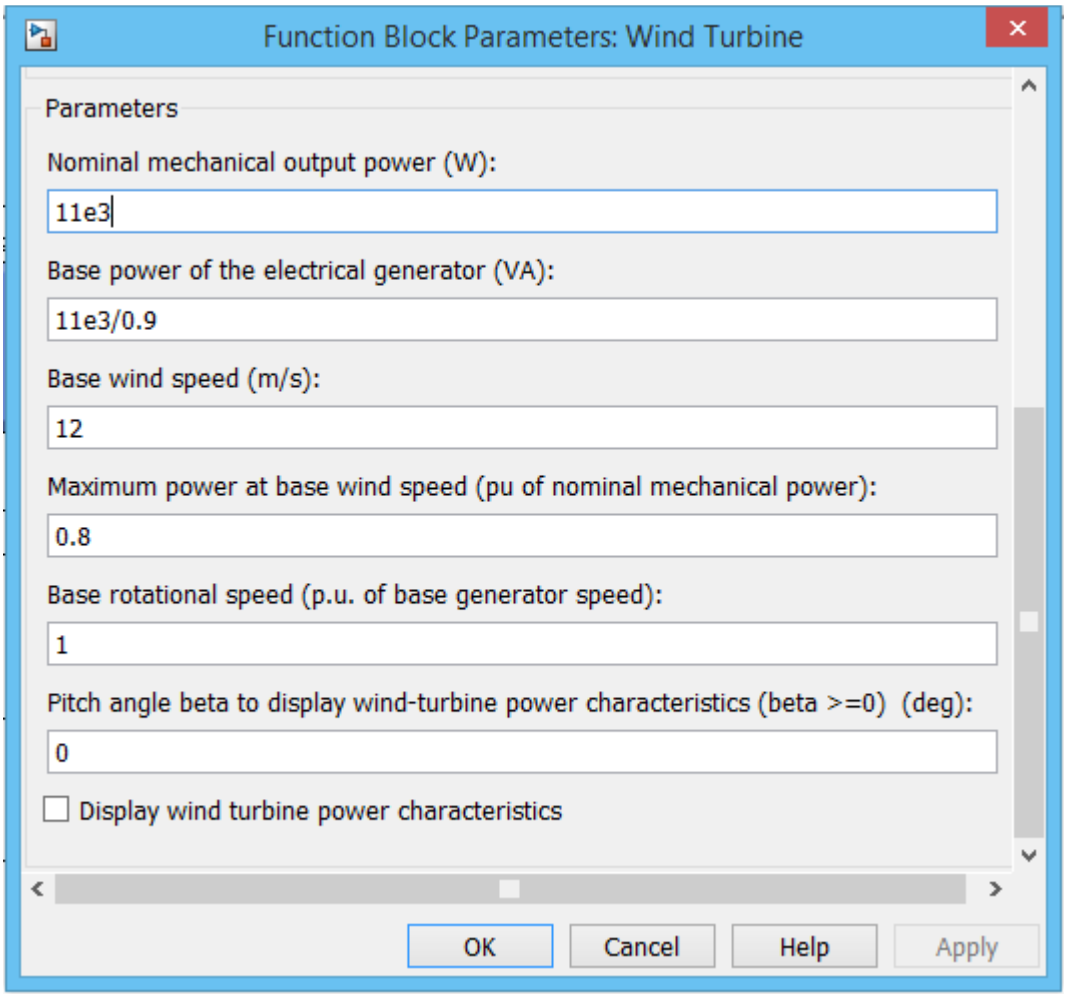

Figure 2.7 Wind turbine interface (Mask of the blockset)

In the Mask, nominal mechanical output power and base power of the electrical generator is used for detection power factor of the generator integrated to the system. Base wind speed is used to determine the speed where the maximum power is extracted (it can also be considered rated speed). Maximum power at base wind speed is needed to imitate the loss of the turbine.

This blockset lacks of dynamic conditions of a turbine – that is, turbine model presents us steady state performance of a turbine. Drive train of the turbine cannot be simulated in this simulator. Thus, it should be also added to the simulation. In the

next section, drive train and the other factors affecting dynamic performance will be detailed.

2.4.3. Kinetic Model of the Wind Turbine Used in the Simulation

Dynamic performance of a wind turbine is critical for transient stability analysis [8]. Transients occurred in the shaft of turbine is a more crucial problem for escpecillay fixed speed wind turbines since they are connected to the grid directly. On the contrary, effect of transients of dynamic conditions can be tolerated via power converters of the variable speed wind turbines (VSWT) [9]. However, drive train is still a research area since power converters used in VSWT should be designed accordingly. Thus, steady state model of the wind turbine is accompanied with the kinetic model in the simulation.

Kinetic model consists of the drive train (inertia, shaft stiffness, damping) and the other phenomenons (tower shadow and wind shear).

Drive trains can be classified as six-mass model, three-mass model, transformed three-mass model, two-mass model and one-mass model. All models can be found in Figure 2.8. In six-mass model, three blades' inertia, hub inertia, gearbox inertia, generator inertia, shaft stiffness of all the rotating parts and damping coefficients have been included. For a detailed study, six-mass model should be set up and all the parameters should be taken into account in the simulation. In three mass model, turbine has been thought as a big disk that includes hub and blades' inertia and damping and stiffness of the blades have been ignored. In two mass model, system is thought to be directly coupled and have equivalent shaft stiffness. Finally, in one mass model, WTG (wind turbine-generator) has been thought to be a single rotating mass. In our simulation, two-mass model has been carried out since HIL simulator that will be detailed in the next chapters is a direct driven system. Since HIL setup lacks of gearbox, the gearbox is not considered in two-mass model. Two-mass model has been established with the Equations of 2.7-2.10 [13]. For future works, drive

train can be modified to see the effects of drag and lift components at the blades to whole system.

$$2H_t \frac{dw_t}{dt} = T_{wt} - T_{shaft} \tag{2.7}$$

$$\frac{1}{w_{elb}} \frac{d\phi_{tw}}{dt} = w_t - w_r \tag{2.8}$$

$$2H_g \frac{dw_r}{dt} = T_{shaft} - T_g \tag{2.9}$$

$$T_{shaft} = K_{shaft}\phi_{tw} + D_t \frac{d\phi_{tw}}{dt} \tag{2.10}$$

where H_t and H_g are the inertia constants of the turbine and PMSG respectively, ϕ_{tw} is angle of twist, w_t is the angular speed of the wind turbine in per unit, w_r is the shaft speed of the generator in per unit, w_{elb} is the electrical base speed, T_{shaft} is the torque of the shaft, K_{shaft} is the stiffness of the shaft and D_t is the damping constant [13]. Inertias of the turbine and PMSG are set by taking generator inertia as base value. While inertia of the generator is set to 1 p.u., inertia of the turbine is set to 12 by taking into consideration typical wind turbines [62]. Shaft stiffness and damping factor is set to 0.3 and 0.01 respectively. Electrical base speed is 750 rpm, which is the rated speed of the generator. The other variables (shaft torque and wind turbine torque) are consequences of the models instantly at the simulation period. Shaft twist angle is again calculated according to Equation (2.8). This angle is used to calculate shaft torque at the kinetic model.

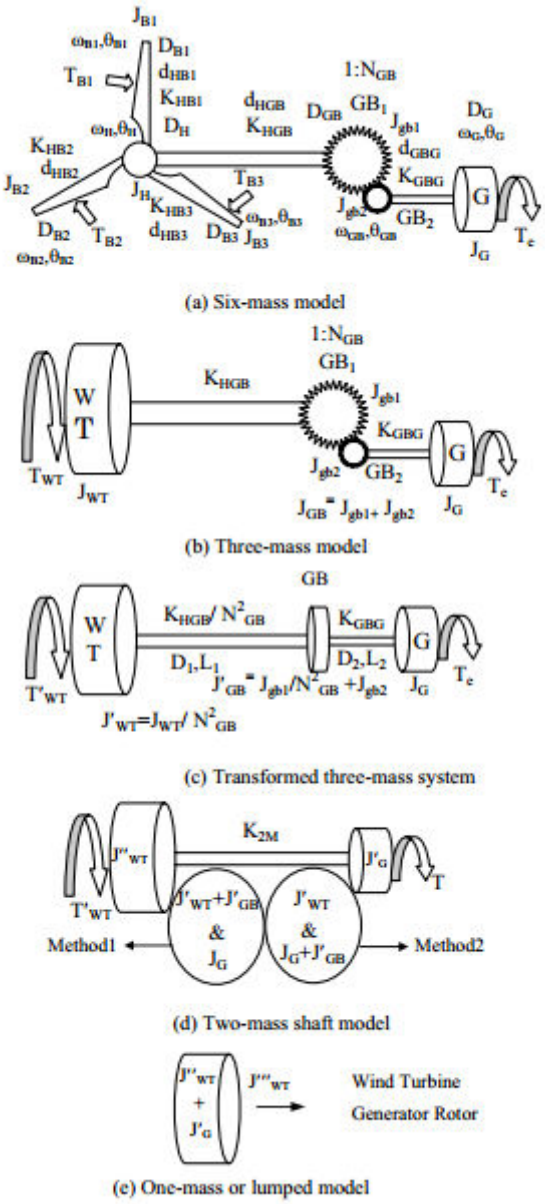

Figure 2.8 Drive train models [9]

Other phenomenons such as tower shadow and wind shear has been added to the kinetic model, too. Tower shadow can be stated as small change of output power due to interruption of airflow when each blade passes through tower. Placing a tower disrupts airflow by the side of the airflow. Thus, rotating blades experiences different airflows at that instant. This imbalance of the blades due to different airflows causes

a small dip in the net output torque of the turbine [10]. Tower shadow can be modeled by adding a decrease in net output torque of the turbine for each 2π/3 rad section of the blade as in Figure 2.9 [11]. The characteristics of the torque ripple depend on the physical structures of the blades and the tower [12]. A representative model of the tower shadow effect can be seen in Figure 2.9.

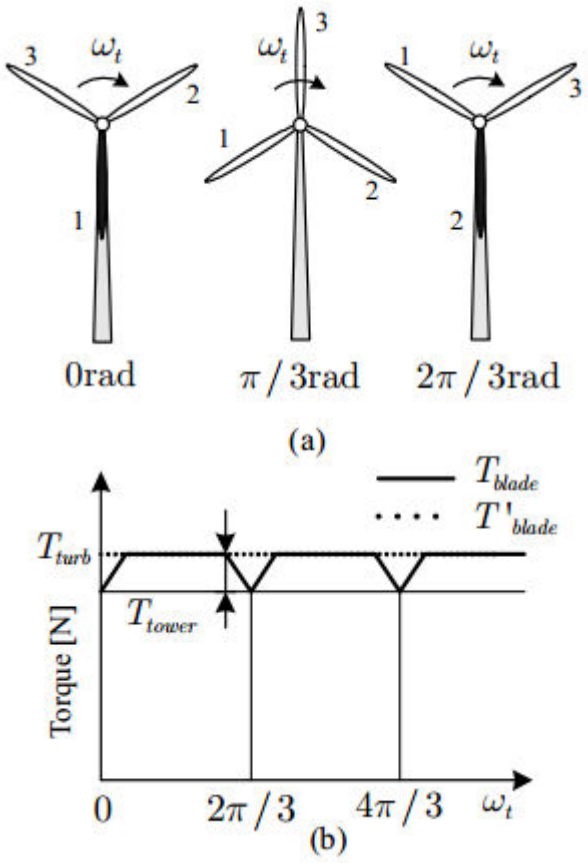

Figure 2.9 (a) Rotor position at ω_t = 0, 2π/3, 4π/3 rad (black blade creates the tower effect), (b) Ramp shape of torque ripple modeling for upwind tower effect [12]

The torque component of the tower shadow can be modeled as,

$$T_{ts} = -t_{ts}\cos\theta \tag{2.11}$$

where θ is the angle of the blades to the tower and t_{ts} is a constant which should be set by the user.

Wind shear creates oscillations in the net output torque of the turbine as well. This oscillation comes out due to changing wind speed for different heights. In other words, it is known that wind speed increases with increasing height as seen in Figure 2.10. Thus, for rotating blades, it can be said that the blades experiences different wind speeds. This causes a torque oscillation in the turbine. The wind speed can be formulated by taking into consideration height of the blades as,

$$\frac{v_2}{v_1} = (\frac{h_1}{h_2})^{\alpha} \tag{2.12}$$

where h_1 and h_2 represent height of the blades and v_1 and v_2 show the speed of the blades, respectively. 'a' is a constant which shows the characteristics of the territory that the turbine is placed onto. The change in the torque due to changing speed of the blades can be showed as,

$$T_{ws} = -t_{ws}\, cos\theta \tag{2.13}$$

Tower shadow and wind shear creates a decrease at the net output torque for each 120^0 revolution of the blades as seen in Figure 2.9. The decrease can be set by changing t_{ws} and t_{ts} constants in the simulation according to desired wind condition.

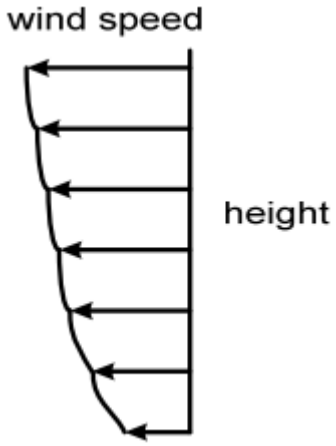

Figure 2.10 Wind shear [11]

In the kinetic model, both tower shadow and wind shear effects have been unified to one formula same as Equation (2.11). Kinetic model has been set up at the software simulator as in Figure 2.11.

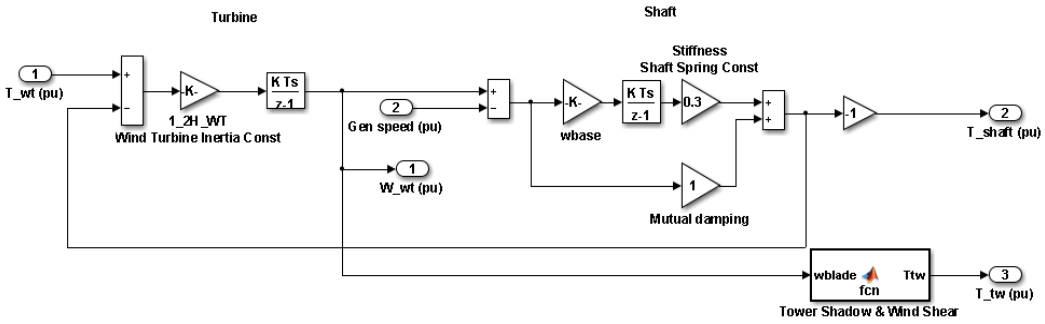

Figure 2.11 Kinetic model of the wind turbine model

Aerodynamic and kinetic models are explained in this section. To summarize, wind turbine results in a torque output after taking the generator speed, pitch angle and wind speed. In the model, dynamic conditions are also taken into consideration. For the future purposes, different dynamic conditions can also be added to this model.

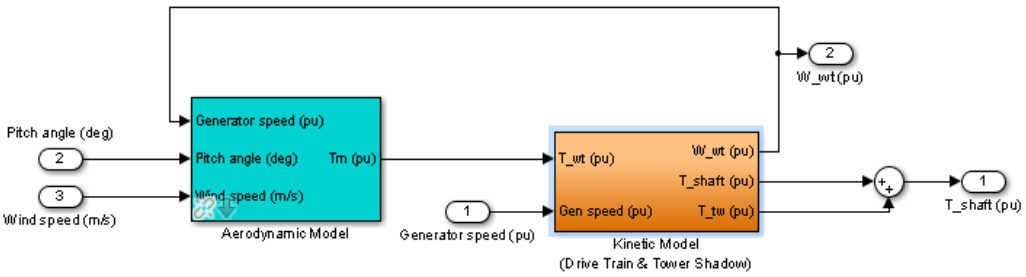

Figure 2.12 Wind turbine model at software simulator

2.5. Generator Model

Turbine types are detailed in section 2.1.2 and it is concluded that variable speed wind turbines dominate market share by 2013. Until 2003, fixed speed wind turbines with squirrel cage induction generator (Type A) were leading in the wind turbine industry. With the increased awareness of power quality and grid codes, control of the power and its quality made the designers to pass to VSWTs. By 2008, VSWTs (mostly Type C, DFIG generator) captured 85% of the market share and the fixed speed wind turbine manufacturers stopped or limited their production [6]. Although Type C wind turbines dominate the market, Type D wind turbines increase its share in the market. Main distinction between the Type C and Type D comes from the scaling of the power converters and their drive trains. Their differences can be seen at Table 2.1.

Table 2.1 Comparison between Type C and Type D wind turbines

	Type C	**Type D**
Generator Type	Doubly Fed Induction Generator (DFIG)	Permanent Magnet Synchronous Generator
Gearbox	Available	-
Converter Scale	Partial Scale	Full Scale

In Type C wind turbines, DFIG connects to the turbine with the help of multistage gearbox. Stator of the DFIG generator is connected to the grid directly while rotor of the DFIG is connected through a power converter. Since a part of the energy is passed out to the grid from converter, partial scale operation is possible. The converters are almost 25% rated power of the complete system. In addition, the filters used at the point of common coupling (PCC) are also 0.25 p.u. size [3]. Since the converters and filters are reduced, the cost of the conversion system is decreased.

Disadvantages of the using DFIG generators can be sequenced as [3]:

- Need for gearbox and high speed transmission reduce the transmission efficieny. Furthermore, gearbox usually requires maintenance due to its complex structure.
- DFIG generated turbines mostly use water cooling systems, increasing cost of the system
- They starts to operate at higher wind speeds larger than that of the PMSG generated turbines
- Less compact structure when compared to the PMSG

Type D wind turbines are called direct driven wind turbines in industry. Type D wind turbines mostly use permanent magnet synchronous generators in their design.

PMSMs shelters large air gaps which reduces flux linkages. Thus, low speed PMSMs can be produced smaller than DFIGs when its power rating is taken into consideration [6]. Thus, using PMSG allow turbine operating at low speeds. That is, there is no need to a gearbox. Eliminating gearbox decreases cost quite amount. Moreover, system maintenance is decreased. Maintenance is a critical problem for especially off-shore wind turbines [14]-[15]. Since off-shore turbines located in the water (sea, ocean etc.) to extract more power, their maintenance is harder than on-shore turbines and this increases the operational cost of these turbines. Furthermore, PMSGs do not need field windings since permanent magnets create required flux around the rotor. Thus, there is no need to supply field current. This results in reduced heat dissipation and higher efficiency. At the beginning of 2000s, cost of PMSGs has been overrated compared to DFIG due to containing magnets inside. Starting of the utilizing NdFeB permanent magnet materials, cost of the PMSG has been dropped considerably. The statistics also support that development such that size of global direct drive market reached 28.1% in 2013 with an increase from 19.5% in 2012 [7].

Although direct driven PMSG turbines improve, there are still some disadvantages. High energy PM materials decreases the cost of PMSG; however, PM materials are still makes it an expensive option. Furthermore, manufacturing and assembling is hard compared with the DFIG. Since PM materials can be demagnetized in harsh environment, generator should be designed such that temperature of the generator rotor must stay below 80^0C. This makes the design process harder than DFIG. Even if PMSG cannot be ahead of DFIG with all the parameters, technology of PMSGs has been developing so rapid that direct driven systems are thought to surpass in the market share in the near future [15]. Thus, PMSG has been selected as the generator to be implemented in HIL system.

In the simulation, permanent synchronous generator has been modeled via using the PMSG model of SimPowerSystems in Simulink. This machine operates either in motoring or generating mode. Sign of mechanical torque determines whether it is in motoring or generating mode (positive for motoring, negative for generating). This

model presents dynamics of a three-phase PMSM with sinusoidal back electromotive force (EMF).

Electrical model has been established with below assumptions [16]:

- Smooth air gap model, neglecting cogging torque between permanent magnet and stator teeth
- Position-independent inductance, neglecting reluctance torque
- Electrical conduction loss model, neglecting core losses in magnetic materials of machine and neglecting frequency dependence of stator resistance R
- Linear magnetic model, neglecting magnetic saturation
- Linear friction model, viscous and coulomb terms

Electrical model equations and parameter verification has been done in the rotor reference frame (dq frame). Stator referred quantities which are in the rotor reference frame can be seen as,

$$\frac{d}{dt}i_d = \frac{1}{L_d}v_d - \frac{R}{L_d}i_d + \frac{L_d}{L_q}pw_r i_q \tag{2.14}$$

$$\frac{d}{dt}i_q = \frac{1}{L_q}v_q - \frac{R}{L_q}i_q - \frac{L_d}{L_q}pw_r i_d - \frac{\lambda pw_r}{L_q} \tag{2.15}$$

$$T_e = \frac{3}{2}p\left[\lambda i_q + \left(L_d - L_q\right)i_d i_q\right] \tag{2.16}$$

Table 2.2 Electrical model parameters [16]

L_d, L_q	d and q axis inductances
R	Resistance of the stator winding
i_q, i_d	q and d axis currents
V_q, V_d	q and d axis voltages
w_r	Angular velocity of the rotor
λ	Amplitude of the flux induced by the permanent magnets of the rotor in the stator phases
p	Number of pole pairs
T_e	Electromagnetic torque

In the model, q and d axis inductances also have a relationship with the stator inductance as showed in Equation (2.17).

$$L_{ab} = L_d + L_q + \left(L_q - L_d\right)\cos\left(2\emptyset_e + \frac{\pi}{3}\right) \tag{2.17}$$

$\emptyset_e$ represents the electrical angle of the motor.

According to Park transformation, those relationships in (2.18)-(2.20) can be written [63]:

$$w_e = pw_r \tag{2.18}$$

$$T_{em} = \frac{3}{2}p\lambda i_q \tag{2.19}$$

$$T_{em} = K_t i_q \tag{2.20}$$

All the parameters required to model a generator convenient to Park transformation has been given at the below sections.

2.5.1. Stator Resistance

Measurement of phase resistance has been done by applying DC current. DC current has been set to 10 A limits at the DC power supply. Positive channel has been connected to phase A and negative one to phase B. Measurements from DC supply:

Table 2.3 DC current and voltages for stator resistance measurement

DC Current	10A
DC Voltage	10.05V

$$2R_s = \frac{10.05}{10} = 1.005\ \Omega \tag{2.21}$$

$$R_s = \frac{1.005}{2} = 0.50025\ \approx 0.5\ \Omega \tag{2.22}$$

2.5.2. Q-axis inductance (L_q)

This test has been applied according to IEEE P1812 standards [64]. PM motor has been excited between phase B and C together and thus resultant flux oriented exactly at 90^0 electrical degrees. The rotor aligns itself at the q-axis of stationary d-q frame on the stator side. After fixing the rotor, supply voltage from mains has been applied with the help of an autotransformer.

Measurement results are:

Table 2.4 q-axis inductance measurement data

Frequency (f)	50 Hz
Terminal Voltage(V_t)	16.34 V_{rms}
Stator resistance	0.5 Ω
Current (I)	2.94 A_{rms}
Power factor angle	-82.91^0

By using Equation (2.23), L_q can be calculated.

$$I = \frac{V_t}{\sqrt{w^2L^2 + R_s^2}} \tag{2.23}$$

$$L_q = 17.64\, mH \tag{2.24}$$

2.5.3. D-axis inductance (L_d)

This test has been applied according to IEEE P1812 standards. PM motor has been excited from phase A by connecting phase B and C together and thus resultant flux oriented exactly along the magnetic axis of phase-A. The rotor aligns itself at the d-axis of stationary d-q frame on the stator side. After fixing the rotor, supply voltage from mains has been applied with the help of an autotransformer.

Measurement results are:

Table 2.5 d-axis inductance measurement data

Frequency (f)	50 Hz
Terminal Voltage(V_t)	16.34 V_{rms}
Stator resistance	0.5 Ω
Current (I)	2.94 A_{rms}
Power factor angle	-82.91^0

By using Equation (2.25), L_d can be calculated:

$$I = \frac{V_t}{\sqrt{w^2 L^2 + R_s^2}} \tag{2.25}$$

$$L_d = 16.83\ mH \tag{2.26}$$

2.5.4. Open Circuit Characteristics

Open circuit characteristics have been taken out by measuring line-to-line voltages at different speeds. PMSG has been driven by an induction machine. Measurements taken from PMSG can be seen in Table 2.6. Open circuit characteristics can be seen in Figure 2.13 as well.

Table 2.6 Open circuit voltage measurements

Hz	wr (rpm)	wr (rad/s)	Ea (V_L-L)	k [Ea (V_L-L)/wr(rpm)]	k [Ea (V_L-L)/wr(rad/s)]	Ea_peak (V_peak L-L / krpm)
6.67	100.00	10.47	46.40	0.46	4.43	656.20
8.67	130.00	13.61	60.20	0.46	4.42	654.89
13.32	200.00	20.94	92.70	0.46	4.43	655.49
19.98	300.00	31.42	138.96	0.46	4.42	655.06
26.67	400.00	41.89	185.45	0.46	4.43	655.66
33.34	500.00	52.36	231.78	0.46	4.43	655.57
40.00	600.00	62.83	277.95	0.46	4.42	655.13
46.66	700.00	73.30	324.36	0.46	4.42	655.31
50.00	750.00	78.54	347.56	0.46	4.43	655.37

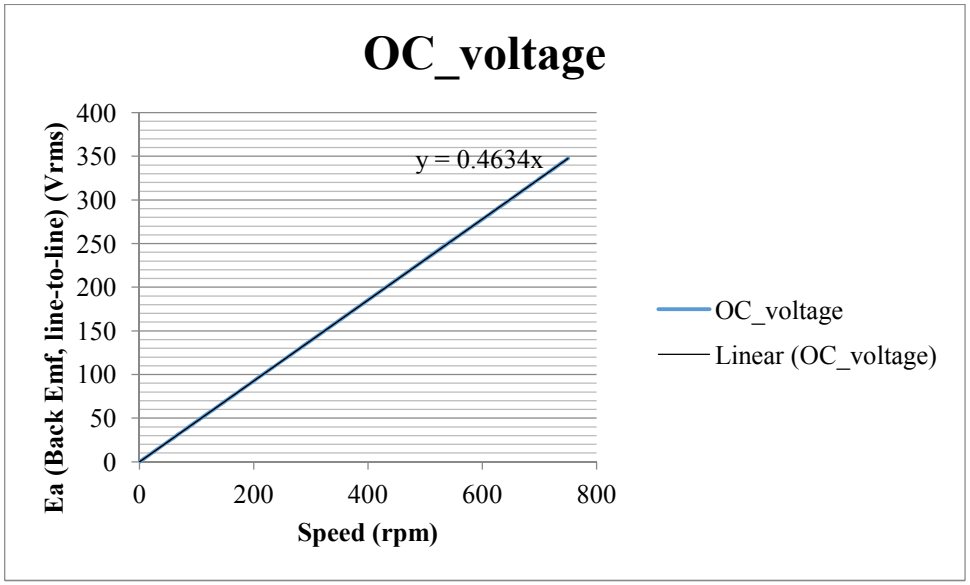

Figure 2.13 Open circuit characteristics of the generator

PMSG model in Matlab desires from user to enter 'Voltage Constant' as "Peak of Line-to-Line (V_{rms})/krpm". According to measurements, the value of 655.15 has been entered.

2.5.5. Torque Constant

The torque constant has been measured by driving PMSG with a drive. Drive creates a torque while I_d = 0 A. Only q axis current created torque. Measurements can be seen in Table 2.7.

At different speeds and I_q current values measurements have been taken. To better estimate the torque constant, core losses should be minimal and machine shouldn't be in magnetic saturation. Thus, low speed and low current driven generator is thought to give more realistic torque constant.

At different torques, torque constant changes due to losses in PMSG. In the simulation, torque constant is desired to be in the form of Nm/A_{peak}. Torque constant is entered to the model and the AC drive as 5.42.

Table 2.7 Torque constant measurements

Speed (rpm)	I (rms)	Torque (Nm)	k (Nm/A_rms)	k (Nm/A_peak)
	4.17	33.20	7.96	5.63
	8.33	64.50	7.74	5.48
	12.48	96.00	7.69	5.44
130.00	16.60	125.90	7.58	5.36

2.5.6. Flux Linkage

Flux linkage has been measured during open circuit tests. Model expects from user to enter "Peak of Line-to-Neutral Voltage (V_{rms})/ w_e (w_e: electrical speed). Measurements can be seen in Table 2.8.

Table 2.8 Flux linkage measurements

Ea_peak(V_L-N)	f	we	Ea_peak(V_L-N) / we
37.88544136	6.67	41.90885	0.903996291
49.15309417	8.67	54.47522	0.90230195
75.68923305	13.32	83.69203	0.904378046
113.4603649	19.98	125.538	0.903792689
151.4192909	26.67	167.5726	0.903604373
189.2475775	33.34	209.4814	0.903409941
226.9452247	40	251.3274	0.902986358
264.838831	46.66	293.1734	0.903352102
283.7815517	50	314.1593	0.903304734

2.5.7. Inertia

System inertia can be found as doing coast down test. However, this information is already given in manufacturer's datasheet. Thus, the coast down test is not implemented.

Inertia of PMSG is 0.0626 kg*m^2.

2.5.8. Viscous Damping Coefficient and Coulomb Friction Constant

Damping coefficient and friction constant can be found by measuring electromagnetic torque at different speeds at no-load. However, this is hard to distinguish from the other losses of the generator (rotor loss, windage loss, core (iron loss)) [55]. Thus, a model representing core and mechanical losses have been generated, which will be detailed at the next section.

2.5.9. Core, Friction and Windage Loss

In this study, PMSM model assumes no core (iron) loss, rotor loss and windage loss. However, core losses in a PMSM are considerably high when compared to total loss.

To exemplify, a 120kW permanent magnet machine has been tested to measure all the losses [55]. Measurement from this machine can be seen in Table 2.9.

As seen in Table 2.9, 72 % of total losses from at a 120kW machine come from stator loss. In the model, copper loss is included. However, core loss and rotor loss are assumed to be zero. Simulating with ignoring these losses causes wrong power input-output balance. To get a closer simulation of experimental setup, loss of PMSG has been modeled according to [56].

Table 2.9 120 kW PM machine losses

Stator Loss	Copper Loss (W)	1308
	Core (Iron) Loss (W)	1262
Rotor Loss	Shaft Loss (W)	15.9
	PM Loss (W)	206
Windage Loss (W)		874
Total Loss (W)		3666
Rated Output Power (W)		120,000
PM Efficiency (%)		97

Paper [56] claims that no-load core loss and mechanical loss can be separated by fitting the experimental results according to their physical models. By using curve fitting method, relation between R_{c1} and V_i is estimated. Mechanical loss is estimated with a function dependent to rotating speed of the machine. Then, load tests have been done and conventional permanent magnet machine model is modified as seen in Figure 2.14, adding resistor R_{c2}. This resistor aims to find armature reaction on the core loss.

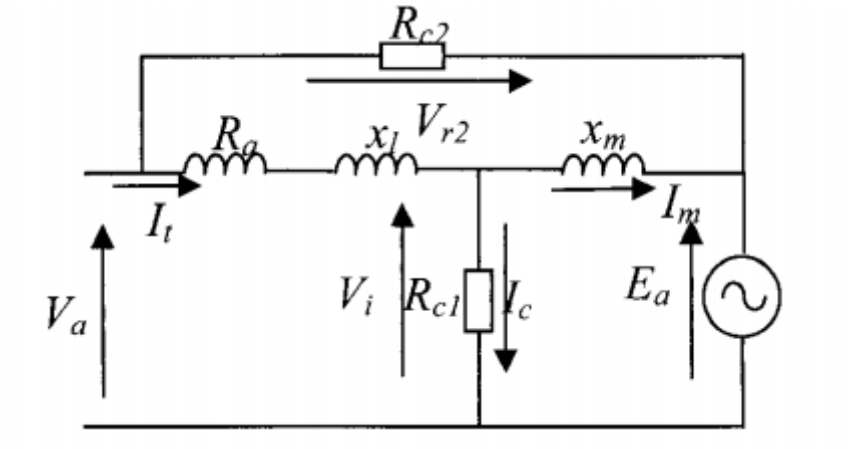

Figure 2.14 Per phase equivalent circuit considering core losses [56]

Power balance of a machine can be written as:

$$P_{in} = P_{cu} + P_c + P_{mech} + P_{out} \tag{2.27}$$

Measuring the difference between input and output power, losses can be found. Then using $P_{cu} = \sum I^2R$, total core loss and mechanical loss have been found. Measurements of losses are:

Table 2.10 Core and mechanical losses of the generator

F (Hz)	Vi (Vrms)	w_r (rpm)	Core+Mech Loss
6.67	46.4	100	12
8.67	60.2	130	15
13.32	92.7	200	23
19.98	138.96	300	38
26.67	185.45	400	58
33.34	231.78	500	81
40	277.95	600	109
46.66	324.36	700	136
50	347.56	750	152

No-load core loss can be formulated as:

$$P_c = P_{hr} + 2C_e(fB^2) + C_a(fB)^{\frac{3}{2}} \tag{2.28}$$

Mechanical loss is generally a function of the rotor speed and can be expressed as:

$$P_{mech} = a_1 w_r + a_2 w_r^2 + a_2 w_r^3 \tag{2.29}$$

Core loss can be related to the internal voltage, V_i, which is proportional to the product of frequency and flux linkage, i.e., $f\lambda_m$, or fB since λ_m is proportional to B. Therefore, considering Equation (2.28) and $P_{hr} = C_h f B^h$, where h is a constant, then, core and mechanical losses can be combined to one equation:

$$P_c + P_{mech} = C_h f^{1-h} V_i^h + C_e V_i^2 + C_a V_i^{\frac{3}{2}} + a_1 w_r + a_2 w_r^2 + a_2 w_r^3 \tag{2.30}$$

Coefficients in Equation (2.30) can be found by least square curve fitting method in Matlab. Thus, core and mechanical loss can be separated mathematically. From the no-load test, coefficients are: C_a=0.006, C_e=4e-4, C_h=5.2e-8, a1=6.1e-2, a2=2.1e-7, a3=1.2e-8, h=7.95. The results of the curve fitting method and the measurements can be seen in Figure 2.15 and it can be said that the method is applicable. There is a slight difference at the 300 rpm as seen in Figure 2.15. The difference can be minimized by decreasing the error rate of the least square method if needed.

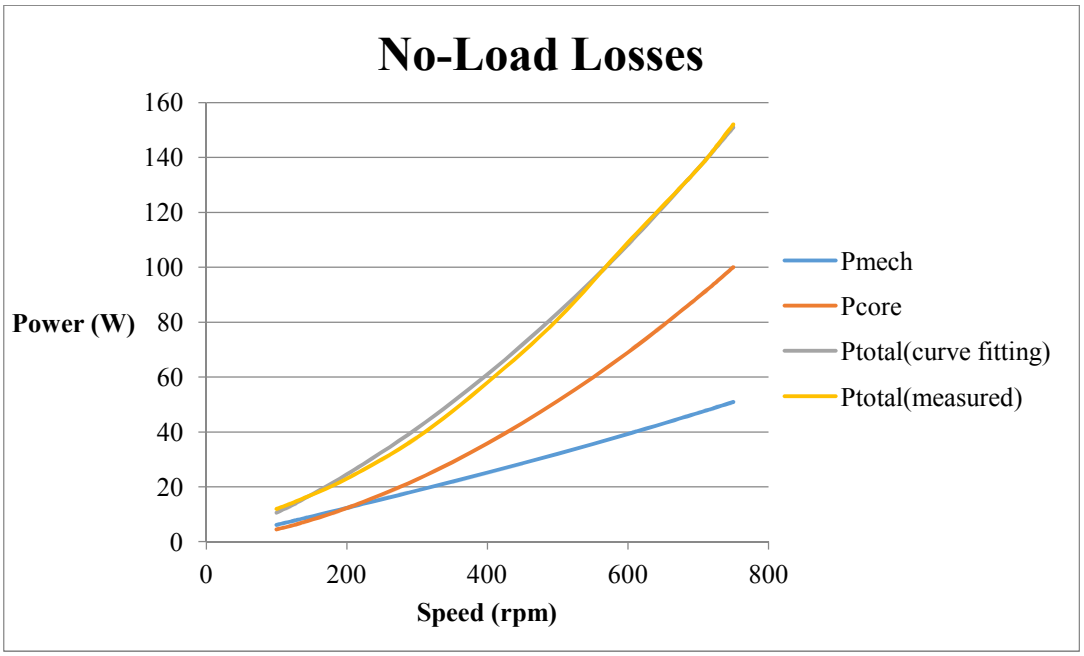

Figure 2.15 No-load losses of the generator (measured and curve fitting method results)

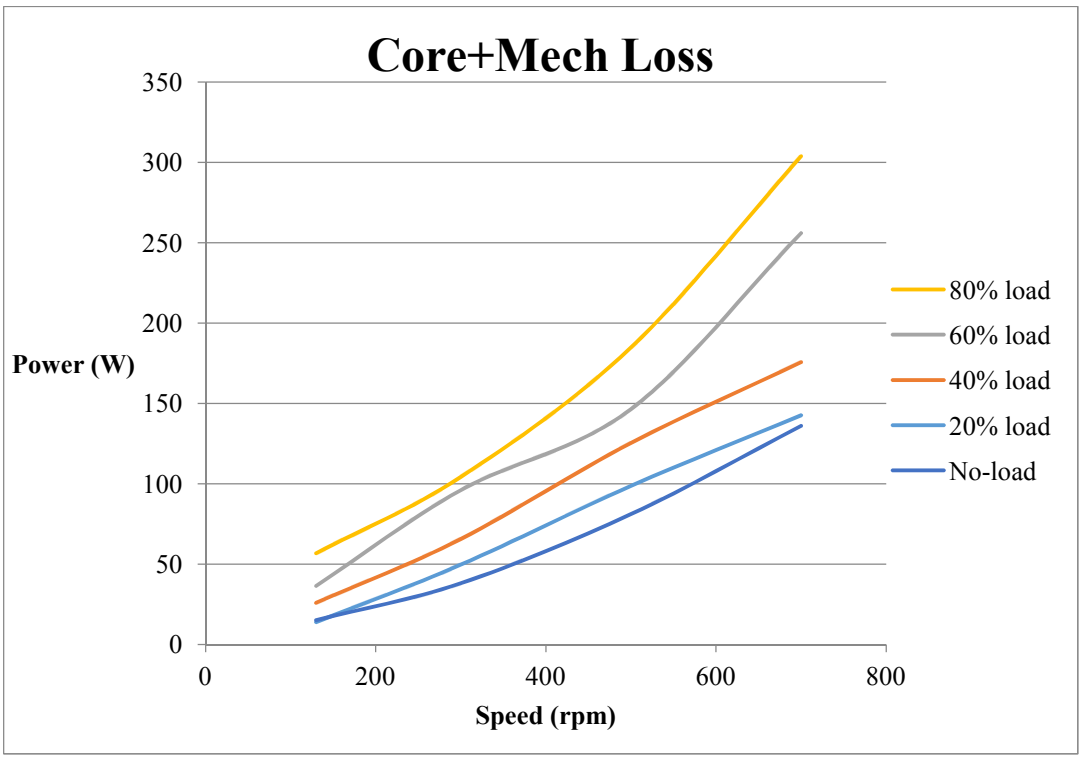

Figure 2.16 $P_c + P_{mech}$ measured by no-load and load tests

After separating the no-load losses, armature reaction is considered from load-tests. Figure 2.16 presents a comparative analysis. Increasing load increases core loss due to armature reaction. According to [56], this increase can be modeled with an extra resistor placed parallel to R_a and X_m as seen in Figure 2.14.

Extra resistor is found with the Equations (2.31) – (2.33):

$$V_{r2} = E_a cos\partial + jE_a sin\partial - V_a \tag{2.31}$$

$$E_a = w\lambda_m \tag{2.32}$$

$$R_{c2} = \frac{3V_{r2}^2}{P_{c2}} \tag{2.33}$$

To find P_{c2}, mechanical and core losses under no-load are subtracted from those losses measured under load. Then, R_{c2} is calculated. In our system, extra resistor is found to be 1.266 Ω.

Loss model has been created via mask in Simulink. This mask includes no-load and load core loss calculations. Generated code in this mask and Simulink model of 'Loss Model' can be seen in Figure 2.17.

Loss model takes PMSG output power (lossless power), stator current, frequency, back emf and speed of the generator. Using this information, net output power for PMSG has been calculated and it is given to regenerative drive neural network. Doing that, losses of the PMSG has been considered. This model lacks at one point: temperature dependency of the measured parameters. Loss model works assuming no temperature variation. This can be added in the future work as a development to the model.

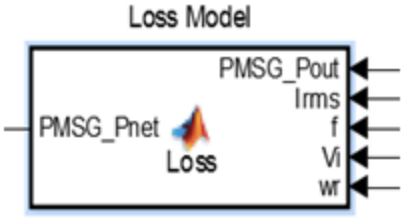

Figure 2.17 Loss model of PMSG generated in Simulink

2.6. Converters' Models

In the software simulator, there are two converters: AC/DC converter and grid side converter (DC/AC). These converters are detailed in the upcoming sections.

2.6.1. AC/DC Converter

For the variable speed operation, power converters are critical both to control variable speed and to control power quality at the grid side. AC/DC converter (drive of the generator) is used as:

- to rectify AC output voltage of the generator to a DC link,
- to control speed of the shaft according to maximum power point tracking algorithm

AC/DC converter has been realized in Matlab/Simulink by using the 'PM Synchronous Motor Drive' model [65]. The premade model of the converter in Simulink is divided mainly into three parts; three-phase inverter, speed controller and vector controller as seen in Figure 2.18.

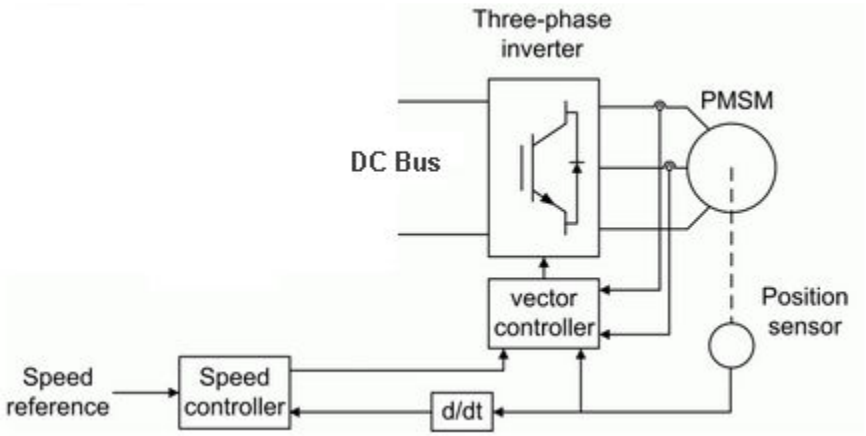

Figure 2.18 Schematic of the AC/DC converter in Simulink

The main task of the converter is to rectify variable frequency AC voltage to a stabilized DC link. By using DC constant voltage, generator can also be controlled. In the simulation, AC/DC converter is used also to adjust speed of the generator at the MPP point. Speed controller is supplied by PI regulator by creating references appropriate to MPPT controller reference. The output of the speed controller is given to the vector controller block to generate torque reference, which is achieved by the three-phase inverter. Input variables of the vector controller can be sequenced as torque reference from speed controller, rotor angle and phase currents. The rotor (mechanical) angle is converted to electrical angle in the vector controller. Electrical angle is used to convert *dq* frame references (torque reference) to *abc* frame. Since the torque is controlled by active current (in other words I_q current), I_d reference current is set to 0 in the vector controller. After generating reference *abc* currents, current controller subblock uses both reference and actual currents. By using them, required PWM signals for the three-phase inverter are generated. The switching control block takes its set frequency by the user as seen in Figure 2.19 and Figure 2.20.

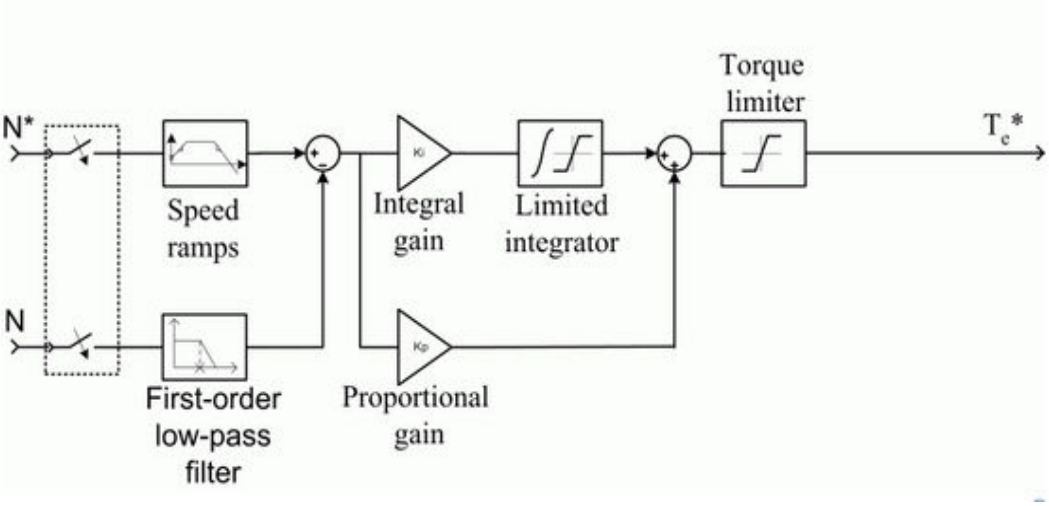

Figure 2.19 Speed controller of the rotor side converter

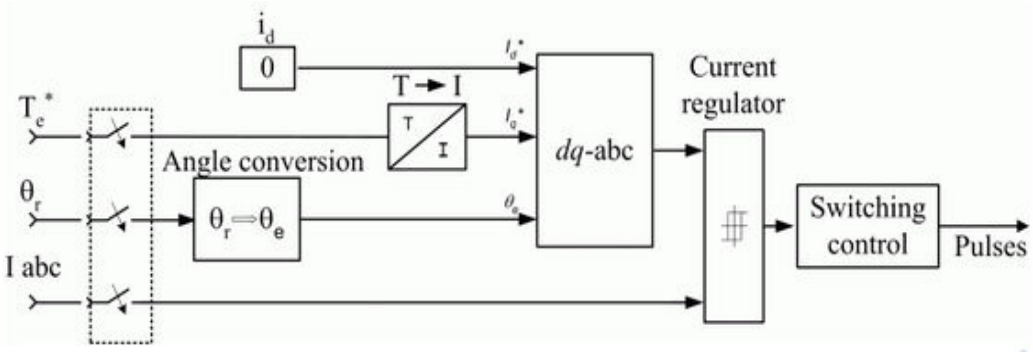

Figure 2.20 Vector controller of the rotor side converter

Pulses generated at the vector control are sent to the three-phase inverter where the stator currents of a three-phase generator are controlled. That is, electromagnetic torque of the generator is controlled by this way.

AC/DC converter accepts mechanical torque generated by the kinetic model of the wind turbine model. It also gets a speed reference from the maximum power point tracking (MPPT) controller. To follow the speed reference, internal electromagnetic torque is controlled by taking into consideration the mechanical model Equation

(2.20). However, to simulate the inverter used in the HIL system similar with the simulator, acceleration and deceleration speed ramps should be adjusted by the user, too. In addition, scale of the inverter should be adjusted by entering torque output limits for the converter to obtain realistic results in the simulator. Thus, there is an interface for the user to set values mentioned above as seen in Figure 2.21.

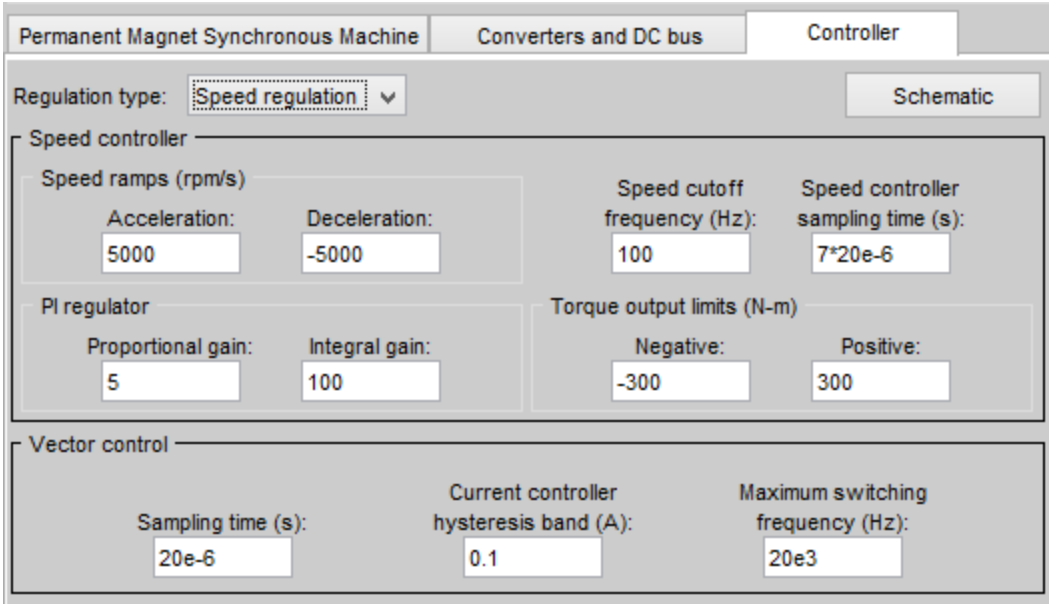

Figure 2.21 Controller parameters at the interface of the rotor side converter

Speed controller sampling time is set to a multiple of sampling time of the simulation as seen in Figure 2.21, which is set as 7*20e-6 in the simulation. This is also a critical point, which is emphasized in MPPT section. Turbine responds any changes in the shaft speed after a while since it has a considerably high inertia. This sampling time, thus, should be higher than the system sampling time to see result of a change in the system.

2.6.2. Grid Side Converter

Grid side converter can be summarized such that it converts DC link bus voltage to the AC voltage in order to supply AC current to the national grid. It is generally voltage source inverter with six or twelve switches (switch number changes according to level of the inverter) . IGBTs with antiparallel diode have been used as switches for the grid side converter in wind energy conversion systems. Grid side converters have mainly two objectives; 1) to stabilize DC link voltage 2) to control power quality. For variable speed variable pitch wind turbines, active power is controlled directly by means of the generator torque and pitch control, and indirectly through DC link voltage control. Keeping the DC link voltage at a constant level assures that the total available active power is transferred to the grid. Since the DC-link completely decouples the reactive power of the generator from the reactive power of the grid, the reactive power injected to the grid can be controlled by the grid side converter as seen in Figure 2.22.

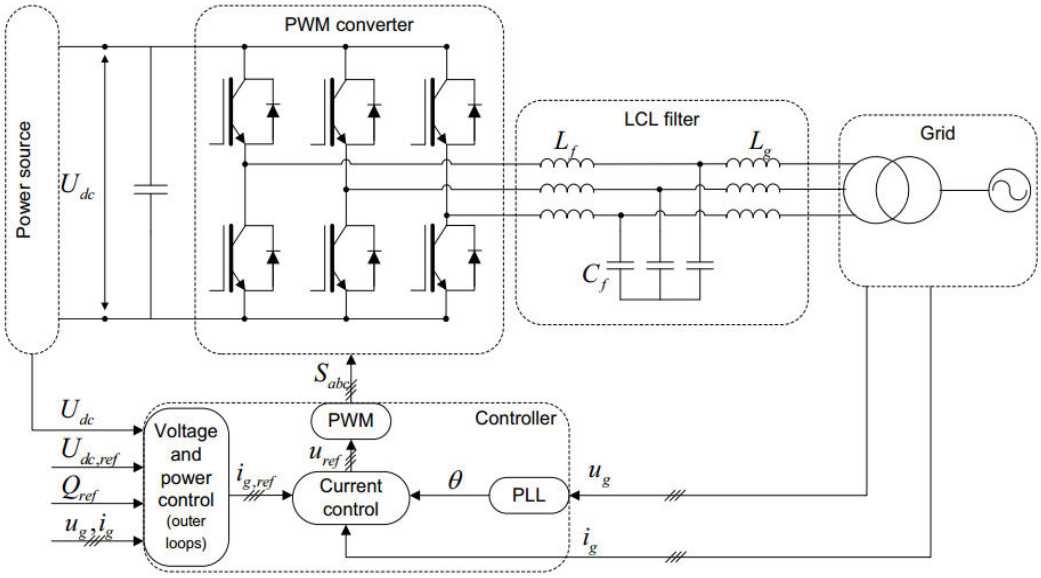

Figure 2.22 Grid side converter control system [17]

In the grid side converter, there are two cascaded control loops. The outer loop, which acts slower, controls 1) reactive power delivered to the grid, 2) DC-link voltage. The outer loop generates the reference currents for the inner loop, which acts in faster dynamics. The inner loop, current control, is subjected to the grid via phase locked loop (PLL) controllers and it should respond fast to satisfy grid codes. PLL is used for the coordinate transformation and accepts three phase grid voltage to generate phase angle reference [18]. Grid side converters are connected to the grid via filters (mostly LC or LCL filters). The values of the LCL filter are given in section 2.2. There are two sources of the harmonic distortion in the wind energy conversion systems. Low frequency harmonics are caused due to distortion in the grid voltage (especially 5^{th} and 7^{th} harmonics). High frequency harmonics, on the other hand, are caused due to switching of the IGBTs (that is, PWM frequency, which is 6 kHz for the simulation). These harmonics are filtered out with the LCL filters placed at the output of the converter [17].

The grid side converter is modeled as in Figure 2.23 in Simulink by using the model of "AC/DC Three-Level Converter" [66]. Grid side converter model mainly consisted of DC bus capacitors, IGBT block (three-level bridge, twelve IGBTs) and controller as seen in Figure 2.24. For DC link, 2 mF capacitors have been used to imitate HIL setup. The IGBT block involves 6 IGBT switches. The on-state resistance (R_{on}) is set to 1 mΩ. Forward voltages for IGBT and anti-parallel diodes are set to 0.8V. Fall time and tail time (turn-off characteristics) are set 1μs and 2μs, respectively. In the simulation, the snubbers are not activated for this time.

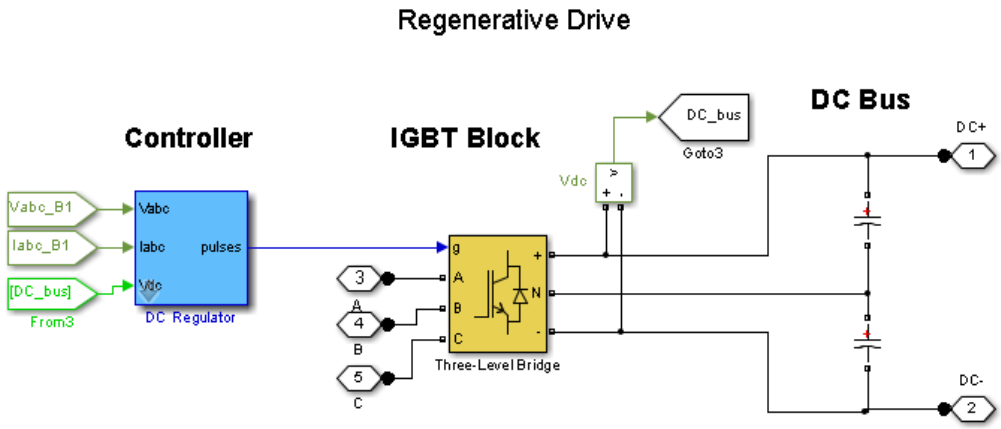

Figure 2.23 Simulink model of the grid side converter

Controller in the simulator consists of PLL, dc voltage regulator and current control blocks. PLL and dc voltage regulator blocks monitor the voltages and create references for the current control loops. Current control loop provides AC current injection to the grid by controlling the switches in the three-level bridges. Reactive power injection is not implemented in this stage. Moreover, grid side converter modifications will be applied at the Chapter 4 while we are conducting tests to see the effect of islanding operation at the grid. Thus, it is not detailed any more in this chapter.

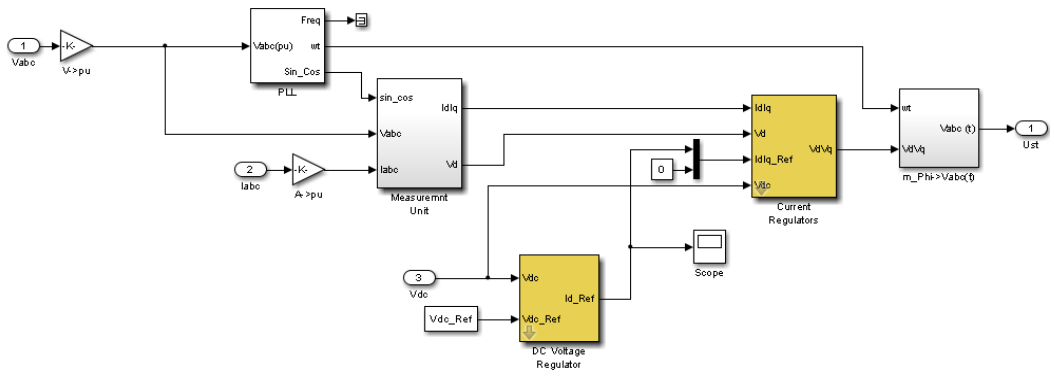

Figure 2.24 Controller of the grid side converter

The back-to-back converters that are modeled in Simulink are planned to be use for the analysis of the islanding operation. However, it should be noted that the internal configuration of the converters (AC drives) cannot be known exactly. Thus, to satisfy the need of a software simulator which will operate as HIL setup, a neural network based model of the back-to-back converters is needed. Hence, a study has been conducted to model the back-to-back converters in Simulink. The details are given at the next section.

2.6.3. Neural Network Modelling of Back-to-Back Converters

The software simulator is established to reflect the characteristics of the wind energy conversion system from all the perspectives. The wind turbine and generator can be modeled thanks to having enough information of the physical structures. The grid side filters and grid connection can also be modeled since the components usually passive elements and can be directly placed into the software. However, modeling of the power electronics of the system (AC/DC/AC converters) may not be achieved precisely due to lack of information about the internal structure of the drives. Thus, there should be a model which imitates the characteristics of the converters in the software simulator.

The model is desired to get the net output power of the HIL system when it runs at the software simulator. Since the AC drives include switches, diodes and other electronic components (converters, inductances etc.), they are thought to bring losses at different speeds and different input powers. Thus, a model which uses the output power of the generator and the frequency at the operation instant and results in net output power can satisfy the need of the software simulator.

The model can be developed by using curve fitting functions. However, the nonlinearities are hard to determine for such a complex electronics. Thus, curve fitting solutions are thought to be inefficient for this study. On the other side, utilizing neural network structures can result in a good manner. Neural networks consist of “neurons” which are inspired from the human biology. The neurons are

thought to process many conditions and their characteristics are thought to change with the experiments during lifetime. With this inspiration, this technique is called neural network.

To call a model as neural network, it should consist of many neurons (or nodes) which include “weighs”. The weighs can be stated as the coefficient of a function in a neural network. The weighs are determined adaptively using “training” methods. Training means the determination of the weighs in the “functions”. The functions are placed into the nodes and they are mostly non-linear functions. A single neuron can include either one or many nonlinear functions.

The model is desired to be set up with the neurons which process the output power of the generator and the operating frequency. Thus, there should be data which will be supplied to the neural network training procedure. According to data gathered in the laboratory, a neural network structure which is called as ‘fitnet’ (function fitting neural network) has been developed in MATLAB [57]. There are several neural network structures such as pattern recognition, clustering etc. However, these are used for complex input systems. Data fitting (fitnet) method is sufficient for this study.

In the simulation, the neural network has been set up with two hidden layers. Hidden layers can be stated that the internal top functions which include many nonlinear adaptive weighted functions. Increasing the number of hidden layers decrease the error rate. However, processing time of the network lasts longer in especially embedded systems. Thus, a balance should be kept between the accuracy and the processing time. Number of hidden layers has been decided with trial-and-error method. Its performance is found insufficient with one hidden layer and its number is increased to 2 as seen in Figure 2.25.

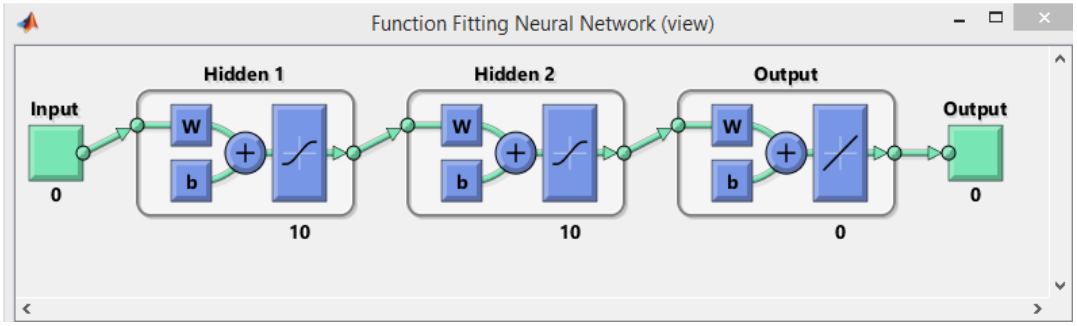

Figure 2.25 Neural network model of back-to-back converters (overview)

After setting up the neural network, the weighs in the hidden layers should be determined with training procedure. With the training, the network "learns" the pattern of the studied structure. There are several "learning" techniques such as supervised and unsupervised learning, reinforcement learning. Unsupervised learning and reinforcement learning techniques aims to minimize the "cost" which can be described as the mismatch between the real output value and generated output value from the network. These techniques require some of input data "x". According to minimization of the cost, the mean input data are filled in the training section and the model is established. These techniques are said to give errors higher than the supervised learning due to lack of input information. On the other side, supervised learning algorithm needs both input "x" and output "y" with the cost of the system. The priority of this learning technique is to reach the output value with minimal cost. However, in other techniques, it is vital to reach limited cost even if output or input cannot be matched precisely.

In our system, supervised learning is preferred because input and output set can be supplied by the user. The performance criterion of the neural network is determined via mean squared error. If the gradient of the network is achieved to be less than 10^{-7}, the training procedure is stopped and neural network is established. To minimize the mean squared error, mostly preferred technique is Levenberg-Marquardt algorithm. This algorithm is used to solve least square problems in the literature. During training operation, the entire data set is not used. A high population of data is used

for training and the remaining ones for the test and the validation. For our study, 70% of the data has been used for the training procedure. Increasing the data rate or decreasing mean squared error directly affects the “iteration” number. The iteration is named as “epoch” in neural network structures as seen in Figure 2.26. To have a fast debugging of the network, minimum number of iterations should be attained. The network that we use is established at the 6th iteration. If a higher performance is required, the iteration number of the network can be increased. Iteration changes the weighs of the neurons by observing the error for each loop.

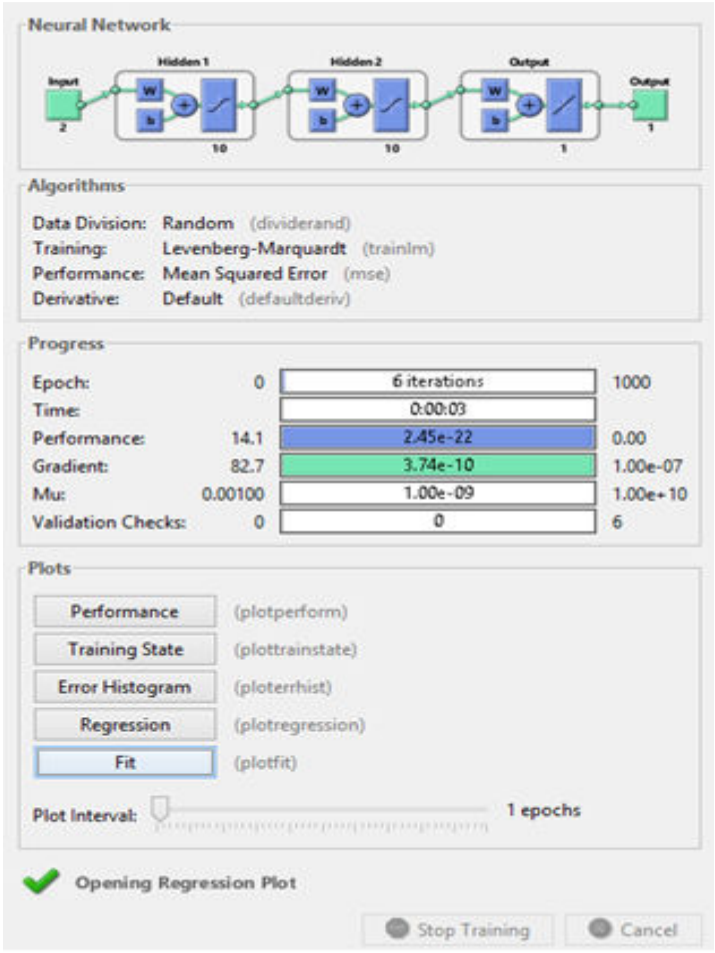

Figure 2.26 Neural network training and performance parameters

To evaluate the performance of a neural network, it is tested with the real data at the end of the process. The performance of a neural network has been decided by using

regression maps. Regression means the relationship of the real outputs taken from the system and the targets established by neural network. To evaluate the performance, regression maps of training, validation, test and all the data have been drawn as seen in Figure 2.27. In Figure 2.27, the solid lines express the best linear fit of the network. The dashed lines show the perfect targets at the network and the circles in the graphs represent the real data. The 'R' which is placed onto each graph is a representation of the relationship between output and target from the perspective of "linearity". If it is '1', there is an exact linear relationship between outputs and targets. As if seen in Figure 2.27, the training results in as R=1, which characterizes the linear relationship between the output and targets. It should be noted that training result of R=1 does not implement that system is linearly modeled. This linearity is achieved between the data selected from the entire data of which 70% is selected for this study. If the validation and test of the network results higher than R=0.9, the network is established. Since the validation and the test are finished via R=0.96 and R=0.94, the network is said to be established with "fitnet" model in MATLAB. The most important graph can be said as the one named as "All" in Figure 2.27. This graph shows the relationship between the entire data (output) and targets. The R value is 0.87 for this study. It means that there is an almost linear relationship between the input and output of the network. This result shows the validity of choosing neural network by thinking the model of the converters to be nonlinear. The performance of the network can also be seen in this graph by observing the data and the dashed lines. Some of the data which are located at the right hand side of the graph become distant from the dashed lines. These data represents the output power at the high rotating speed (such as 700 rpm). By evaluating this graph, it can also be said that the performance of the network falls down at higher speeds. This evaluation will be clear when the software simulator and HIL emulator is compared at Chapter 3 as well.

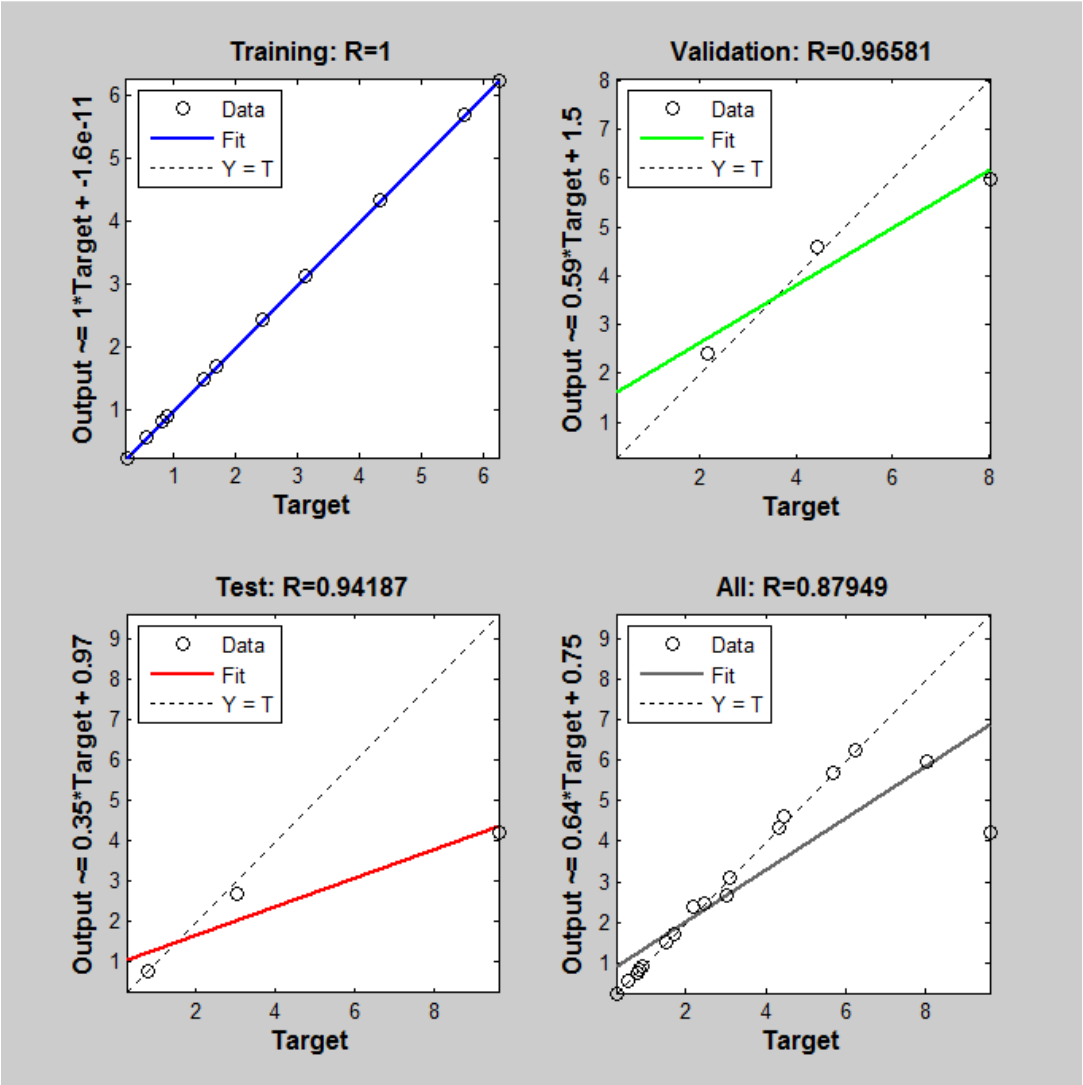

Figure 2.27 Regression mappings of neural network

2.7. Grid Connection

In the software simulator, grid connection to the 3-phase source has been supplied with 380V, line-to-line voltages. However, for the grid connection studies, the simulator is modified such that wind turbine is connected to the local loads and the infinite bus by transformers and tranmission lines. This connection will be detailed in Chapter 4 while explaining the integration of the wind turbines at the fault situations.

2.8. System Controllers

With the increasing awareness to the renewable energies, there is a great interest to improve the share of the wind energy in the total energy consumption. Thus, there is an increasing number of wind turbines and large wind farms which are connected to the national grid. Increasing number of the wind turbines results in more issues both to control the wind turbine and to control the grid-side effects. That is, control techniques should be selected for the specific system properly.

2.8.1. General Considerations for Control of Variable Speed Wind Turbines

For the varible speed wind turbines, the control algorithm has been separated in two region and four zones [20]. Control strategies differ for below the rated power and above it. At below rated powers, there are two zones: torque control and transition. At the Zone 1, turbine starts to operate when the wind speed is over the cut-in. In this zone, generator torque is controlled such that maximum power can be absorbed . In the Zone 2, maximum power point tracking algorithm keeps working; however, increase in the shaft speed is lowered due to high inertia of the system. That creates a smooth transition in this zone. When the wind speed increases so high that the rated power is exceeded, turbine power is limited with pitch control (there are also some other techniques that will be explained in next sections). At the Zone 4, turbine's power can be limited with other control techniques such as using crowbar techniques or passive stall techniques as seen in Figure 2.28.

For all the zones, control techniques have been developed at the software simulator. For below rated power, a MPPT controller which works with the technique of Perturbation & Observation is utilized. Above the rated speed the pitch controller is activated. There will be also a braking (crowbar, chopper) resistor to lmit the load at the extreme conditions (e.g. three-phase fault, islanding etc.). These controllers will be stated at the upcoming subsections.

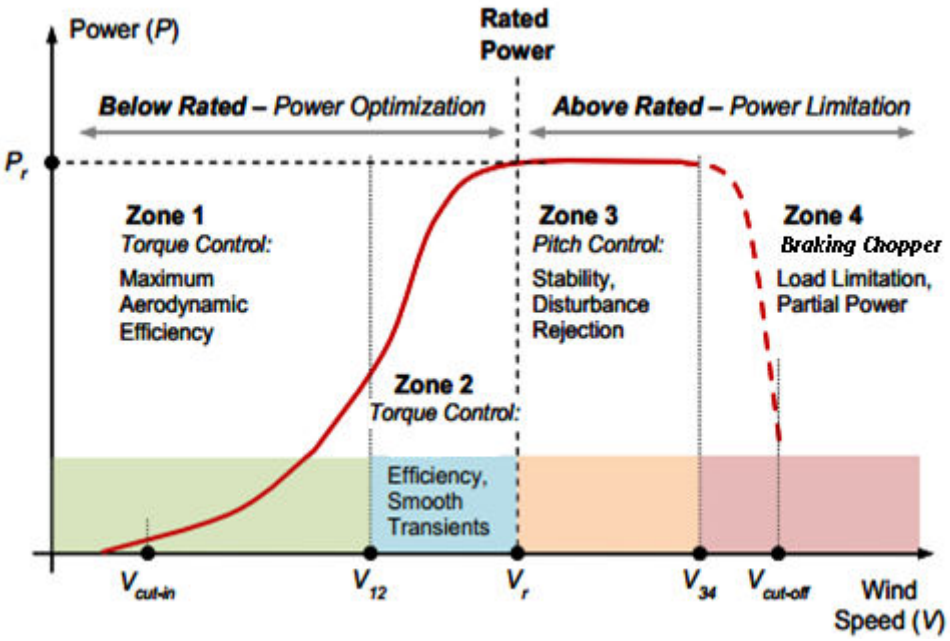

Figure 2.28 Control techniques of a grid connected VSWT

2.8.2. Maximum Power Point Tracking (MPPT) Controller

In order to harvest maximum energy from a wind turbine, turbine should be operated at the optimal-tip speed ratio. Optimal tip-speed ratio is the ratio of the wind speed to the blade's tip speed which maximizes the absorbed energy from the wind. Maximum power point tracking (MPPT) is to achieve a tip-speed ratio as close as possible to the optimal tip speed ratio. If the optimal tip speed ratios are connected together for different wind speeds, MPP curve is obtained. MPP curve for the turbine which has been used in this simulation can be seen in Figure 2.29.

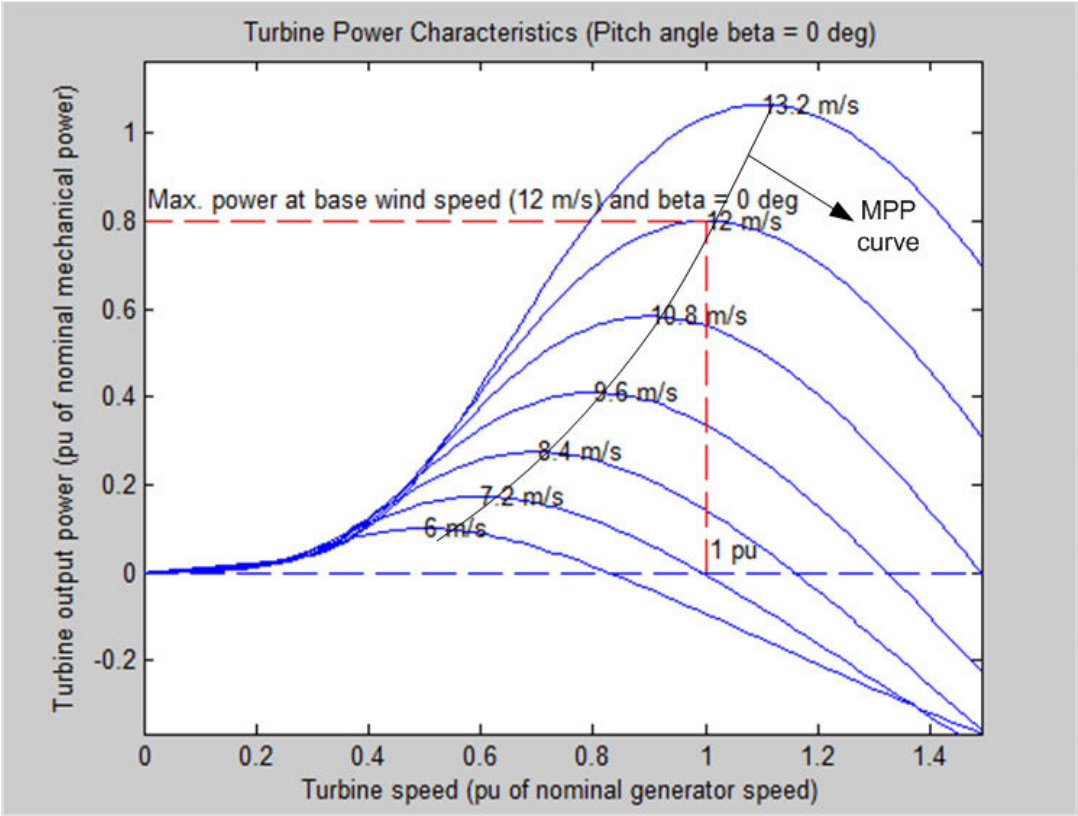

Figure 2.29 MPP curve of the turbine

MPPT strategies in the literature can be divided into two main groups: The first group uses C_p curve of the turbine to calculate optimum operating point- this technique can be named as 'Model Based Control'. The second group has no information about C_p curve, which is called as Perturb & Observe (P&O) or hill-climb search (HCS) [25].

2.8.2.1. Model Based Control

This method needs a predetermined equation of C_p. Using this equation and with additional information, maximum power point (MPP) is determined. Additional information here is rotation speed of the turbine and wind speed. The application of

this method in the literature can be classified in two groups and briefly explained in the following section.

2.8.2.1.1. Tip-Speed Ratio Control

This method requires wind speed, turbine speed and C_p curve. Using this information, reference speed of the turbine found. Using a PI or PID controller, generator's torque has been controlled and system's speed is set to desired point [27]

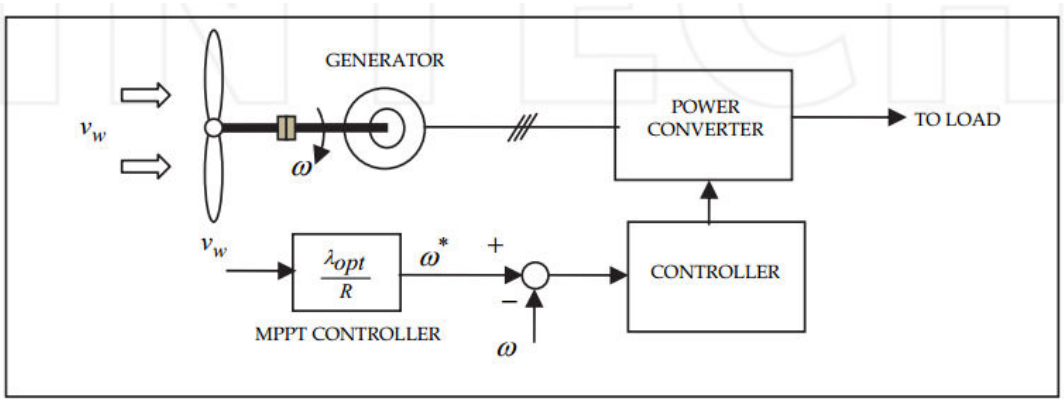

Figure 2.30 Tip speed ratio control of WECS [27]

2.8.2.1.2. Power Signal Feedback Control

This method requires turbine rotating speed and C_p. Reference power is generated using C_p curve taking turbine speed as input. Controller tries to find out MPP by minimizing error.

Disadvantages of these two techniques [26] are:

- C_p curve should be measured (with data fields or functions), which is difficult and expensive to implement in practice,

- To find wind speed, an anemometer or estimator should be added to the system, which increases the cost of the system.
- Any changes in C_p curve will worsen the performance.

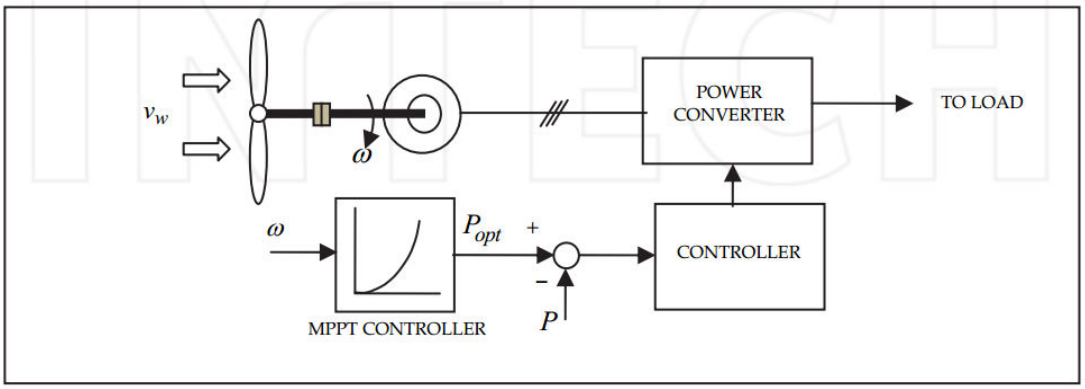

Figure 2.31 Power Signal Feedback Control of WECS [27]

2.8.2.2. Perturbation & Observation Method

The alternative approach for achieving MPPT control is 'Perturbation and Observation' method [28]. This method needs no information about C_p curve. Thus, no measurements of turbine and wind speed are required. This method uses only measured data, which are instant output power and shaft speed. Advantages of this method can be stated as simple structure, easy to implement, minimum parameters required and rapid convergence and strong performance against physical parameter variations.

This method consistently aims to find out shaft speed that achieves maximum power. It can surpass aforementioned difficulties in 'Model Based Control'. This method is based on perturbing the control element in small steps and observing the changes in output power. Principle of P&O can be seen in Figure 2.32.

P&O method uses various control elements, which is seen in Figure 2.33 as 'x'. In the literature, 'x' control element can be rotor speed, generator stator current, PWM duty

cycle etc. The main goal is to change rotor speed to regulate generator torque with its power converters.

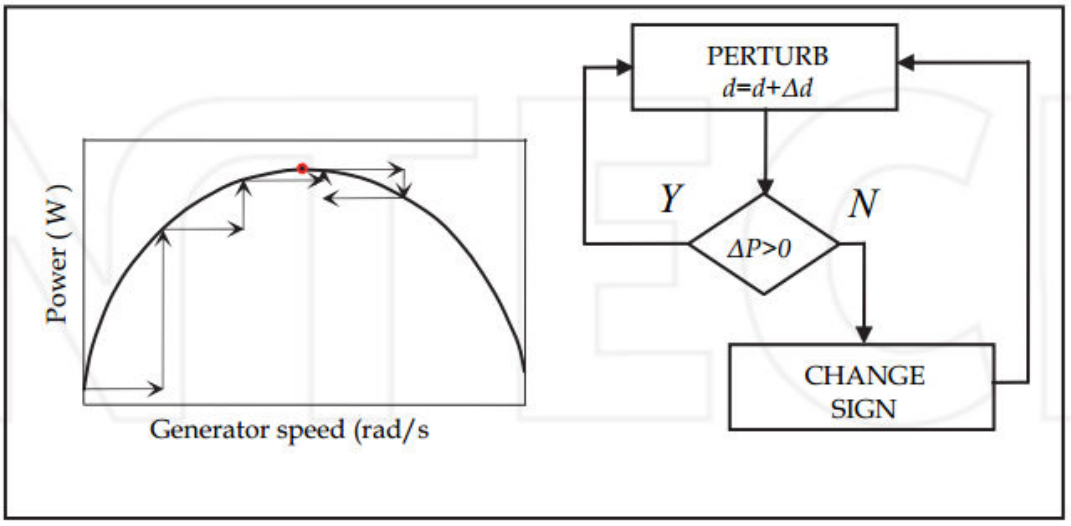

Figure 2.32 Principle of P&O

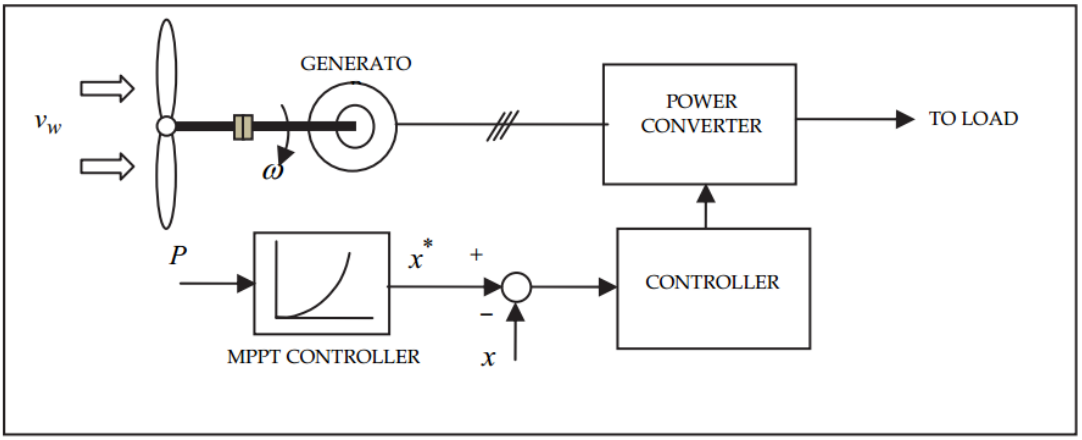

Figure 2.33 P&O control of WECS

In spite of many advantages of P&O method, there are some disadvantages, too. These are [28]:

- steady-state oscillations around MPP,
- a slow tracking speed,
- possibility of perturbation in a wrong direction,
- high rotor speed overshoot under fast wind speed variations.

Steady-state oscillations around MPP are the prime trouble of this method. This can be overcome by using adaptive step-size instead of fixed one. To exemplify, in [29], perturbation step size was parted into eight steps, first one is the smallest and the eighth one is the largest. Looking for convergence to the MPP point, either smaller or larger step size is selected. While getting closer to the MPP, step size is reduced and amplitude of oscillation is decreased.

Slow tracking speed problems come out due to inertia of the turbine. Speed-loop response time which is dependent to inertia determines the sampling period. To work controller efficiently, sampling period should be longer than the one of the controller to assure that measurement of the control variables is performed after that system responded to the previous step [30]. However, if sampling period is kept large, convergence time of the search controller increases. Thus, a correct balance between these sampling times should be found to ensure proper execution of the controller.

To sum up, efficiency of P&O technique can be increased using it with variable step size and in the small inertia systems [26]. Since the experimental setup's inertia is small and the technique used in the simulation includes variable step size, it is convenient for the simulation.

In the simulation, P&O technique has been implemented accordingly with Figure 2.32. P&O technique works as follows:

1. Turbine is operated as if there is no control at the start.
2. By using torque-inertia Equation (2.34), change in shaft speed is found out for the next time step.

$$T_{wt} - T_{shaft} = J\frac{\Delta w_t}{\Delta t} \tag{2.34}$$

3. Speed is increased as much as Δw_t, which is variable speed reference for each time step.
4. At the next time step, wind speed is assumed to be constant during sampling time as seen in Figure 2.34.

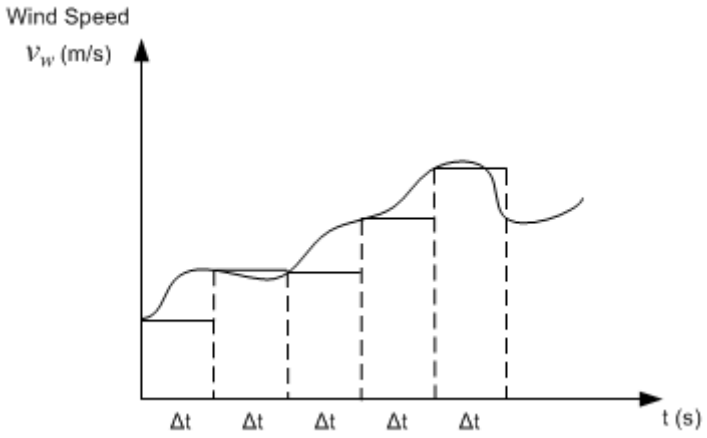

Figure 2.34 Wind speed sampling during P&O

5. For that wind speed, output power is checked whether the operating point is at the maximum or not. If not, perturbation process continues until it is found. Otherwise, it is stopped at that shaft speed.

In the simulation, this MPPT technique has been realized in Simulink by using different functions such as zero-order hold (ZOH), signum etc.. This technique works in Simulink platform as follows:

1. Torque and speed output of the turbine is used to calculate instantaneous power, P[n]
2. Sign (P[n] - P[n-1]) is calculated (P[n-1] is kept with zero order hold)
3. Sign (w[n] - w[n-1]) is calculated (w[n-1] is kept with zero order hold)
4. Rate of change of speed is found by using the sampling period

5. Signum of power and speed change is multiplied
6. If the multiplied result is 1, Δw is added to w[n]. Otherwise, it is subtracted from w[n].
7. Steps 1-6 recursively repeated until MPP is found.

Realization of MPPT in Simulink can be seen in Figure 2.35. MPPT control strategy can be seen as flowchart in Figure 2.36 as well. In the simulation, by dividing w[n]-w[n-1] to Ts (sampling period) maximum allowed speed change of AC drive of generator has been found. According to this rate of change, maximum allowed electromagnetic torque has been applied to generator to get MPP as fast as possible. That is, there are two constraints that rate of change of speed is determined: one of them is system inertia, the other one is driving capacity of AC drive of generator. In the simulation, MPP is aimed to be found as fast as possible. However, it came out with oscillation at the MPP since system cannot response that fast because of the system inertia. These results will be also discussed at Chapter 4, too.

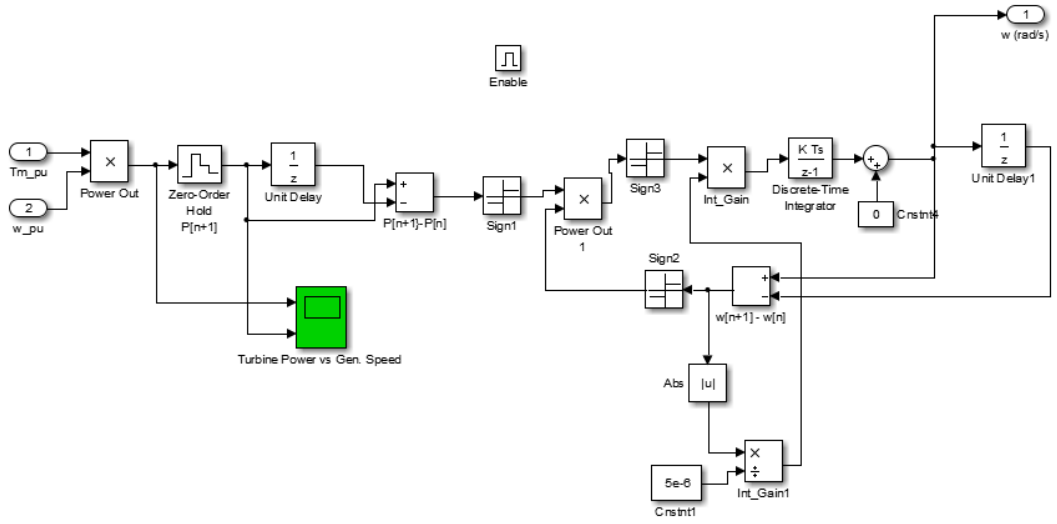

Figure 2.35 MPPT realization in Simulink

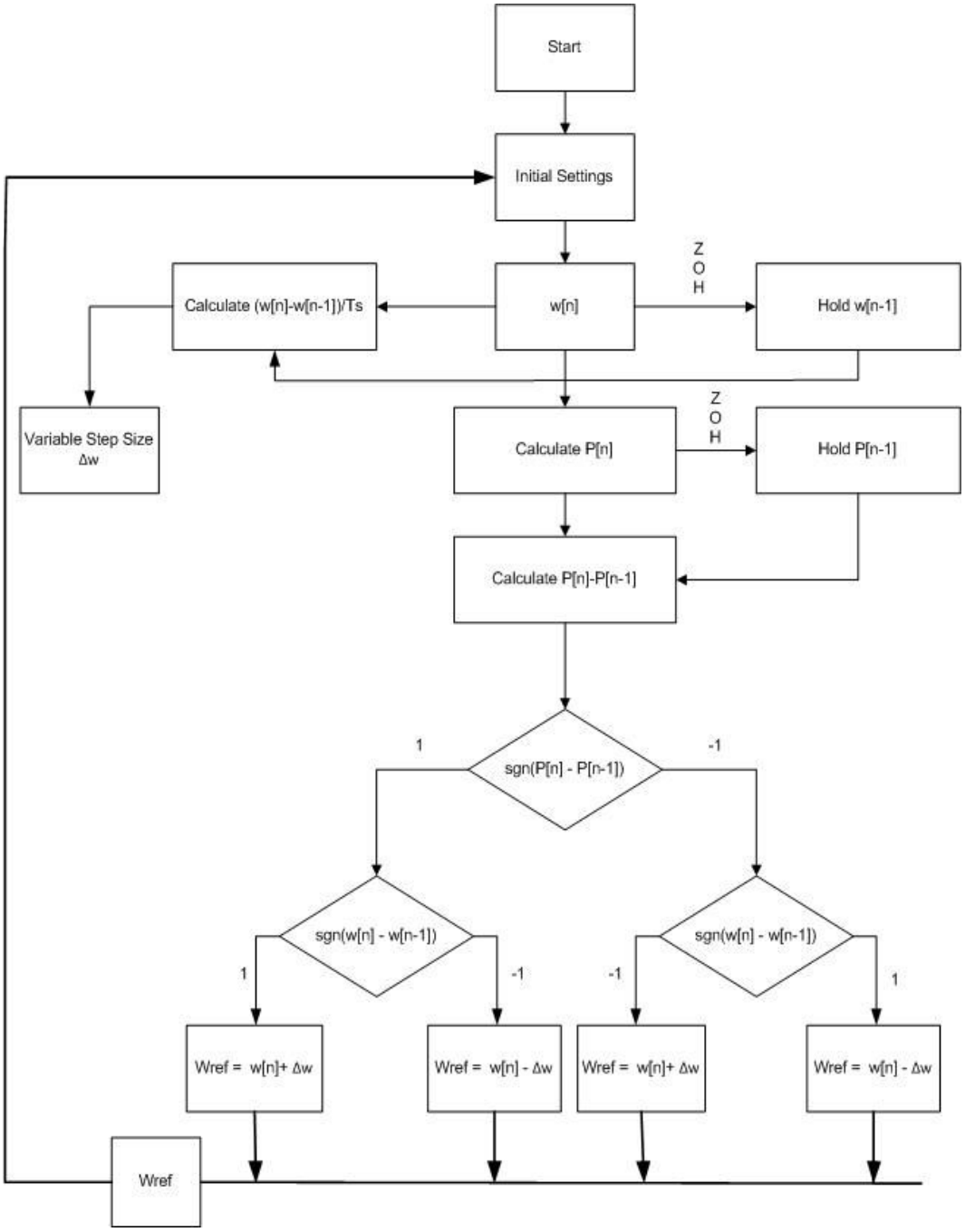

Figure 2.36 Flowchart of the MPPT controller

2.8.3. Braking Resistor (Chopper, Crowbar) Control

Braking resistors are used to suppress excess energy at the resistors not to damage power electronics in the turbine. Braking resistor control is achieved with a switch (mostly IGBT) by turning on/off when DC link increases beyond the safe limit. That is named as activation voltage as seen in Figure 2.37. Braking resistors are mostly activated at transient events such as a voltage dip or grid fault in the power system. Especially in variable speed turbines braking resistor control helps to decrease output torque variations and increase the capability of low-voltage fault ride through conditions.

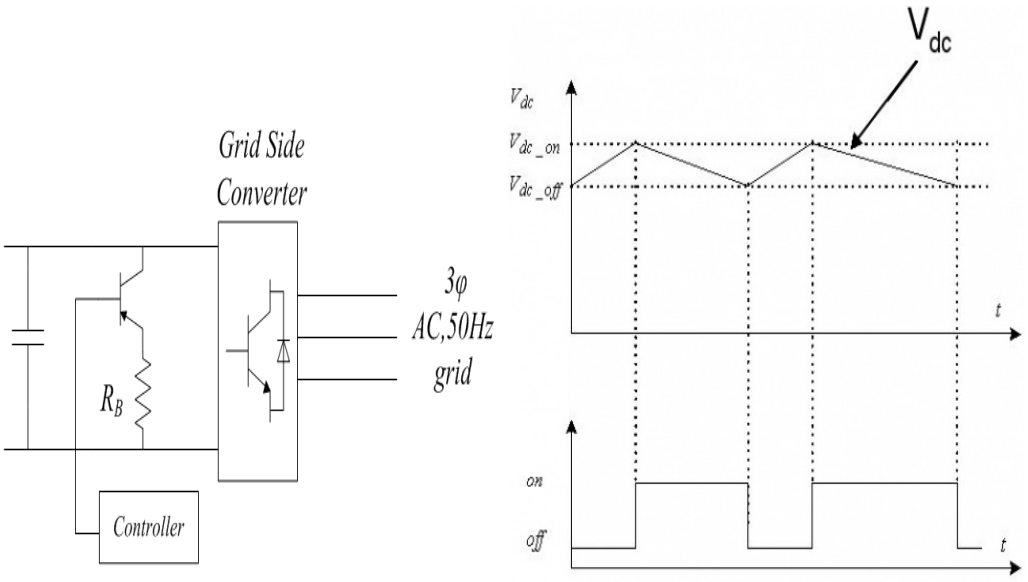

Figure 2.37 Control of braking resistor

In the software simulator, this controller is achieved with an IGBT and PI controller. PI controller checks the DC link voltage with the reference one. Reference DC voltage (activation voltage) is set by the user at the interface of the controller as seen in Figure 2.38. Value of the barking resistor and chopper frequency is also set at the interface. Values seen at the interface are taken from the HIL setup and the HIL system is made to imitate at the software simulator.

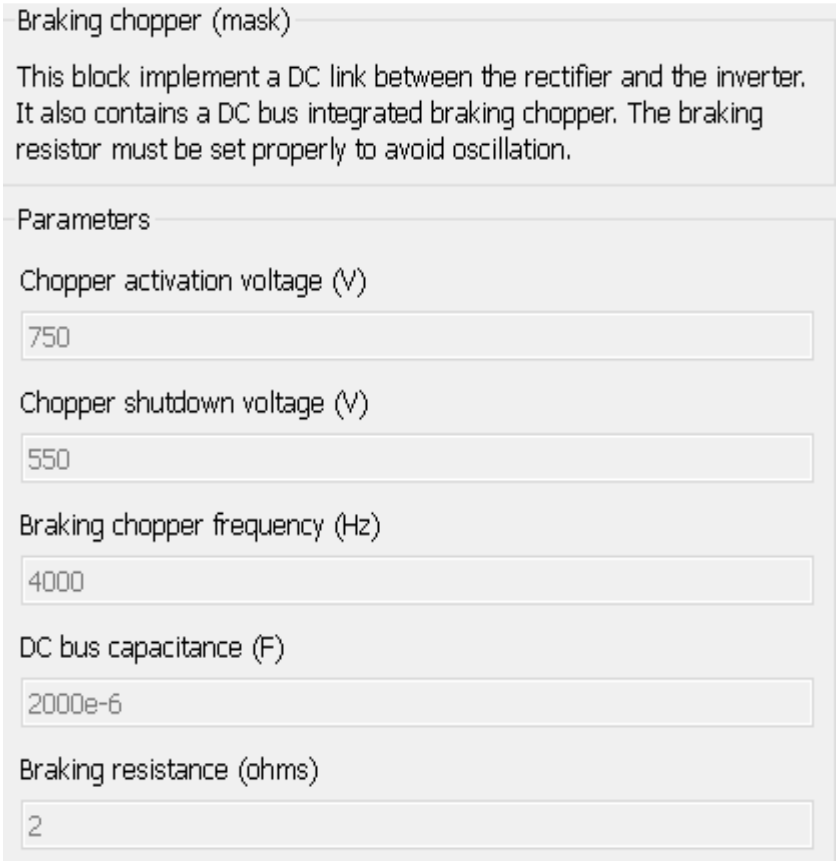

Figure 2.38 Interface of the braking resistor

2.8.4. Pitch Controller

Turbines are designed with some mechanical limits such as maximum aerodynamic torques or rotation speed. Thus, turbine designers set a cut-out speed to stop turning of the rotor blades. However, before cut-out speed is attained, rated power is already reached for almost all types of turbines. In this range (between rated power and cut-out speed), there are some employed active and passive control strategies to deal with high wind speed that would otherwise pose a threat to the turbines and its power electronics [22]. These control techniques can be classified as pitch-regulated and stall-regulated, respectively.

Stall-regulated wind turbines have blades that are fixed to the rotor with an angle. If there is a wind profile blowing higher than a specified speed, turbulence is experienced at the blades. That is called as “stalling”.

Pitch-regulated wind turbines, on the other hand, have an active control that the output power is monitored to catch the rated power and start to operation. When there is a high speed facing the rotor blades, blades are pitched (turned around its own axis) to be unaligned with the wind. Pitching the blades results in decrease in lift and drag forces, which also decreases the torque transferred to the generator.

Stall-regulated systems rely on aerodynamic design of the blades. They are easy to implement and cost-efficient wind turbines. On the other hand, pitch controllers use active control techniques and additional components such as hydraulics and stepper motors to rotate the blade. The additional components increase not only the cost but also the system maintenance. However, noticeable difference between these two strategies comes out at high wind speeds as seen in Figure 2.39.

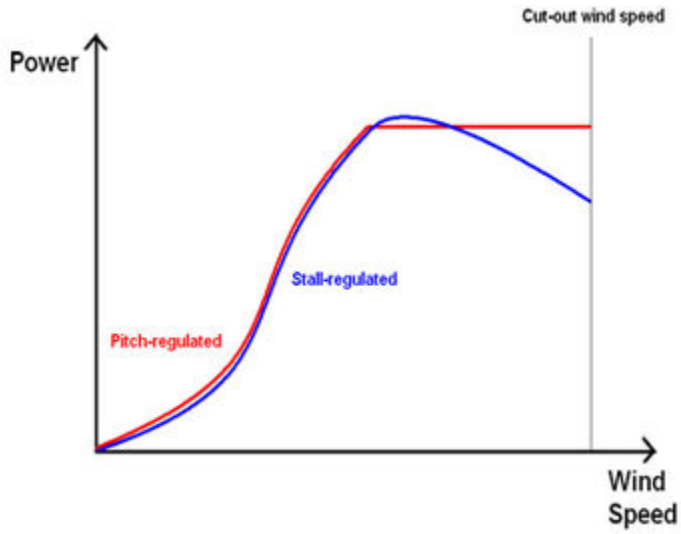

Figure 2.39 Power vs. wind speed graph of pitch-regulated and stall-regulated systems [22]

For stall-regulated systems, there is a decreasing power regime with the increasing speed when the rated power is exceeded. Since the blades are passively controlled, the blades continue to stall at very high speeds and this causes a decrease at the output power noticeably. However, in pitch regulated systems, active power of the turbine is kept constant at very high wind speeds until cut-out speed is obtained. Due to this power surplus, pitch controlled systems are preferred in last 20 years and the market share of the variable pitch wind turbines are almost 90% percent of the total share.

In pitch regulated systems, torque is kept consant at high speeds and the shaft speed is fixed to a pre-defined value. However, in stall regulated systems, the aerodynamic torque is decreased and the rotor speed is decreased, too. Since we explained the deficiency of the passive stall regulated system at the previous paragraph, turbine designers have come out with a new control strategy with the same idea of passive stall control strategy, which is named as active speed stall control. In active speed stall control, the output power is monitored and when the rated power is exceeded, the generator torque is controlled such that rotor speed is accelerated and the absorbed power is decreased [24]. Since the stragety in active speed stall control is same as the passive stall control, this control technique is classified in stall-regulated systems.

Active speed stall control eliminates the decreasing power regime as in passive-stall regulated systems. In addition, active stall control strategy requires no hydraulics or stepper motors to pitch the blades. It can be seen advantageously when it is approached from this perspective. However, disadvantage of this concept is that the generator must reduce the rotor speed even if the wind speed increases in order to force the rotor blades to “stall”. That is, maximum torque of the generator and its drive must be larger than the torque produced at rated power. To exemplify, there is a need of 14MNm torque rating of the generator when active speed stall control is used while there is a need of 10MNm torque rated generator when the pitch control technique is used. That is, using active speed stall control strategy increases the dimensions of the generator and its drives. It results in a higher cost. Altough annual

energy yield of active stall speed controlled wind turbines and pitch controlled wind turbines are almost same [23], increased capital cost of the active stall controlled turbines make the users prefer pitch controlled wind turbines. Thus, in our system, the pitch controlled wind turbines are taken into consideration and the software simulator is set up accordingly.

In the software simulator, pitch control is achieved by using measured power and reference power as inputs. When the power is exceeded, integrator increases the pitch angle. Since the pitch controller is carried out with hydraulic systems or stepper motors, there should be delay (time constant). In the software simulator time constant t_s = 0.25 s is set [33]. The pitch angle controller, shown in Figure 2.40, is realized with anti-windup technique, using a servomechanism model with limitation of both the pitch angle and its rate of change [19]. In typical variable speed pitch turbines, pitch angle β ranges from -2^0 to 30^0 and varies at a maximum rate of ± 10^0/s [34]. Rate limiter and angle limiter has been adjusted according to these specifications.

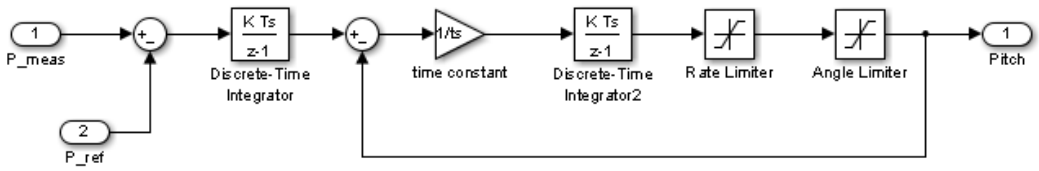

Figure 2.40 Pitch controller realization in Simulink

To visualize effect of pitching the blades on the output power, Figure 2.41 and Figure 2.42 can be investigated. For example, when pitch angle is set to 0^0 and rotor turns with 1 p.u. speed at the 12 m/s wind speed, generated output power from the turbine is 0.8 p.u. If the pitch angle is set to 5^0, for the same wind speed and rotor speed the generated output power decreases to 0.57 p.u. Even if the MPPT is followed and the shaft speed is set to 1.2 p.u. as in Figure 2.42, the maximum output

power is limited to 0.6 p.u. This comparison shows that change of 5^0 of the angles from the upwind results in a 25% decrease in output power. Although pitch controller seems to be slower when compared to other strategies, it presents us a noticeable change in the output power to limit the turbine at extreme conditions.

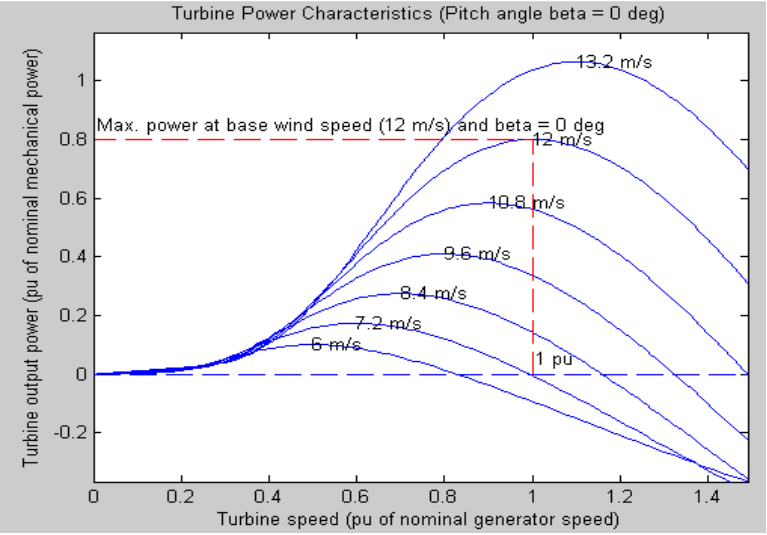

Figure 2.41 Turbine output power when $\beta = 0^0$

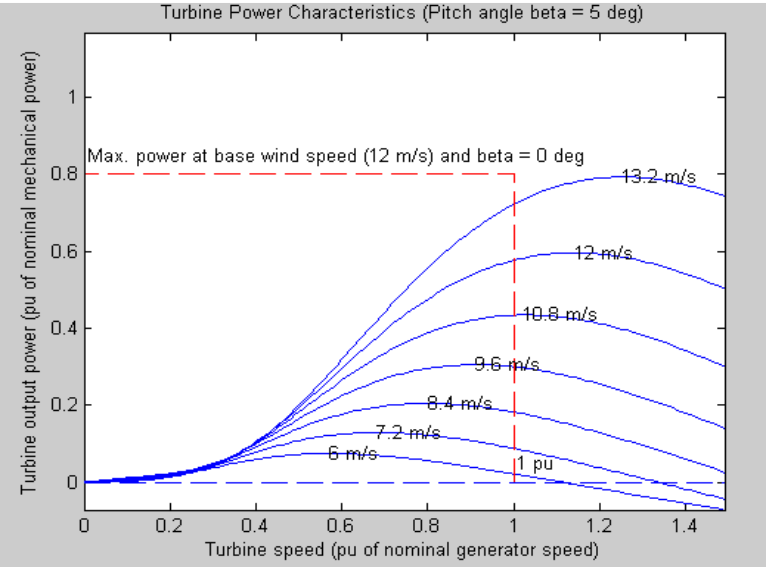

Figure 2.42 Turbine output power when $\beta = 5^0$

Pitch controller in the software simulator is activated whenever the rated power is exceeded. However, this controller will be updated at the Chapter 4 to control the wind turbine when it is operating at islansing mode.

Software simulator which is detailed in previous paragrahs can be seen in Figure 2.43 and Figure 2.44. Figure 2.43 shows the top schematics of the software simulator while Figure 2.44 shows the power electronics and power system components in detail.

2.9. Conclusion to the Chapter 2

In the Chapter 2, a software simulator has been developed. During developing process a wind energy conversion system has been investigated from the wind to the grid connection. During modelling, selection of wind turbine (Type 3, Type4 etc.), its control techniques, mechanical conditions and the HIL setup has been taken into consideration. The aim is to simulate a wind turbine which is compatible with the assembly set up in the laboratory. The lacks in the software simulator will be satisfied during the HIL emulator establishment.

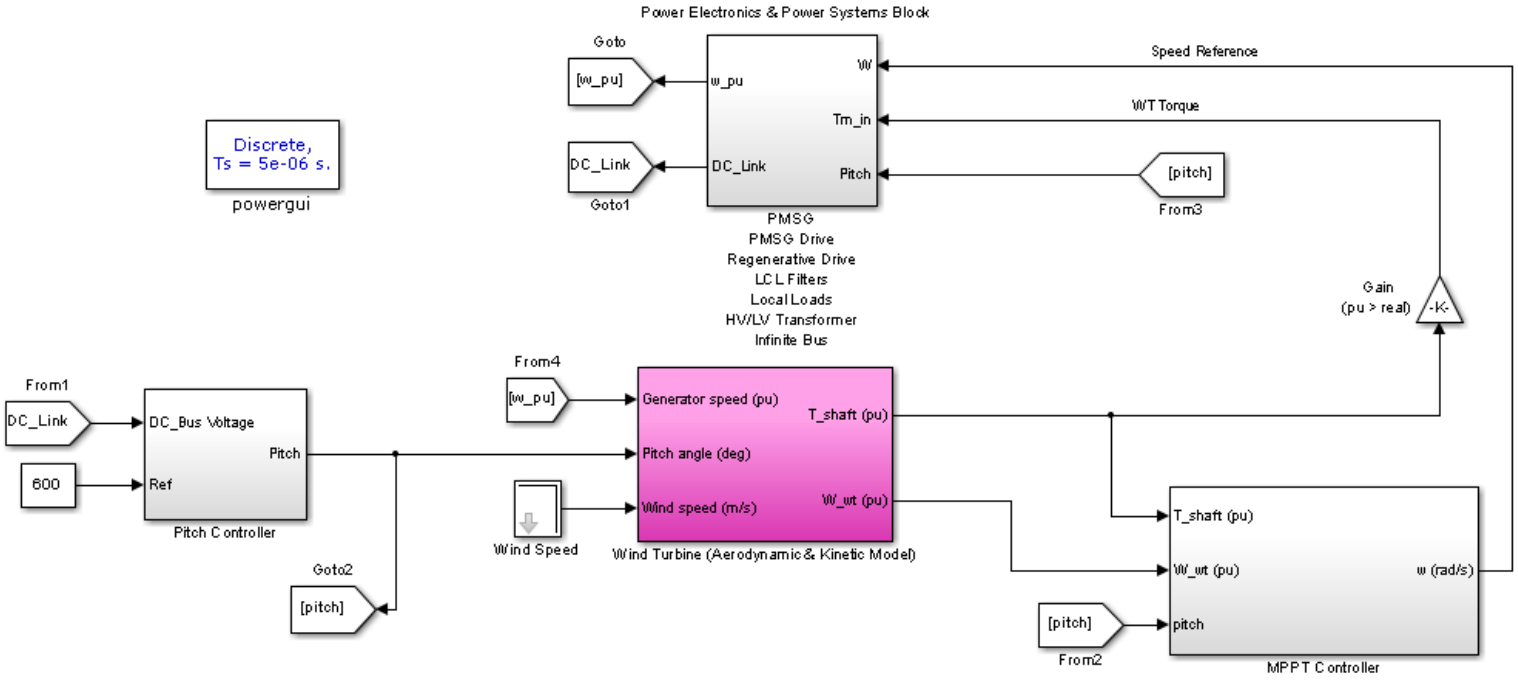

Figure 2.43 Top schematic of the software simulator

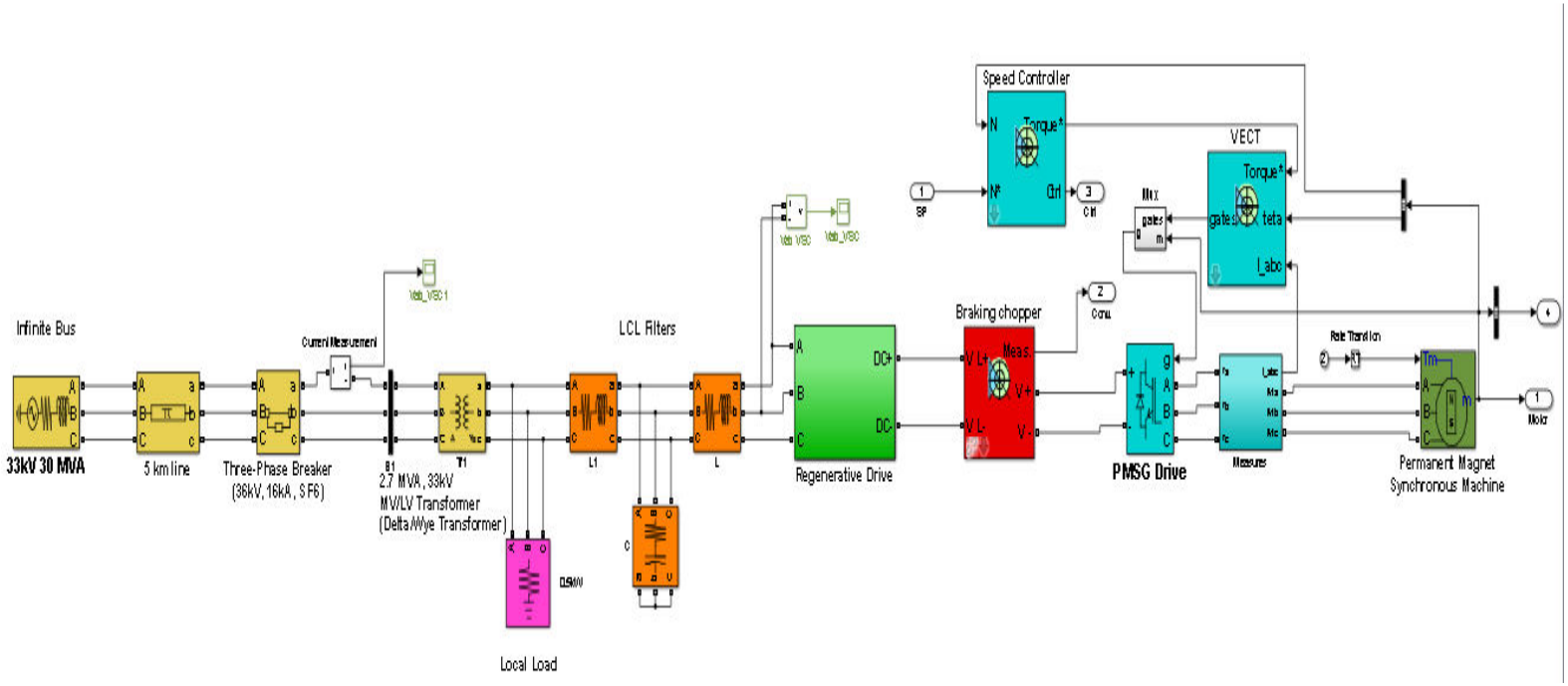

Figure 2.44 Power electronics and power systems block of the software simulator

CHAPTER 3

HARDWARE-IN-THE-LOOP EMULATOR

Over the last thirty years the renewable energy sources gained high importance to meet increasing energy demand. Among these renewable energy sources wind systems became the fastest developing technology. Highly increasing demand for wind energy systems revealed the necessity of control of the turbines. Aerodynamic loops (yaw control, pitch control vs.) and power electronics (torque, speed and power control) are used to control turbines. These control techniques should be studied to increase efficiency, minimize cost arising from dynamically unbalanced conditions and study system behavior under adverse conditions.

To study wind turbine systems, it is necessary to build a real time emulator since a wind turbine may not be available or neither a wind tunnel. The emulator can extract the same behavior as a real wind turbine can produce. For an effective wind simulator, it's both aerodynamic and kinetic characteristics must be close to a real-sized wind turbine. The advantage of an emulator is that different wind turbines and conditions can be imitated as desired through software system. Moreover, safe test environment of the generator and power electronics under hazardous conditions can be accomplished in this simulator.

A wind turbine emulator consists essentially of as seen in Figure 3.1:

- A software system which implements the mathematical model of the wind turbine,
- A physical system that provides the similar references as the real studied system.

Software and physical systems communicate with each other. The real time simulator generates references for the physical system when outputs of the physical system are observed by the software simulator [46].

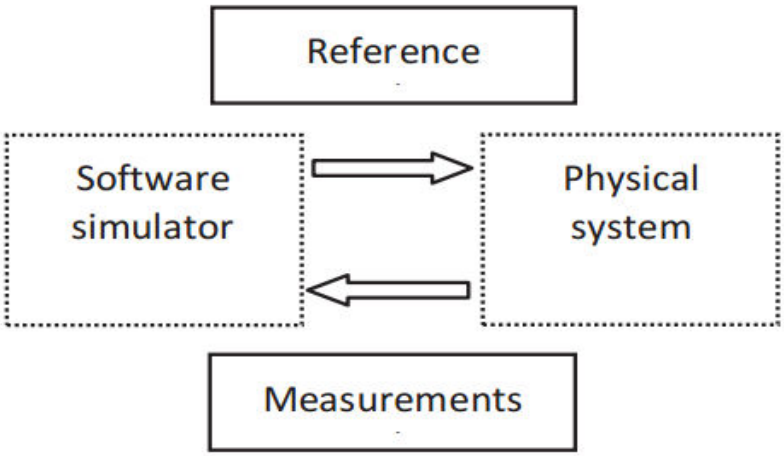

Figure 3.1 General schematic of a HIL simulator [46]

In this study, an emulator for a wind turbine generator is established. This emulator has been studied to research grid-wind turbine relationships and apply developed control algorithms to the experimental test setup via the method of "Hardware-in-the-loop (HIL)".

Hardware-in-the-loop method is composed of two main parts as seen in Figure 3.1: software simulator and physical system. In our study, software simulator includes;

- a wind turbine according to desired mathematical model
- a wind profile which is desired to be analyzed
- a mechanical model which characterizes system inertia and shaft stiffness
- a maximum power point tracker system.

On the other side physical system consists of:

- generator (which is chosen to be a permanent magnet synchronous machine)

- regenerative drive system (back-to-back (AC/DC/AC) converters)
- LCL filters.

For the software simulator, a simulation model has been created in Matlab/Simulink environment. The model, then, has been deployed to NI-Labview environment. Model runs over the Labview platform to send the reference signals and take measurements online. However, this simulation not only included wind turbine, wind profile, mechanical model and maximum power point tracker (MPPT) but also permanent magnet synchronous generator (PMSG) and regenerative drive system (Regen). In the HIL setup, PMSG and Regen models have been discarded since they are already components of the physical system. By simulating physically implemented PMSG and Regen drives, it is aimed that physical system also can be characterized in the simulation environment and users can create or try newly control techniques even without operating the physical system. That is, simulation and hardware system are desired to give similar results.

Wind turbine simulator software creates two references: torque reference and speed reference. Torque reference is calculated according to wind profile and shaft speed as seen in Figure 2.12. Shaft speed is controlled via mechanical model and MPPT together. MPPT takes into consideration response time of the whole system and creates speed reference accordingly. These references are given to the induction machine and permanent magnet synchronous machine and physical system is implemented. Measurements taken from physical system are sent to the simulator and new references for the next time step has been created and this loop continues to the end of wind profile.

There are several studies conducted to represent wind turbine generator system characteristics via HIL method. These studies will be detailed at the section 3.1, “HIL Studies in the Literature”.

3.1. HIL Studies in the Literature

Wind energy conversion systems consist of the following fundamental components: wind turbine, gearbox (except direct drive systems), generator (mostly doubly fed induction generators or permanent magnet synchronous generators), power converters and filters. Developed HIL systems have been used either to solve a problem in these fundamental parts or to increase efficiency and minimize cost. Thus, studies on the literature have many different focuses. To exemplify, some studies focus on wind-wind turbine relation. That is, aerodynamic effects of the wind and the response of the turbine to these effects have been analyzed. In some other studies, power electronic converters are aimed to be improved to increase efficiency. There are also lots of studies conducted to search grid relationships of the turbines at the PCC for sudden changes in the local loads. To comply with standards of network grid such as IEC, filtering techniques at the PCC and fault-ride through capabilities of the WECS have been searched. Many studies using HIL simulators conducted on the area of WECS will be illustrated at the next paragraphs. It will be seen that HIL simulators constitute a majority of the studies to find out new techniques or develop new control algorithms for wind energy conversion systems.

In the literature, some studies just concentrate on wind turbine simulation – gearbox, generator and power converters aren't included- instead of simulating entire wind energy conversion system. To exemplify, in [46], a hardware-in-the-loop emulator for a wind turbine system which will be used to tune and test the generator and the associate power electronics and control has been designed. This simulator has been accomplished by using dSPACE real-time controller. First of all, a simulation study has been conducted in Matlab/Simulink as seen in Figure 3.2. In the simulation, wind turbine has been comprised of aerodynamic and mechanical model. While aerodynamic model produces the instantaneous torque, mechanical model is used to calculate dynamical response of the turbine. In the simulation, PMSG has been modeled but a MPPT strategy has not been considered. PMSG is not connected to the grid via back-to-back converters. Resistive loads have been connected to the output phases of the PMSG. Connecting resistive loads at the output phases of generator

provides variable current drawback whenever the shaft speed is changed. Thus, the torque on the shaft of a turbine is emulated in this simulator via changing rotational speed of the generator. This simulator is not included any power electronic converters that will back up the energy to the grid. This paper just describes how a wind turbine can be emulated in the laboratory environment.

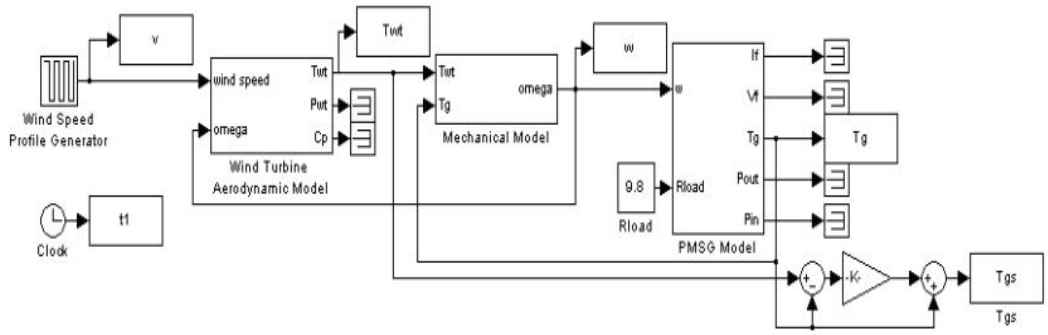

Figure 3.2 Wind turbine Simulink simulation scheme [46]

In the paper it is realized that inertia of the emulator and the MATLAB simulation is different. Thus, a complementary inertia has been utilized while dSPACE is worked on the emulator as seen in Figure 3.3. Complementray inertia is defined as the difference of the real-sized wind turbine and hardware emulator. To find out change of rotor speed in the emulator, this complementary inertia is added to the inertia of the induction machine. By doing that, change of rotor speed in the wind turbine is founded. Then, this derivative is used at the hardware emulator to reflect change of rotor speed truly at the simulator. By using modified inertia model a new torque reference has been created at dSPACE, which is different than the simulation. Then this reference has been sent to the DTC inverter and induction machine has been drived as seen in Figure 3.4.

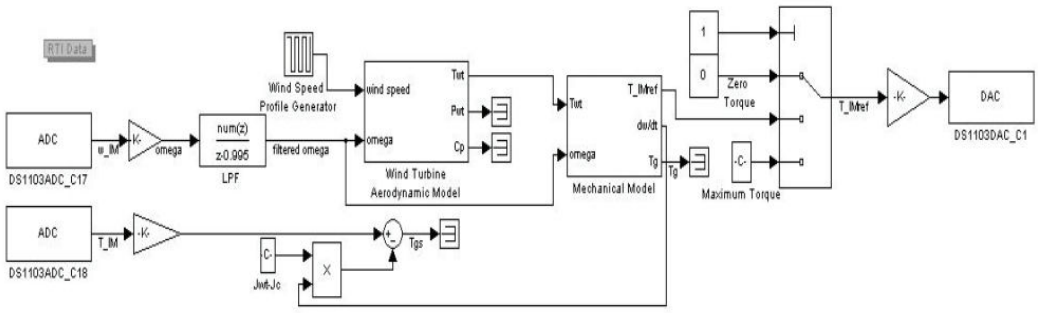

Figure 3.3 Wind turbine dSPACE implementation scheme [46]

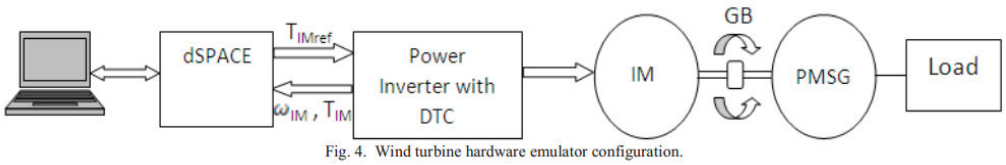

Fig. 4. Wind turbine hardware emulator configuration.

Figure 3.4 Wind turbine hardware-in-the-loop emulator configuration [46]

To conclude, in [46], just a wind turbine has been emulated, not generator and back-to-back converters. Furthermore, dynamical problems such as shaft stiffness, tower effect vs. have not been studied. By using a complementary inertia, difference between simulation and emulation is thought to be eliminated.

In paper [47], it is concluded that there are several techniques that can replicate steady state behavior of a wind turbine with DC motor, IM with IGBT driver, and armature and field control on motor; however, those simulators cannot replicate dynamic behavior of a real wind turbine. This study firstly compares a simulation model and actual wind turbine on frequency domain. It emphasizes that conventional static simulation cannot reproduce dynamic behavior, so new techniques for dynamic simulation should be examined. Then a simplified model of WTS (wind turbine simulator) has been proposed which uses dynamic simulation via a computer, of which turbine characteristics can be changed when different wind turbines have been

researched. To emulate dynamic behavior of a wind turbine, torque equation has been modified which can reflect both steady state and dynamic transient torque components in it. Assuming same generator would be used both in real-time and emulation, the Equation (3.1) and the Equation (3.2) have been unified and the Equation (3.3) has been obtained. Leftmost component of the right hand side of the equation yields transient compensation torque and it implies that it is only different than zero when speed is changing dynamically.

$$T_r/_n = \left(J_r/_n + J_g\right) * \frac{dw_{g_1}}{dt} + T_e \tag{3.1}$$

$$T_m = \left(J_m + J_g\right) * \frac{dw_{g_2}}{dt} + T_e \tag{3.2}$$

$$T_m = T_r/_n - \left(J_r/_{n^2} - J_m\right) * \frac{dw}{dt} \tag{3.3}$$

Then a wind turbine emulator system has been constructed, two permanent magnet synchronous machine has been set back-to-back configuration, one of is driving motor and the other one is acting as generator as seen in Figure 3.5.

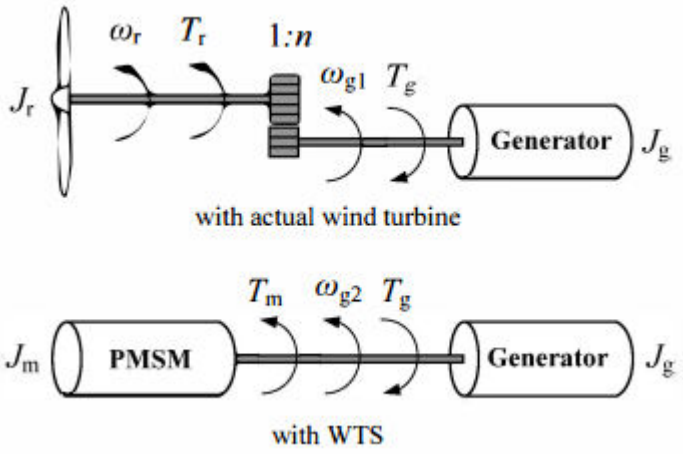

Figure 3.5 Actual wind turbine vs. WT (wind turbine) simulator [47]

To control servo driver of driving motor, a DSP has been used. This component calculate the real-time torque reference according to rotational speed and wind velocity. The servo driver, which runs in torque loop mode, regulates the PMSM to follow the torque reference calculated as seen in Figure 3.6.

Finally, simulation and experimental results have been discussed in the paper. Sudden changes on shaft torque by changing PMSG load resistances have been applied and the simulation and emulation have been compared. It is seen that this convergence to dynamic simualtion is effective.

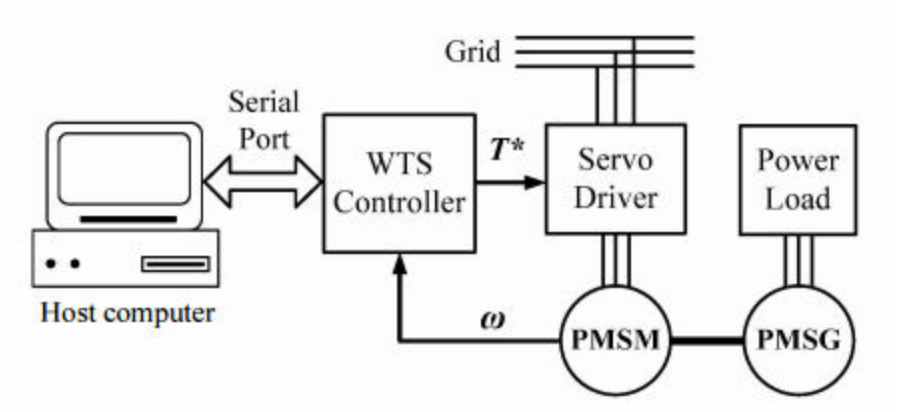

Figure 3.6 System structure of the experimental setup [47]

As seen in [46] and [47], some HIL simulators try to develop a model that represents the wind turbines, not entire WECS. In these studies inertia modeling, dynamic conditions have been studied. However, in some studies entire wind energy conversion system is aimed to be modeled. In [48], implementation of a wind turbine emulator has been accomplished. This study's contribution is that a new torque-speed curve calculation technique has been developed. Without knowing C_p-λ curve of a turbine, its MPP curve can be extracted using geometry of wind turbine (such as rotor radius, inertia, rated power, rated wind speed, start-up and cut-in speeds vs.) and curve-fitting algorithm.

This simulator comprises an induction motor to imitate the characteristics of a wind turbine. By using wind speed and rotating shaft speed, resultant torque of the turbine instantly is found out. Then, this torque reference is used to control output torque of the induction motor. Simulator works as:

1. A wind turbine model is implemented in PC.
2. A wind profile is set to the model (either a data collection or user defined speed profile).
3. Using rotating speed, wind speed and torque measurement; a new torque reference has been calculated for the next time step.
4. This reference is sent to the inverter of the IM.
5. This loop continues until the end of the profile between 3-4.

How a wind turbine is modelled in this simulator can be seen in Figure 3.7. Measurements of torque and speed are obtained by torque meter. Torque reference is sent to the inverter via using MODBUS communication protocol (we have used this protocol,too).

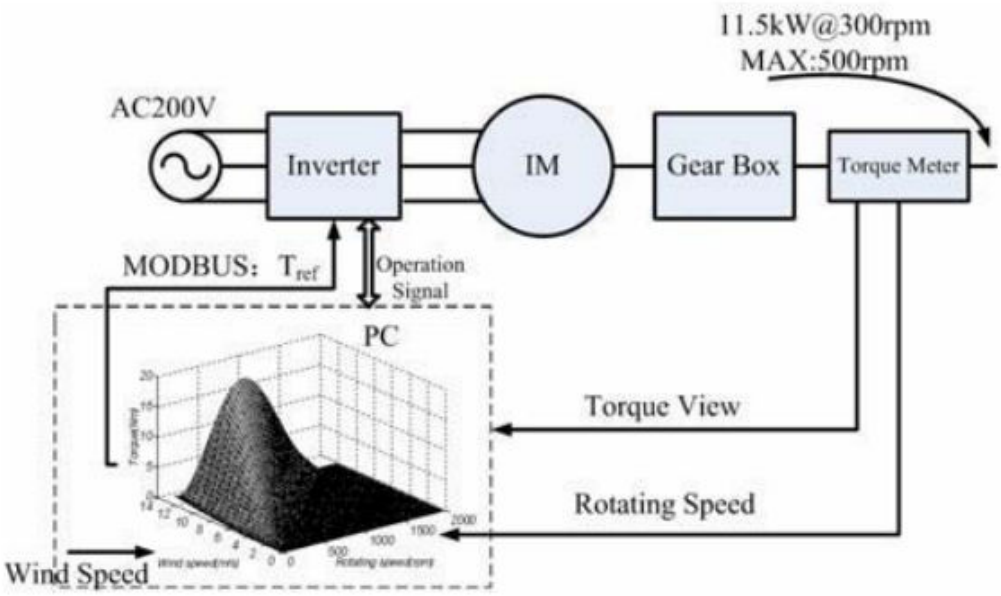

Figure 3.7 Wind turbine emulator configuration [48]

In this simulator, dynamic situations have not been considered much. Whole system is thought to be one-mass. Equation (3.4) has been modified as in Equation (3.5), where Δt is digital sample time period.

$$T_t = J * \frac{dw}{dt} \tag{3.4}$$

$$T = T_w[V_w(t), \omega_w(t)] - J(\omega_w(t) - \omega_w(t - \Delta t))/\Delta t \tag{3.5}$$

By using Equation (3.5), required torque reference is generated at the host PC. If the induction motor is operated at torque loop, wind turbine characteristics can be observed at the shaft of the motor with the help of the inverter as shown in Figure 3.7. In Figure 3.8, wind turbine simulator can be seen, too.

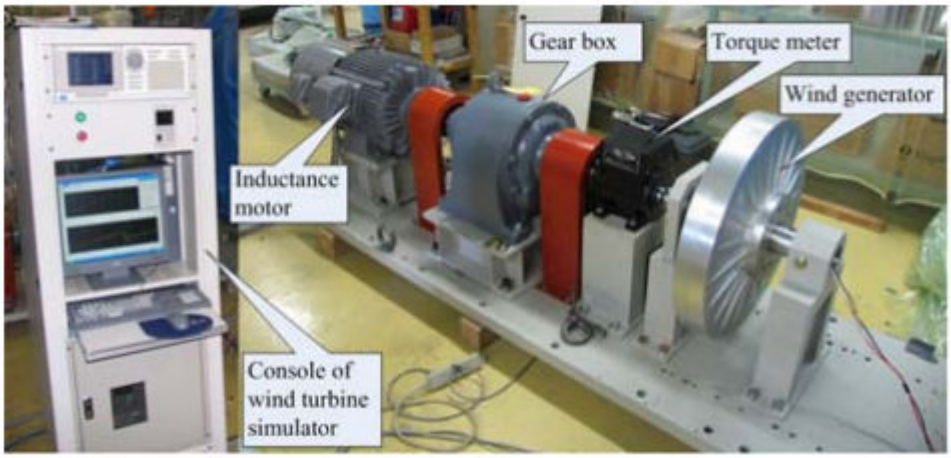

Figure 3.8 Wind turbine simulator[48]

In this paper, 10 kW IPMSG has been used for experimental purposes. This PMSG has fed respectively a rectifier, a DC-DC boost chop and inverter to connect to 3-phase grid. Motivation in this study is to trace MPP curve. Since generator is controlled by a rectifier instead of an inverter, speed can be adjusted only by controlling output current of the rectifier. Using hill-climb technique (called also

P&O technique, which we use in our study), output current of the rectifier is controlled and simulator operates at the MPP.

In [49], a wind turbine simulator have been set up in the laboratory with a 1 kW induction motor as seen in Figure 3.9. Wind turbine simulator includes dSPACE real-time programming device.

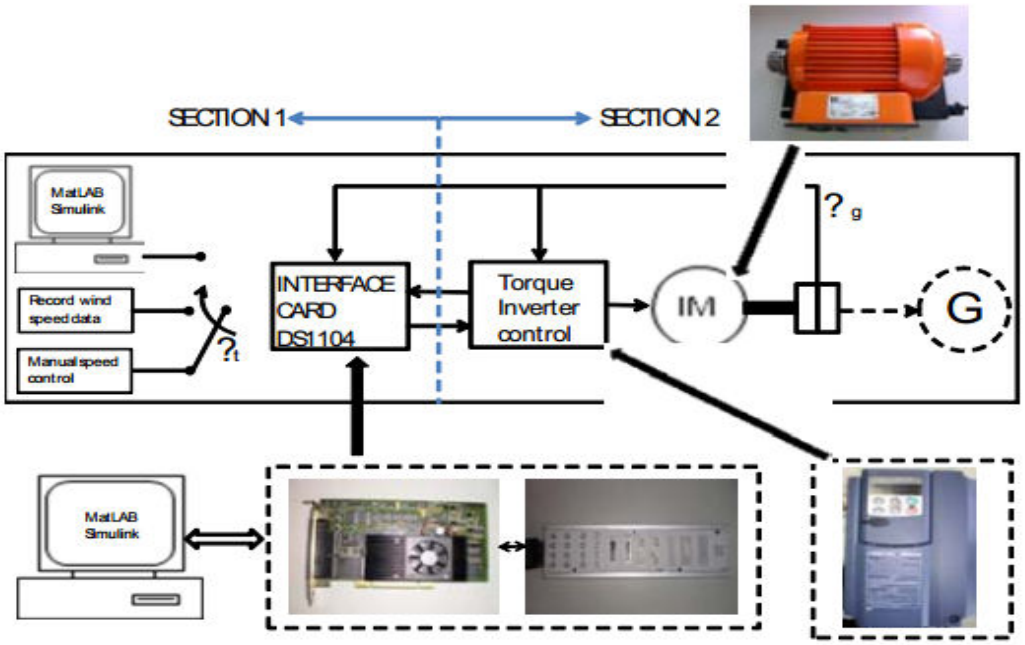

Figure 3.9 Block diagram of real-time wind turbine simulator [49]

Turbine model and wind profile have been run at Matlab/Simulink and dSPACE at real-time. Calculated steady state torque reference has been passed through the model of the rotor blade characteristics of the turbine. The drive which operates at torque loop controls the IM according to this reference. Reference torque is calculated at the DS1104 interface card as seen in Figure 3.10. Using the wind speed characteristics and wind speed, torque reference is calculated for the sampling period. Wind profile is passed by user and rotational speed has got by an optical encoder. At the end of the paper, simulation and experimental results have been discussed and this simulator is concluded to be effective to incorporate different

wind turbines and wind profiles at the laboratory environment easily by using real-time controllers and commercial motors.

In [48] and [49], it is emphasized that a wind energy conversion system can be emulated in the laboratory by using industrial components. The only convern is to replicate the real characteristics of a WECS in the laboratory environment. However, the researchers din't pay attention so much for power electronics and grid-side controllers for a wind energy conversion system. In addition, they ignored dynamic issues (tower shadow, wind shear etc.) and forces acting on the turbine.

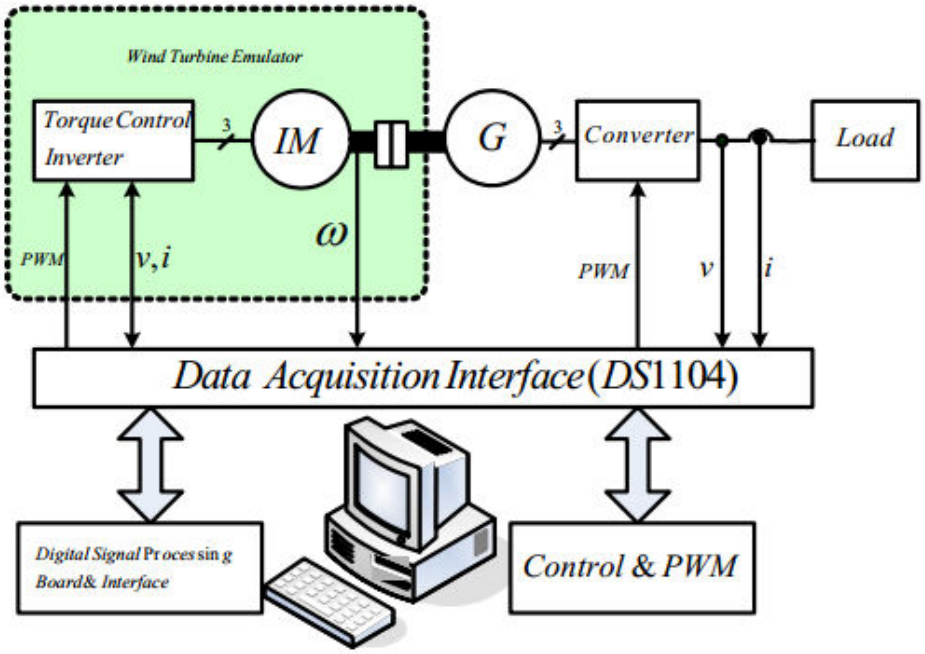

Figure 3.10 Hardware structures of the emulated wind energy system [49]

In [50] and [51], researchers intended to establish a wind turbine emulator by figuring out dynamical issues. Thus, firstly in [50], how to establish a hardware simulator for PMSG VSWTs is discussed. Hardware simulator included two machines; drive motor and generator. This machines are controlled by vector drives. Turbine simulation is achieved by using DSP controllers. In addition, DSPs also

controlled power electronics components. The software simulator comprises from two subsections: aerodynamic and kinetic model of a turbine. In this study NORDEX G70 wind turbine has been analyzed. Aerodynamic model has been established according to measurements of power coefficient and tip-speed ratio. Kinetic model has been created by calculating three blades' inertias. For dynamic conditions, general torque calculation has been used. This study's novelty to the literature is to scale a real turbine to a simulator set. A 1.5MW system has been scaled down to a 2kW simulator.

This study works as: The turbine simulator has been embedded to a DSP. Turbine simulator calculates torque and speed references by taking into consideration wind speed and wind turbine. Then, these references are scaled down to assure rating of the emulator. Torque reference has been passed to AC drive of IM via RS232 communication. On the other side, rotor side inverter operates according to speed references to trace MPP curve as seen in Figure 3.11. Motor torque calculation algorithm can also be seen in Figure 3.12.

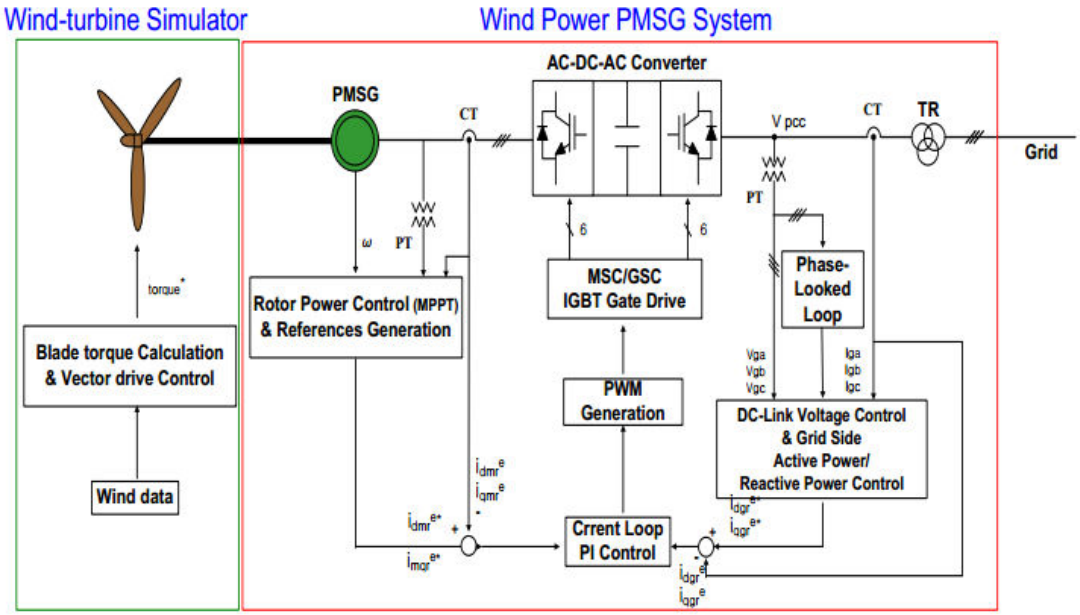

Figure 3.11 Configuration of wind turbine simulator [50]

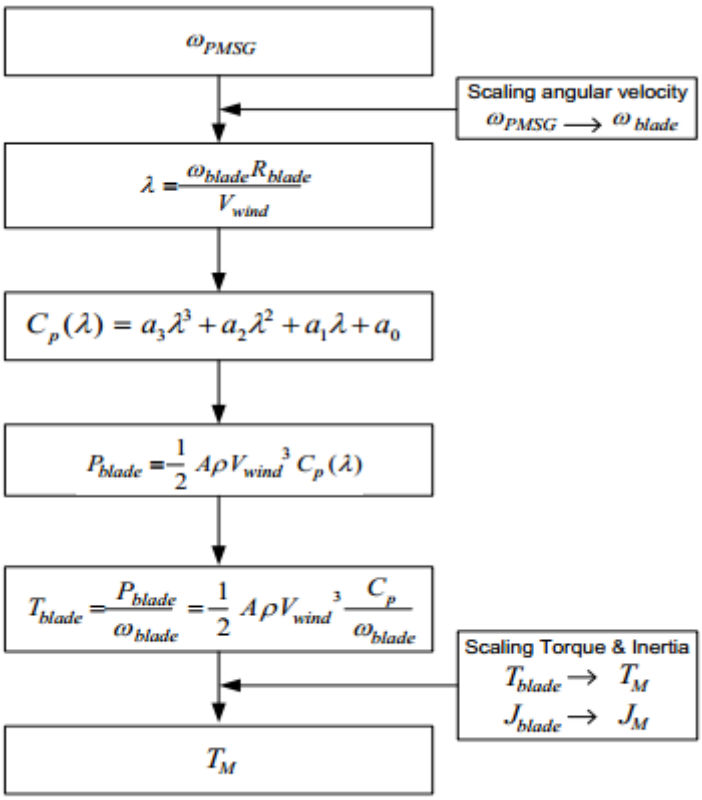

Figure 3.12 Motor torque calculation algorithm [50]

To track maximum power point, converter control in generator side has been accomplished. Optimal tip speed ratio is calculated according to wind profile and reference rotational speed has been given to the converter PI controller. By looking instant rotational and reference speed, error is minimized by controlling d-axis current on the generator side as seen in Figure 3.13.

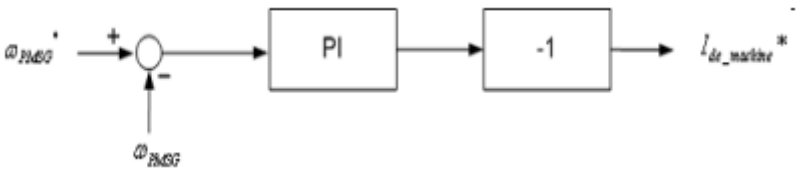

Figure 3.13 Converter d-axis current control scheme [50]

Torque and MPPT calculation techniques and scaling down of the references have been validated both in simulation and HIL environment.

Researchers of [50], then, continued to work on hardware simulator and they decided to improve efficiency of the power converters on the generator side [51]. They claimed that back-to-back converters have high switching loss and bulky structure due to having three-step power conversion, AC/DC/AC. To improve this weakness, a matrix converter has been designed which changes an AC power of one frequency to the desired one directly as seen in Figure 3.14. In fact, researchers started to design a HIL system to say that HIL system is effective to improve new techniques for wind energy conversion systems and then they validated this theorem by designing a new converter. The proposed converter is implemented and a new modulation technique is also proposed. Experiment results showed that using a matrix converter gives positive results both from the perspective of minimizing loss and MPPT technique.

Figure 3.14 Hardware simulator and matrix converter [51]

Although dynamic issues and generator-side converters have been worked out in some studies, researchers continue to investigate different problems by working on wind turbine simulators. To exemplify, in [52], the main focus is again to analyze energy conversion train after the wind turbine segment. However, in this study

several problems analyzed instead of designing a new converter as in [51]. In [52], a wind turbine simulator for laboratory testing has been established. The aim is to test a wind energy conversion drive train which composed of an electric generator, gear-box, electromagnetic brake, power eletronic converters and controllers. This drive train is stimulated with a wind turbine simulator. This simulator consists of a 5.5kW induction motor that is controlled by a variable speed inverter and a Programmable Logic Controller (PLC). The wind turbine simualtor provides the required torque reference signal according to the wind speed input and thus it acts like a wind turbine to the energy conversion system as seen in Figure 3.15.

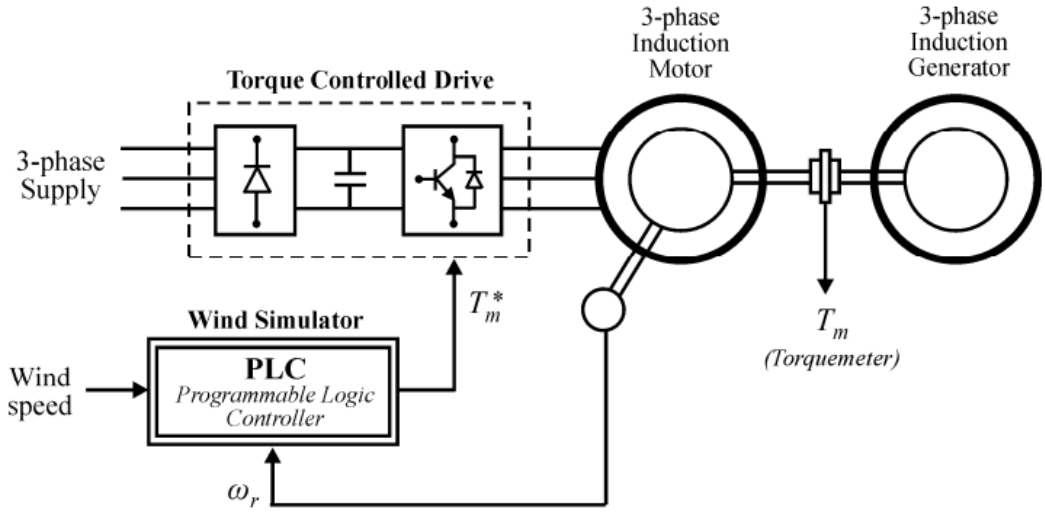

Figure 3.15 Structure of the wind turbine simulator [52]

In the study it is aimed to analyze generation system and its response to aerodynamic effects caused by wind velocity, yaw error, wind shears and tower shadow. Researchers claim that there is a need for a wind simulation system that can incorporate the wind turbine behavior by means of considering torque-speed characteristics and aerodynamic effects. For this purpose a wind turbine is modeled with mathematical formulas in PLC considering other side effects. That PLC obtained input wind speed signal and speed feedback from the electric motor and then using turbine characteristics torque value of the turbine has been calculated. The

three-phase drive is operated with torque control and feeds the electric motor that is acting as the prime mover to the electric generator.

The tested WECS with the wind turbine emulator proposed has been implemented as in Figure 3.16. For generator a 3-phase squirrel cage induction machine has been used. The speed of the shaft is controlled by utilizing indirect vector control method to achieve maximum power point. In this study, since speed is measured at each time step, control technique is named as indirect vector control). For the line-side converters vector control has been also used. This controller aimed to get power factor to unity. At the last stage an LCL filter has been used to reduce the harmanic currents injected to the grid as seen in Figure 3.16.

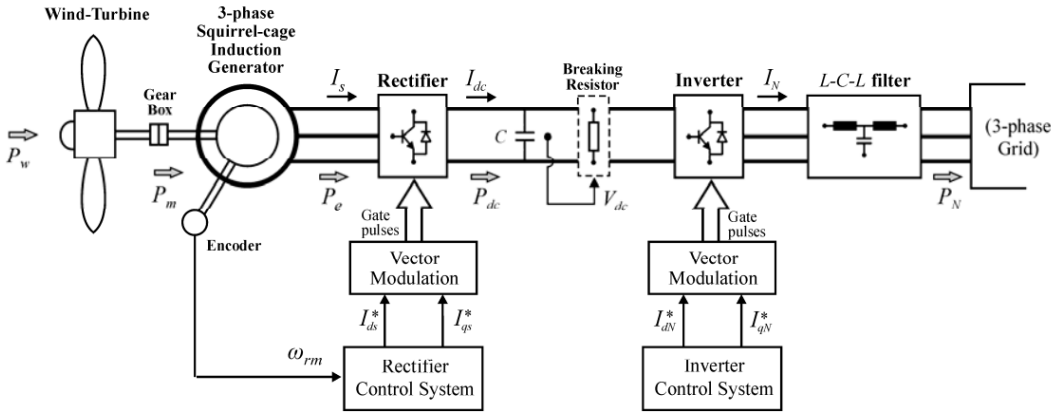

Figure 3.16 Structure of the simulated system at [52]

Described wind turbine simulator and wind energy conversion drive train has been set up in the laboratory as in Figure 3.17. The wind turbine emulator consists of an IM that is driven by an ABB torque controlled drive and a PLC that controls the drive according to simulated wind turbine characteristics. For rectificiation and inverter, dSPACE controllers have been used. The rectifier controller board housed

the MPPT controller in it. Thus, speed of the generator has been controlled and MPPT is followed.

At the last part of the paper efficiency of the emulator has been tested. At constant wind speed and step changes power conversion at the grid-side has been analyzed. Moreoever, performance of the MPPT controller has been shown. Finally start-up of a wind turbine and the emulator has been compared and it is concluded that wind turbine-generator emulator is applicable to test and improve control techniques.

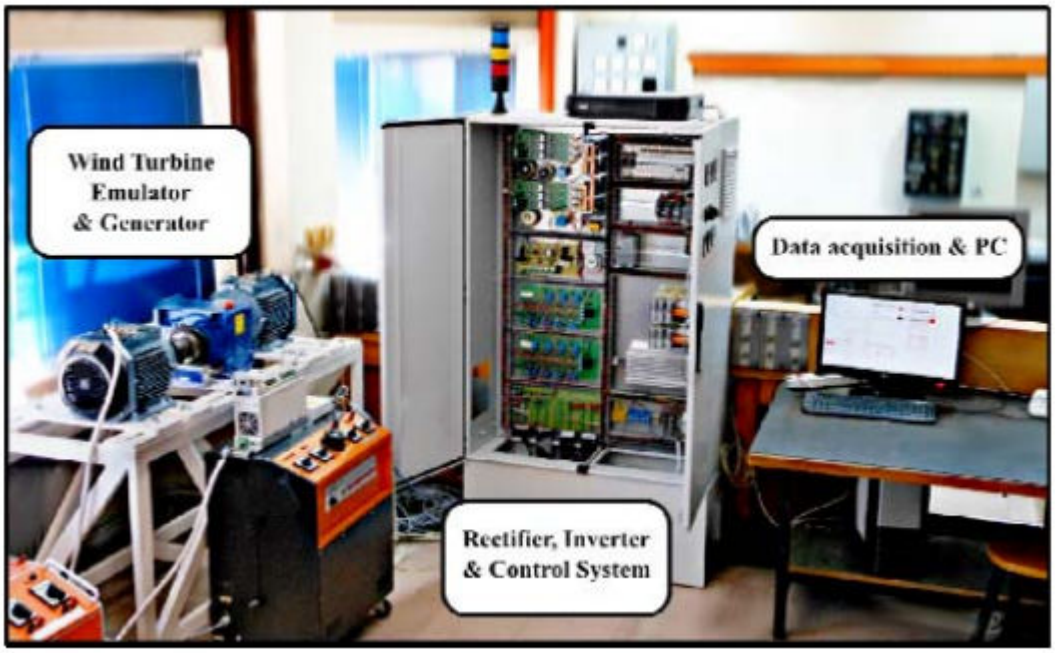

Figure 3.17 Experimental WECS on a laboratory test bench. It consists of an induction generator, the wind turbine emulator, power converters and digital controllers [52]

While some studies focus on generation side of the WECS as in [52], some simulators center on turbine problems for their study [53]. In [53], a hardware simulator has been improved to see the effects of tower shadow and wind shear. It is claimed that a simulator is needed since software simulator cannot replicate the dynamic behavior of a turbine. Wind turbine simulator has been performed using a

permanent magnet synchronous motor (PMSM). The wind turbine simulator consists of a microcontroller, an intelligent power module (IPM) inverter, a PMSM and Control Desk. The Control Desk needs wind speed and the rotation speed of PMSG. By using these two variables, torque of the real-sized wind turbine has been obtained as seen in Figure 3.18.

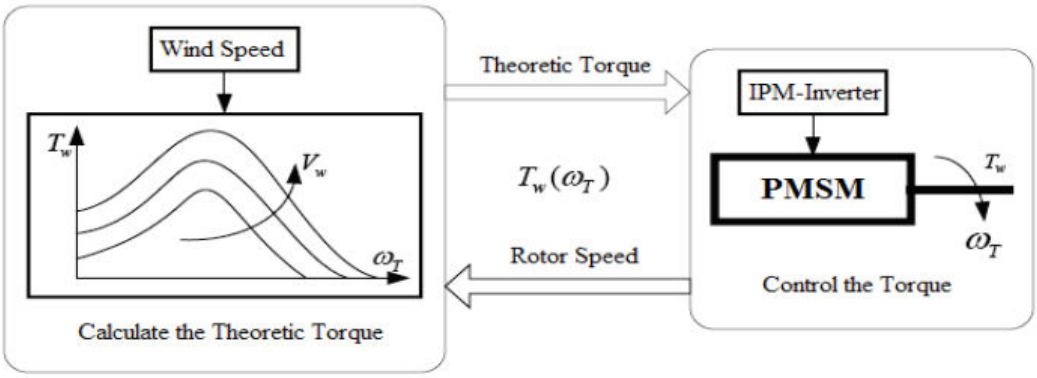

Figure 3.18 Control strategy of the wind turbine simulator [53]

Control schematic of the wind turbine can be divided into two parts: Control Desk and control of PMSM. To obtain the theoretic torque, the Control Desk reads wind velocity from user generated file and rotor speed from an encoder. Tower shadow and wind shear has been taken under consideration while calculating therotical torque. After this step, torque reference has been applied to space vector modulated inverter. Using SVPWM modulation technique, direct-axis current is set to zero and by controlling just quadrature-axis current desired torque has been obtained at the end of the shaft as seen in Figure 3.19.

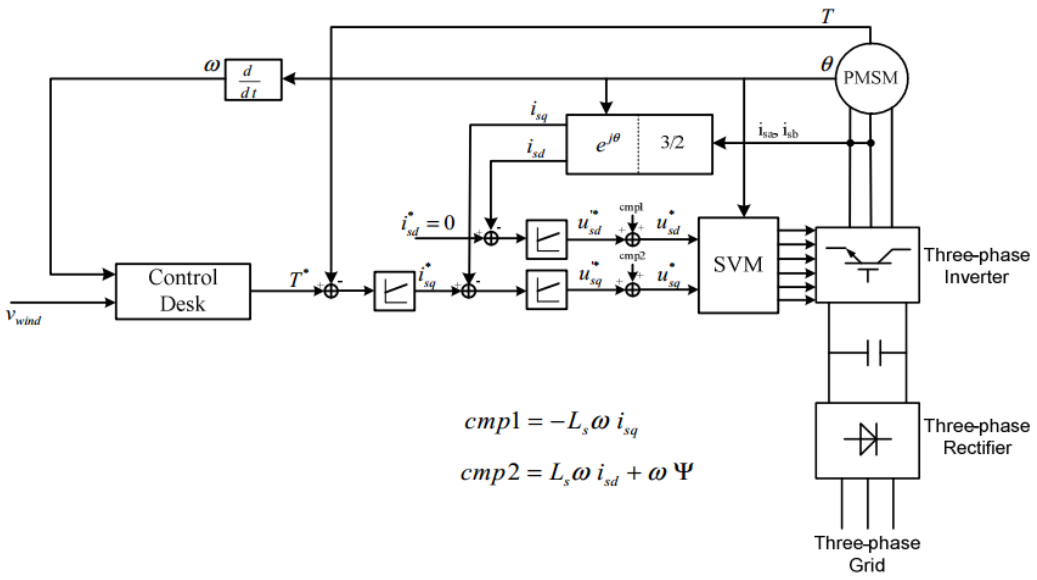

Figure 3.19 Control schematic diagram of the PMSM [53]

At the last stage of the paper, simulation and emulation results have been compared from the perspective of tower shadow and wind shear. In the results section, change of output power and torque at the shaft has been analyzed and it is seen that this effects can be replicated in the hardware emulator.

To conclude, wind turbine hardware emulators have been established for several purposes. Some of them concentrate on replicating wind turbine, while some of them focus on entire wind energy conversion system. If we elaborate on these, it is also seen there are lots of studies to search either generator-side electronics, converters, related problems or turbine dynamics, wind effects etc. Thus, studies upon wind energy conversion train in the laboratory environment show the necessity of the hardware emulators. In this study, it is aimed to establish a HIL setup which imitates both steady state and dynamic characteristics of a wind energy conversion system. Using the HIL setup the islanding operation is desired to be investigated. The problems occurred at the interruption of the electric flow from or to the grid is desired to be monitored. Efficiency of the control techniques will be observed via this HIL setup. The setup shows the characteristics of a standard HIL setup mostly

encountered in the literature. Since the HIL setup that we develop mostly concentrate on islanding operation, the gearbox is not included to the emulator at this moment. If dynamical issues are desired to be analyzed, it can be added to the setup by not changing the overall strategy of the simulator.

3.2. Physical Structure of the HIL Emulator

In this study, a hardware-in-the-loop wind energy conversion system emulator is constructed in the laboratory. This emulator has been established to research grid-wind turbine relationships and apply developed control algorithms to the experimental test setup via the method of HIL. In other words, HIL setup is dedicated to develop control techniques for islanding operation. In the setup, islanding detection algorithms and efficiency of the control techniques is aimed to be analyzed. Furthermore, the HIL setup can also be used for other studies such as increasing efficiency of electronics, trial of the new components (generators, inverters etc.), observing dynamic conditions (tower shadow, yaw effect etc.) and new filtering techniques.

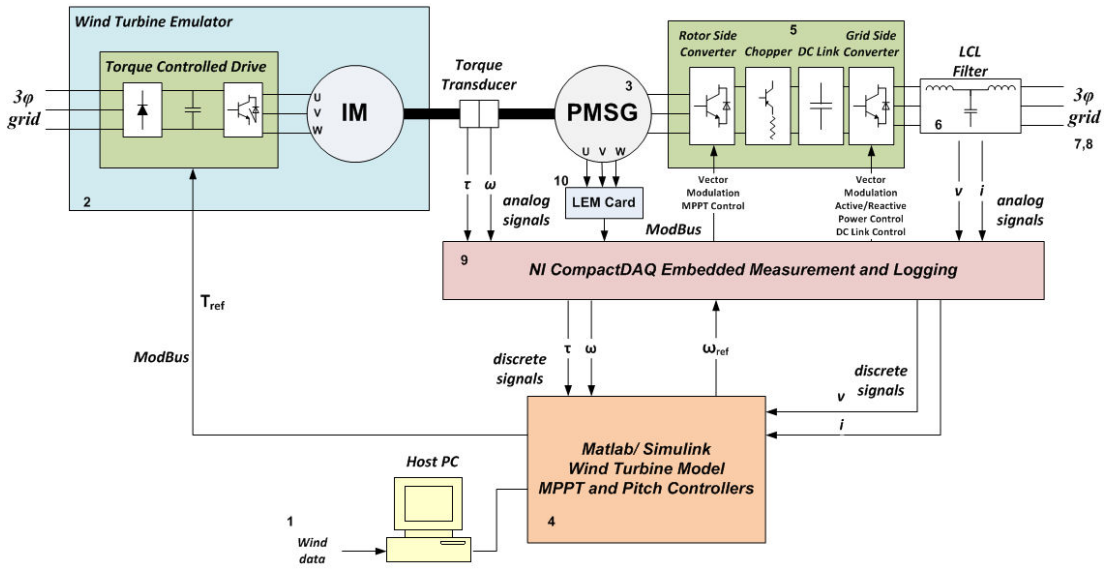

Figure 3.20 Schematic of the HIL setup established in the laboratory

HIL setup is constituted to emulate a wind turbine, which is variable speed variable pitch, direct driven generator (permanent magnet synchronous machine), back-to-back converters (AC/DC/AC) and filters (LCL and EMC). Figure 3.20 illustrates the hardware set up in the laboratory. All the blocks in the HIL setup is numbered in Figure 3.20 as in Figure 2.1 in Chapter 2.

The block '1' represents the wind data which should be supplied by the user. The wind data should be set of a data which consists of speed in m/s for each 50 ms at an 'excel' file. This file is loaded into the host PC by the user. Then, the module of "Read From Measurement File" is implemented in Labview to pass into values to the program.

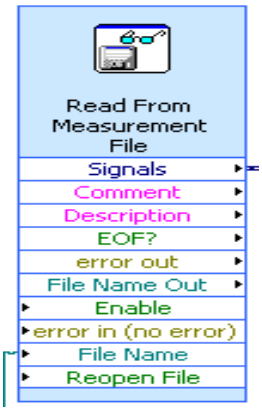

Figure 3.21 The module of 'Read From Measurement Module'

The block '2' is used to emulate wind turbine in the HIL setup. Wind turbine emulator consists of an induction machine which is rated at 11kW and an AC drive which is rated at 11.4 kW. The AC drive can be explained as the variable PWM switching source to drive a motor. The AC drive consists of four main parts: the rectifier, DC link, the controller and the switches. The AC drive in the HIL setup is directly connected to the three-phase grid (220 VAC, 50 Hz). This variable voltage is rectified in the drive to a set value, which is 550V for the drives used in the setup. Then the DC voltage is stored in the internal DC link capacitors. This DC voltage is

utilized at the internal bridge circuits. Bridge circuits of the AC drives consist of six IGBTs. IGBTs create the required PWM switching scheme according to the references generated by the internal controller. The controller is adjusted by the user. That is, which control technique should be applied at the controller (such as open-loop V/f, closed-loop vector, closed-loop servo or regenerative mode) is selected by the user. In this setup, the AC drive is configured to be operated at the closed-loop vector mode which means FOC without position feedback.

The block '3' is the generator which is used to generate electrical source to the grid. The generator is an 11 kW permanent magnet synchronous generator. The generator is controlled again via an AC drive. The AC drive is configured to be in 'closed-loop servo' mode. Closed-loop servo mode is almost same as closed-loop vector mode except for a difference. FOC operation is implemented by using closed loop current operation. To utilize this configuration, the position feedback should be supplied to the AC drive. The generator in the setup supplies the required encoder references to the drive.

The block '4' contains the wind turbine model, MPPT and pitch controllers which are implemented in Simulink. The wind turbine model in the host PC supplies the torque reference to the AC drive of the wind turbine emulator. The MPPT controller attends the torque and speed of the shaft via torque transducer and creates the speed reference which will be utilized by the AC drive of the generator. The pitch controller is implemented in case of an excess power is generated at the grid side.

The block '5' consists of the AC/DC/AC converters and braking chopper. AC/DC/AC configuration is provided via two AC drives which are connected back-to-back by placing a DC link capacitor at the middle point. The AC drive which is connected to the PMSG rectifies the variable voltage variable frequency source to a DC voltage. By using this DC voltage, the speed of the generator is controlled. The DC link voltage is also utilized by a second AC drive, which operates as regenerative drive to supply excess power to the grid. The braking chopper is connected to the DC

bus of the AC drives to dissipate excess energy if the regenerative drive cannot achieve to transmit extra energy.

The block ‘6’ is used to filter harmonics generated at the switching frequency. The switching frequency of the HIL setup is adjusted to 6 kHz. The cut-off frequency of the filter is set to 2 kHz by adjusting inductance and capacitances properly.

The block ‘7, 8’ can be named as the loads and grid connection. In the HIL setup, there is no load for the moment. The loads are to be connected at the islanding operation. The grid connection is again to the central grid, which is 220 VAC, 50 Hz.

The block ‘9’ represents the measurement and logging module of the National Instruments Technology. The module operates in conjunction with Labview, which is the software interface of the National Instruments. By using this data acquisition module, both the analog signals can be discretized (or digitized) and the information can be monitored at the software interface.

The block ’10’ is an electronic card which consists of current and voltage sensors, named as LEMs. The generated currents and voltages are retrieved by these LEM sensors. LEM transducers measure the voltage and current and supply a current relative to the input. The current is retrieved by the DAQ modules to analyze the operation at the Labview interface.

All the blocks expressed at the upper paragraphs and seen in Figure 3.20 can be observed at Figure 3.22 as well. The detailed explanation of the HIL setup will be given in below sections. Firstly, how a wind turbine is emulated in the HIL setup is declared. Then, the measurement techniques and the components will be revelead by taking into consideration delays, response times and accuracy. For the last, experiments and results conducted in the HIL setup will be given and a comparison of software simulator and the HIL setup is made.

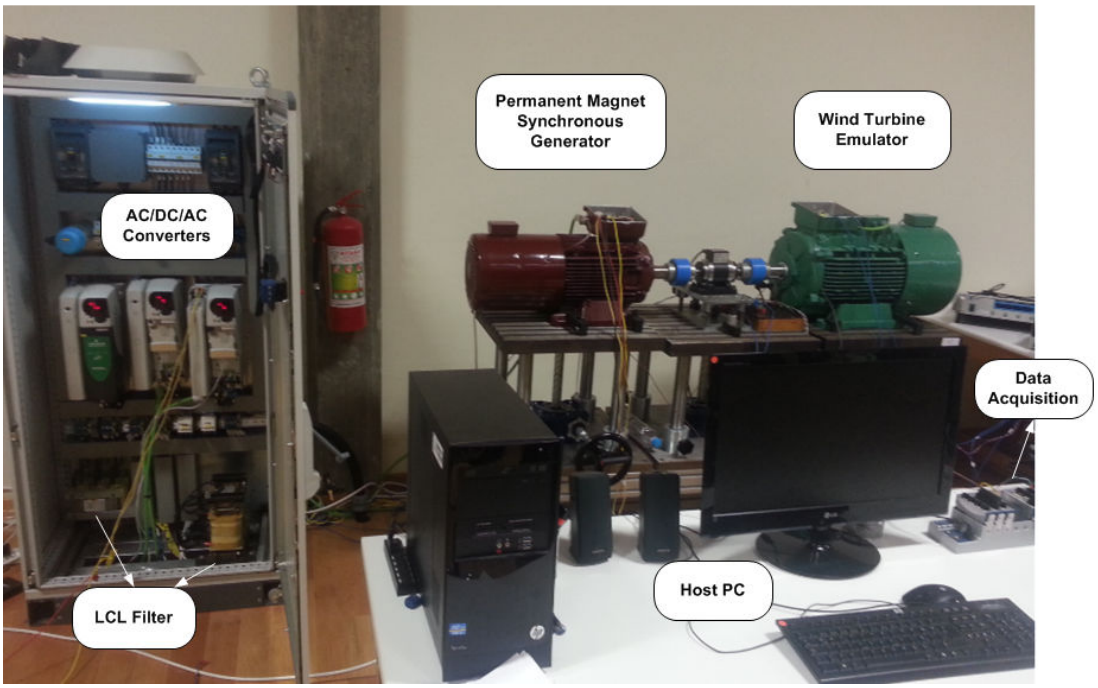

Figure 3.22 HIL emulator setup in the laboratory

3.3. Measurement Techniques of the HIL

For proper operation of the HIL emulator, it should be noticed that the measurements should be taken with right precision. The critical measurements can be sequenced as shaft torque, rotating speed, generated AC voltages at the phase outputs of the generator and the total net output power

3.3.1. Shaft Speed and Torque Measurements

The shaft torque and speed measurements have been recorded via a rotary encoder which is named as “Magtrol SA TMB 312/411”. This encoder has rated torque of 200 Nm and rated speed of 4000 rpm. The motor-generator set in the HIL setup can achieve maximum 142,5 Nm torque and 1000 rpm speed at the shaft. Thus, it can be said that the limits of the encoder are appropriate for our measurements.

The rotary encoder at the setup has been connected to Magtrol 6400 torque transducer display. This component supplies us required two outputs (torque and speed) with BNC connectors. The torque is supplied as ±10VDC which is adjusted according to measured torque value. The rated torque of 200 Nm has been divided into 20V (from -10V to 10V). That is, for every step of 10Nm torque increase/decrease, the analog voltage changes 1V. By using this equation, the torque value is taken to the Labview platform in the electrical units. The analog output has been retrieved by using NI 9225 CompactDAQ component (NI DAQ measurement modules can be seen in Figure 3.27. In addition, 'DAQ' is an abbreviation used by NI to represent its portable analog and digital signal conditioning data acquisiton platform). This component consists of three analog input channel, which can read until 300 Vrms simultaneously. Since it is known that rotary encoder has a sensivity of 25 mV/Nm, the measurement device should have a resolution rate of higher than the error rate. The NI9225 module has a 24-bit resolution (one bit error creates 17.8 μV), which is sufficient for the setup.

The transducer display also supplies shaft speed in rpm by a BNC connector. The measured speed in rpm is converted to electrical signal by using moduation technique. In other words, for a shaft rotating at a speed of 300 rpm, the transducer provides 300 Hz, digital (0 V for logic '0' and 5 V for logic '1') at the BNC connector. The shaft speed is discretized and taken to the Labview again using NI9225 module.

The torque and speed is taken inside of the Labview platform by using "DAQ Assistant Express VI" module (named as "Speed & Torque" in Figure 3.23). Since the speed is given to the Labview in frequency reference, "Timing and Transition VI" module has been utilized to measure the frequency of the digital input signal. The shaft torque is measured by "Amplitude and Levels Express VI" due to taking an analog input voltage from the transducer. The measured values have been converted in the Labview and the speed and shaft torque is measured by the way. The precise measurement of the shaft torque and speed is critical because the input power of the generator should be known to verify loss models generated in the software simulator.

In addition, the shaft speed is utilized by the MPPT controller to achieve maximum power point operation at the HIL setup.

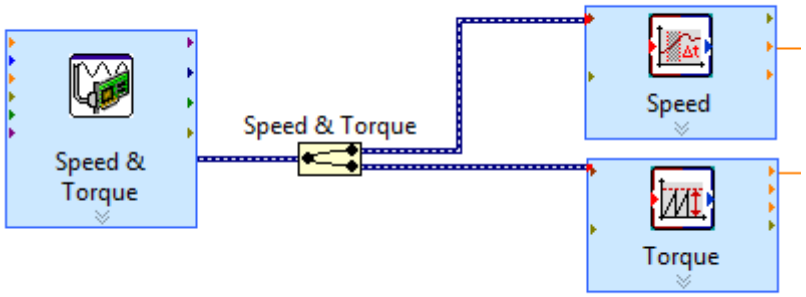

Figure 3.23 Speed and torque measurement at the Labview platform

3.3.2. Voltage and Current Measurements

The measurements of the voltage and the current is vital to follow MPPT operation in the HIL setup. The measured voltage and current is utilized to calculate the net output power of the generator. Following the output power, the HIL setup is aimed to operate at the maximum point for the specified wind speed.

As if known, the voltages at the phase outputs of the generator is in a configuration of PWM square waveform. This is due to control of the generator by the AC/DC converter in the power electronics section. In addition, the generator used in the HIL setup does not provide any star point at its surface. That is, it is internally 'wye' connected and there is no neutral point for the measurement. Thus, the measurements should be achieved from the phase-to-phase voltages at the generator. However, the phase-to-phase voltages can be reached to 380 Vrms for the speeds close to the rated one. The available DAQ module in the setup is NI9225, which can accept analog voltages until 300 Vrms. Due to these reasons, it is noticed that both the voltage should be lowered and filtered for a precise measurement. In addition, it should be

noted that the PWM switching scheme is a high frequency (6 kHz) operation and it can disrupt the operation of the DAQ modules while the system runs (this condition has been tried out in the setup and it is seen that DAQ modules response very wrong!). Thus, the need of isolation of the generator from the DAQ modules is observed.

To lower voltage, filter the PWM switching scheme and isolation, an electronic card which consists of LEM voltage sensors and RC filter has been designed as seen in Figure 3.24. For the voltage sensor, LV 25P has been used due to fast response (40 µs), good accuracy (<2% for T=25^{0}C) and low thermal drift (±0.1 mA change at the output current between T=25^{0}C and 70^{0}C). LV25P provides a current proportional to the input current of the primary side circuit. The conversion ratio for the LV25P is 1:2.5. In other words, a current of 2.5 multiple of the primary side circuit flows through the secondary circuit. Since it involves a primary and secondary circuit, it provides us a galvanic isolation. The voltage measurement at the secondary side has been achieved by placing a resistor, which is 274 Ω in Figure 3.24. The measured voltage, then, filtered via a RC filter of which the cut-off frequency is set to 2 kHz to eliminate harmonics occurred at the PWM switching frequency. Then, the voltage measurement has been passed to the Labview using NI 9225 analog input module. This module has a 50k sample rate, which is enough to observe AC voltages at 50 Hz.

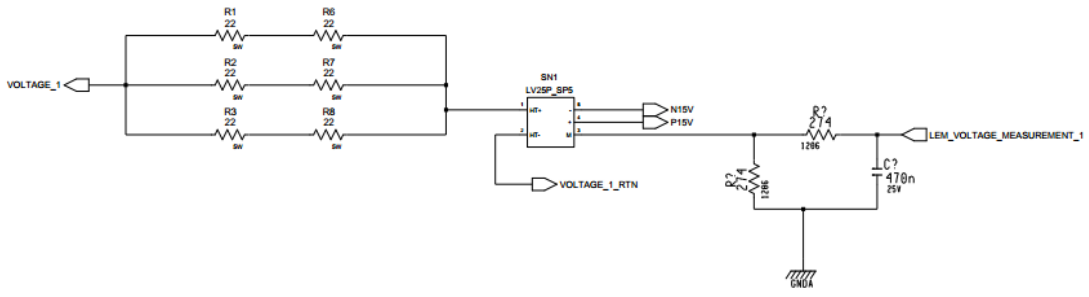

Figure 3.24 Voltage measurement via LEM sensors

The current measurement of each phase has been achieved again at the electronic card by using another LEM sensor, of which the model names is LA55P as seen in Figure 3.25. This current transducer uses Hall effect to measure the current. Hall effect can be stated as the voltage induced across an electrical conductor due to current flowing in the conductor and created resultant magnetic field perpendicular to the current. The phase cables has been passed through these sensors and the voltage induced at the internal circuit of the sensors has been supplied via a current reference which is proportional to the flowing current. The conversion ratio of the transducer is 1:1000. In other words, for a current flowing as 1A at the phase cable is reflected at the output of the sensor as 1 mA. This current is passed through a resistor and the voltage of the resistor is measured by using DAQ module.

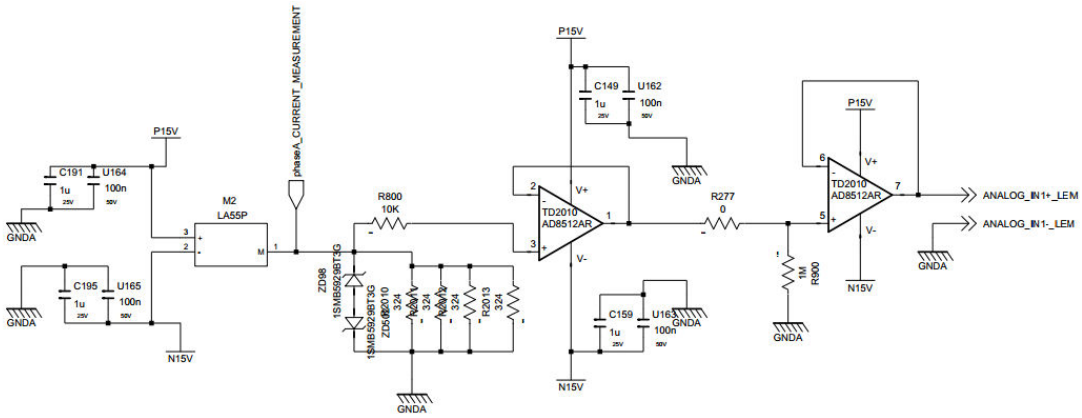

Figure 3.25 Current measurement via LEM sensors

The generated three phase voltages at the LEM card have been passed to Labview platform. 'DAQ Assistant VI' module is adjusted to sample the input at 50ks, which is the maximum rate for the module. Even if measured voltages and currents flow at 50 Hz, 20µs sampling rate takes 1000 samples for each period. This is emphasized to show the accuracy of the measurement. The amplitude and frequency of the voltages and currents has been measured by using 'Amplitude and Levels Express VI' and 'Timing and Transition VIs'. However, for this measurement, a 'Power VI' which can be seen in Figure 3.26 is added different than the speed and torque measurement

VIs. This is due to having a phase difference of 30^0 degrees between the voltages and the phase currents since the measurement of the voltages at the generator side has been generated as 'phase-to-phase'. The 'Power VI' supplies us the phase difference between the voltage and the current and then it is subracted at the Labview platform and accurate power result can be calculated.

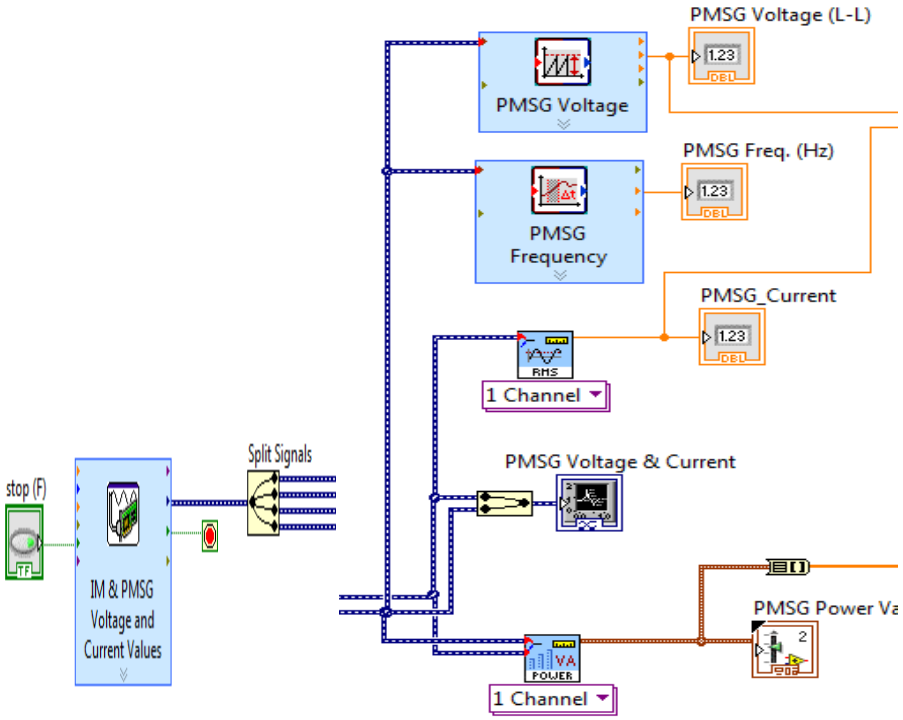

(a) (b)

Figure 3.26 Voltage, current and power measurement at the Labview platform, (a) represents the 'DAQ Assistant VI' and (b) represents the 'Timing and Transition VI', 'Amplitude and Levels Express VI' and 'Power VI'

To conclude measurement section, the shaft speed, torque, voltage and current measurements can be reflected to the software side (Labview) by digitizing the analog signals in a fast and accurate way. It should be remembered that all the measurements have been verified by a second measuring device. Since the PMSG in

the setup supplies position feedback to the AC/DC converter, speed is verified from the converter interface. The applied torque is adjusted at the AC drive of the induction motor and it shows the torque at its screen continuously. By observing this, torque measurement is also verified. For the last, voltage, current and power measurements have been confirmed by using harmonic tester which is named as Hioki 3193.

3.4. Control of the HIL Emulator

In previous sections of 3.2 and 3.3, the physical structure of the HIL setup is overviewed and the measurement techniques have been identified. If Figure 3.20 is taken into consideration, the block '1' can be said to be expressed in section 3.2. The measurement section details the block '9' in section 3.3. Thus, in this section, remaining blocks will be clearified while the control of the blocks are expressed.

3.4.1. Control of Wind Turbine Emulator

For the wind turbine emulator, there is a wind turbine model set up in Simulink by taking into consideration both aerodynamic and mechanical conditions. Then, this model is deployed to the NI-Labview program. The deployed model forms the block '4'. This block is created to trace continuously torque and speed at the shaft and generate control signals upon request of the general system.

Labview is an emulation platform that many digital data acquisiton (DAQ) and measurement modules can be used and controlled. The generated models in the Labview needs three variables: wind speed, pitch angle and the shaft speed. Wind speed is entered by the user to the Labview program. Pitch controller is found at the block of '4' in Labview from the software simulator. The only measurement for the wind turbine emulator is done from the shaft via a rotary encoder. This encoder supplies us both the torque and speed of the shaft simultaneously as described in 3.3.1. The shaft speed and torque information have been generated as analog signals

at the encoder. Thus, analog signals are measured via NI-DAQ and supplied into Labview program as seen in Figure 3.27. After getting these three variables, wind model generates a torque reference.

Figure 3.27 NI-DAQ measurement modules

After producing the torque reference, it should be sent to the induction motor which will emulate wind turbine characteristics. The motor used in the HIL setup is an 11 kW, 8 pole squirrel-cage induction motor as seen in [69] and it is driven by an 11 kW AC drive [54] that is connected to the mains. Since the model generates torque reference in pu, it is converted to a scalar value by multiplying it with the nominal torque of the induction machine which is 142.5 Nm in Labview.

The AC drive is configured as in closed-loop vector mode. The drive is operated without position feedback. That is, closed-loop vector mode control generates its position feedback internally. Figure 3.28 shows the closed loop vector mode in vector diagram. To operate in vector mode, AC drive needs stator resistance, rated frequency, transient inductance and rated voltage. Except the transient inductance, all other parameters are presented at the datasheet of the induction machine. To measure the transient inductance, a “auto-tune” test is conducted on the machine. The drive is selected to be in the auto-tune mode and AC drive supplies a current when the motor is stationary. While measuring transient inductance, current-loop gains (K_p and K_i) are also calculated automatically, which are 185 and 404 respectively. Current-loop gains are critical for the response of the system. If the gains are set properly, for the 6

kHz operation, there is a delay of 581 µs. This is critical since the Labview turbine model should sent the torque reference to the drive after this duration is passed. Otherwise, the control loop results in a faulty operation.

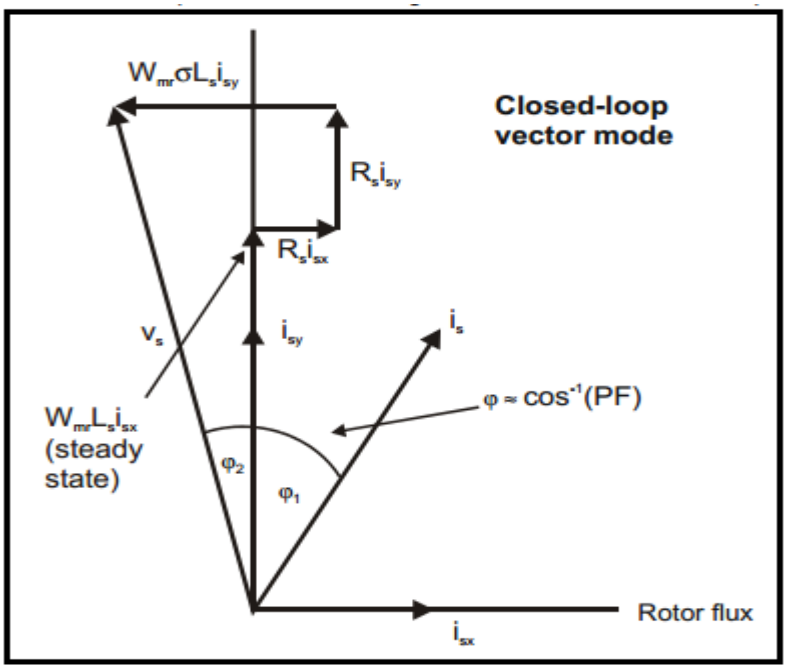

Figure 3.28 Closed-loop vector mode [54]

Table 3.1 Current (torque) controller delays [54]

Switching frequency (kHz)	Current control sample time (µs)	Gain bandwidth (Hz)	Delay (µs)
3	167	TBA	1,160
4	125	TBA	875
6	83	TBA	581
8	125	TBA	625
12	83	TBA	415
16	125	TBA	625

The active current is the torque producing current for a motor and the reactive current is the magnetizing of flux producing current for a motor drive. AC drive

supplies needed torque according to this active current. Torque applied from AC drive is,

$$T_m = K_t I_a \tag{3.6}$$

where T_m is mechanical torque of the induction motor (IM), K_t is the torque constant and I_a is the active current. In closed-loop vector mode, the drive calculates the motor torque per amp (K_t) using the motor parameters as shown in Equation (3.7) assuming a motor efficiency of 90%. This assumption is reasonable for our motor since the efficiency of the used IM is 86% at rated load.

$$K_t = \frac{\sqrt{3} * V_{rated} * I_{rated} * Rated\ pf * Eff}{Rated\ speed\ (rad\ s^{-1}) x Rated\ active\ current} \tag{3.7}$$

The sampling time of injection of wind speed data to the HIL setup is decided to be 50 ms. It is chosen since the system is thought to barely response due to high inertia of motor-generator set. In addition, the sampling time of 50 ms is appropriate to have a good measurement and take the response from the controllers truly (the response of the controller is 581 µs, which is very low than the sampling rate). Thus, it is thought that there is no need to extract parameters of the IM in this study due to having enough information for the wind turbine emulator that it satisfies the proper operation. However, the generator parameters are extracted to set the rotor side converter precisely. These values have been given at Chapter 2 in detail.

Torque reference of the IM is sent to the IM drive via an ethernet protocol: ModBus. The communication protocol is established as fast as possible to increase the reliability of the emulation. Details of the ModBus will be given in next sections, so it is not detailed here. In this section, the block of numbered '2' has been explained in detail while the control algorithm is explained. In the next section, control of the generator and its AC/DC drive will be detailed.

3.4.2. Control of the Generator and AC/DC Converter

In the HIL setup, 11 kW, 8-pole, 21 A permanent magnet synchronous generator in [70] has been used due to reasons that are explained in Chapter 2. This generator is directly driven by the IM at the torque of wind turbine produced. The generator is controlled via MPPT controller which is developed in Simulink. The MPPT controller continuously checks whether the generator is rotating at the speed producing maximum current. For the power measurement, again DAQ modules have been used. DAQ modules are connected to the output phases of the generator and power measurements have been taken as declared in 3.3.2. The related voltage and current signals will be shown in the "3.5. Experiments & Results" section.

Permanent magnet synchronous generator (PMSG) has been controlled in servo mode by the rotor side converter. This converter is controlled to keep speed at the reference which is supplied from MPPT controller via ModBus. Speed reference is sent to the AC/DC converter with a maximum rate of 789 µs if the gains are set properly. The AC drive desires to set generator parameters to calculate the current loop gains precisely. Moreover, the parameters are used at the software simulator as well. Thus, the parameters are defined at Chapter 2 in detail.

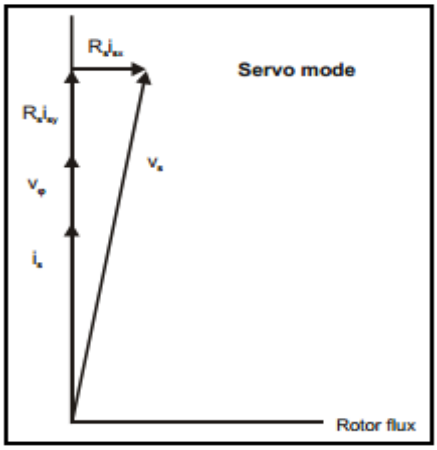

Figure 3.29 Servo mode of the AC/DC converter [54]

Table 3.2 Speed controller delays [54]

Switching frequency (kHz)	Sample period for speed feedback (μs)	Speed controller delay (μs)	Current/torque controller delay (μs)	Total delay (μs)
3	125	167	1160	1452
4	125	125	875	1125
6	125	83	581	789
8	125	125	625	875
12	125	83	415	623
16	125	125	625	875

As seen in Table 3.2, the total delay can reach to 1.45 ms at maximum. Thus, it is logical to define a sampling time bigger than this response time. However, it should also be noted that the response of the physical system is slower compared to the delay of the controller. Thus, the sampling time of 50 ms for the MPPT controller is thought to be reasonable for this system.

Since speed controlled drive (AC/DC converter of the generator) has a longer delay, the reading of the analog signal from DAQ modules have been accomplished with 1 ms delay after Master (starter of the communication at ModBus protocol) send its reference to the drive. These delays are thought to differ results at the simulator and emulator. Thus, the sampling time of the overall system should be decided by taking into consideration these issues as well.

By explaining the control dynamics of the generator and its drive, the blocks of '3' and '5' are also be stated. The remaining blocks which are not detailed here are LCL filters and grid connection. Since the LCL filters are passive components and there is no control of them, they are not explained here in detail. The choice of the inductances and capacitances of the filters have been highlihted at Chapter 2. For the grid connection, there is a control of power factor at the DC/AC converter. The converter is adjusted to supply excess energy with unity power factor at 50 Hz. This control algorithm is adjusted at the start of the study and no change is considered for the verification of the HIL setup. This parameter, for example, can be also changed to see the effects of power factor at islanding operation. However, it is beyond the scope of this study and not detailed here.

3.5. Experiments and Results

In the HIL setup, Labview program has been used to gather data from the setup and apply control techniques and references to the physical components. Gathering data has been achieved by establishing DAQ modules which are bought from the National Instruments. Applying references, on the other side, has been achieved via ModBus as seen in Figure 3.30.

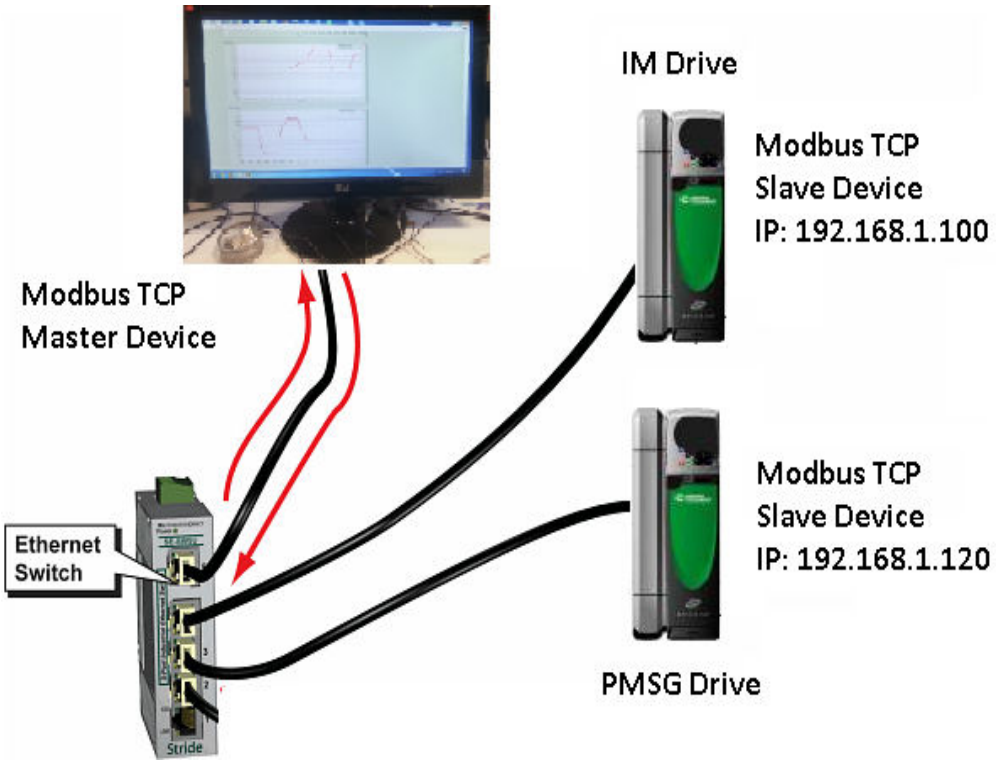

Figure 3.30 ModBus communication scheme for the HIL setup

In the ModBus communication protocol, one device is selected as Master and the others are set Slave devices. The communication can be started or ended by only the master device. In the HIL setup, the torque and speed references are sent to the IM and PMSG drives at 100Mbps. However, the update rates of the AC drives are 4ms. Even if the ModBus can generate its 32-bit data to the slaves, the response of the drives are limited. Thus, for the sake of operation, the messaging has been updated

from the master to the slave with a rate of 5ms. In the Labview, an interface of the ModBus has been established as seen in Figure 3.31. The interface requires the IP addresses of the slave nodes and the “writing mode”. Writing mode is described as sending data from the master to the slave. Either multiple write or single write can be applied. Since the delay of the setup is too high, there is no need to do a multiple write. Thus, single write has been achieved. For the IM, torque reference (Pr 4.08, modbus register 407) and for the PM speed reference (Pr 1.21, modbus register 120) has been utilized.

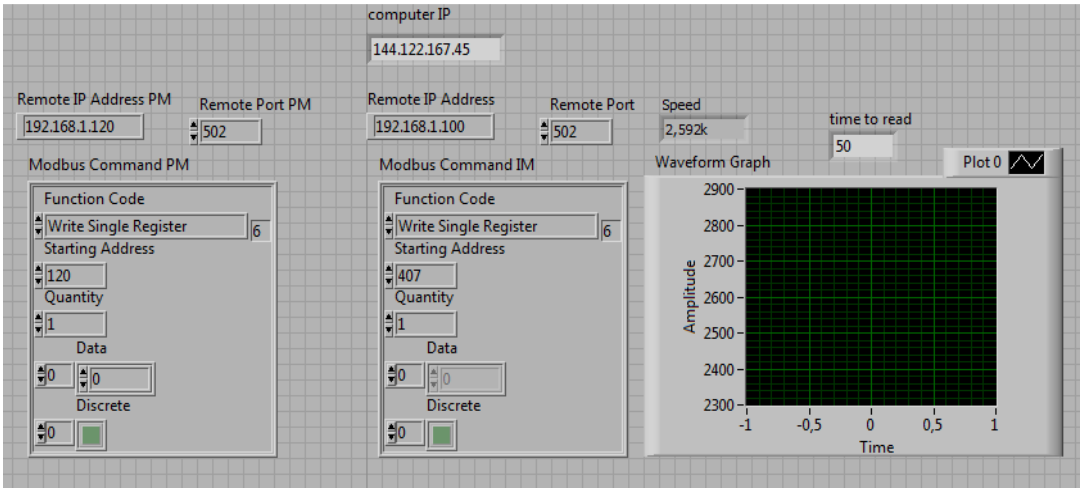

Figure 3.31 ModBus interface of the HIL setup

The drives are also has current-loop and sampling delay as stated in Table 3.1 and Table 3.2. It should be remembered that the sampling time of the system is selected by considering the differences between the converters. Using DAQ modules, all the analog and digital signals have been attained at the Labview program as seen in Figure 3.32 and Figure 3.33. All the voltage and currents generated at IM and PMSG, shaft speed and torque, active and reactive power, power factor of the machines can be gathered. Figure 3.32 is the interface of the Labview platform. All gathered data is presented via this interface. The interface is updated for each second. Figure 3.33 is added to show how the voltages and currents can be seen at the interface continuously and simultaneously. The Labview platform gives the chance

to user to use its interface as an oscilloscope as well. The values at the interface also can be saved to a file using 'Write to Measurement File VI' module at Labview if needed.

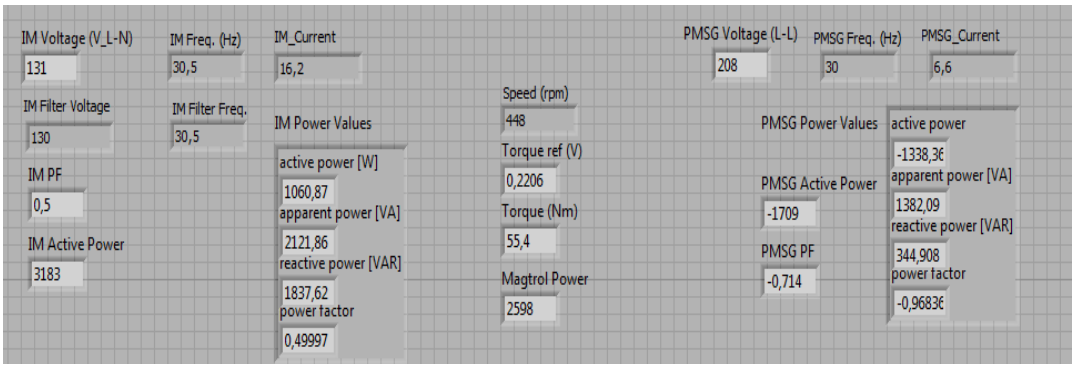

Figure 3.32 Measurement collected from the HIL setup (via DAQ modules)

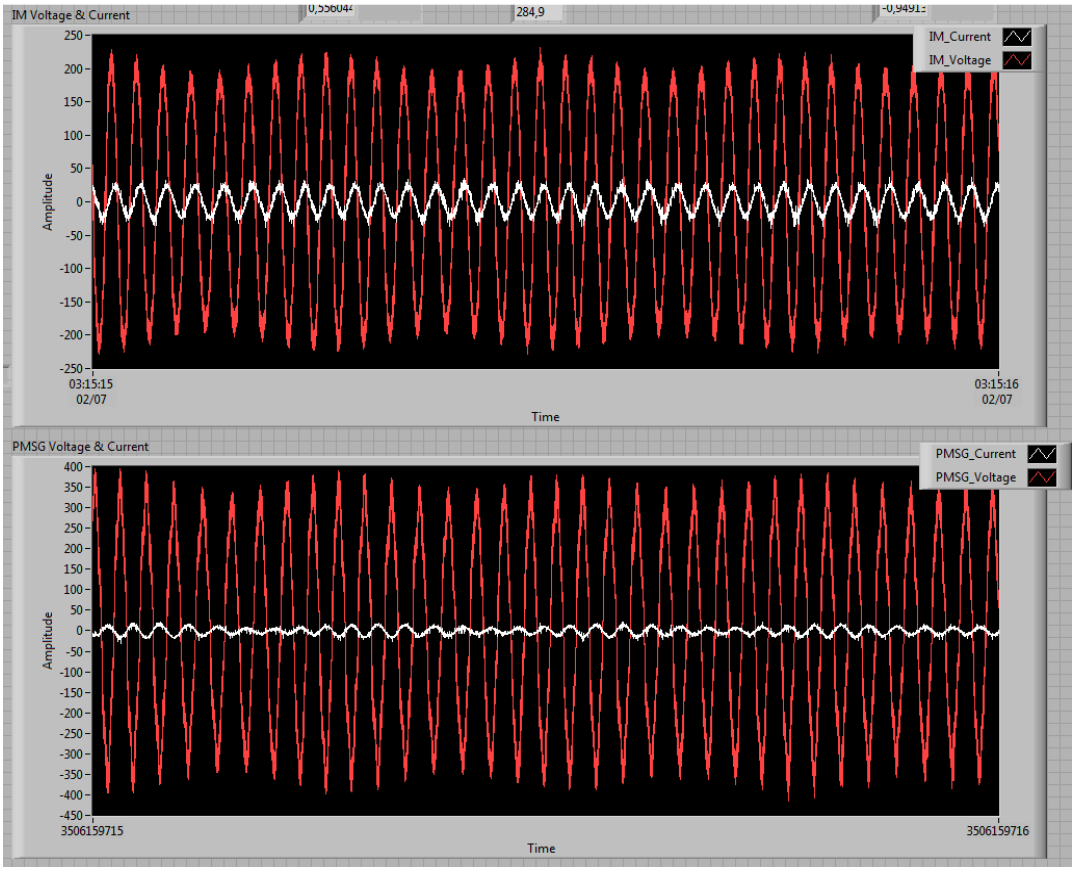

Figure 3.33 Sample voltage and current measurement at the phases of IM and PMSG

3.5.1. Turbine Power Characteristics of Wind Turbine Simulator and HIL Emulator

To compare a wind energy conversion system software and hardware simulator, it is reasonable to start with turbine power characteristics. Turbine power characteristics means the output power of the turbine for different wind speeds and shaft speeds (pitch angle is assumed to be constant and zero for this study). To extract the output power characteristics, the wind turbine model in the software simulator and the HIL emulator is run until its rated wind speed (which is 12 m/s for our system) and until its rated shaft speed (which is 1 in p.u for the software simulator and 750 rpm for the hardware emulator). The output power of the simulator has been drawn at the Simulink as seen in Figure 3.34 (the blue lines belong to software simulator). Then, the same operation has been applied to the HIL setup and the output power has been saved at the Labview platform by using 'Write to Measurement File'. The recorded values have been marked in Figure 3.34 as 'stars'. As seen in Figure 3.34, the simulator and emulator values are compatible although there are slight errors (maximum 8% difference between the simulator and the emulator). The errors are thought to occur due to the slowness of the developed ModBus Communication interface.

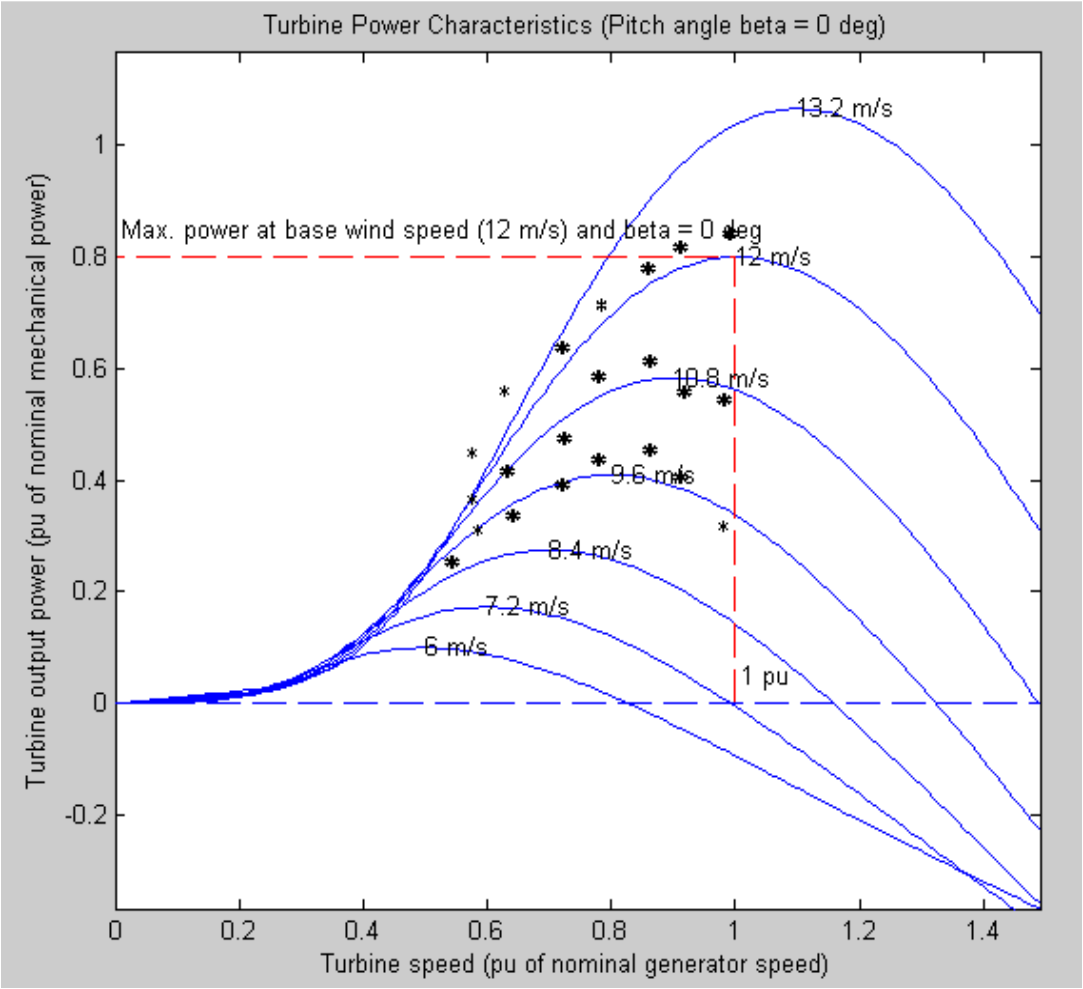

Figure 3.34 Output power and shaft speed for wind turbine simulator and HIL emulator (blue lines represents the output power of the software simulator while stars express the output characteristics of the HIL emulator)

3.5.2. Output Power of PMSG and Regenerative Drive for Software Simulator and HIL Emulator

By using Labview interface, power outputs of the PMSG and grid side converter has been gathered and tabulated in

Table 3.4, which is located at the end of the Chapter 3. If the table is analyzed, it is seen that PMSG output power at the HIL setup and at the software simulator are

similar. If the regenerative drive output power is analyzed, it is seen that values are compatible for especially at middle speed 300-500 rpm (frequencies of 20-33.3 Hz). At the tip points of the operation (for low and high frequencies of 0-6.67 and 46.6-50 Hz) the error is increased up to 54%. This analysis is also done at the neural network section. For a good neural net study, the datas used for the training of the neural network should pass the rated values. In other words, if the rated speed of the system is 750 rpm, the power outputs at 900 or 1000 rpm should be passed to neural network training algorithm to get a better fit.

3.5.3. MPPT Controller Performance at Step Changes of Wind Speed for Software Simulator and HIL Emulator

To see the performance of the MPPT controller and the wind turbine model, a wind profile which changes in a step response is applied both to the simulator and the HIL emulator. A wind profile is set, which changes for every 5 seconds in a step waveform. The start of the wind speed is 8 m/s from 0 to 5 seconds. From the turbine characteristics, the optimal speed can be calculated as multiplying the ratio of the instantaneous wind speed to base wind speed with rated speed (base speed) of the generator. For 8 m/s wind speed, the optimal shaft speed is 500 rpm [(8m/s / 12 m/s)*750rpm=500rpm]. It should be noted that rotating speed of 500 rpm is an enormous speed for a real-sized wind turbine. For the HIL study, the rated speed is selected as being 750 rpm. However, it can be changed as 75 rpm both in simulator and at the HIL emulator if desired. The wind speed is changed continuosly for each 5 seconds from 8 to 11.2, then 11.2 to 6.4 and lastly 6.4 to 9.6 m/s. When the wind profile shown in Figure 3.35 has been applied, the shaft speed is controlled to be in the software simulator as in Figure 3.35. It is known that for a wind speed of 11.2 m/s the optimal speed is 700rpm, for 6.4 m/s it is 400 and for 9.6 m/s it is 600 rpm. Thus, it can be expressed that the MPPT controller works well at the software simulator.

If the same profile is applied to the HIL emulator, the wind profile is obtained as in Figure 3.36. As seen in both graphs, the responses are almost same except the

overshoots at the settling point of the shaft speed. Overshoots at the software simulator keeps lower than 20rpm. However, the overshoots at the settling instant for HIL emulator reach to 50rpm. It should be noted that the overshoot is inevitable due to response of the controller. However, the differences of 30 rpm is thought to come from the response time of the ModBus interface. The developed ModBus interface is prepared at the Labview platform. It responses barely slower than 50 ms (which reaches sometimes to 75 ms). Thus, the true reference cannot be reached to the AC drives and the overshoot increases for that moment. This can be solved by developing a new interface at a different platform such as Visual, Matlab etc.

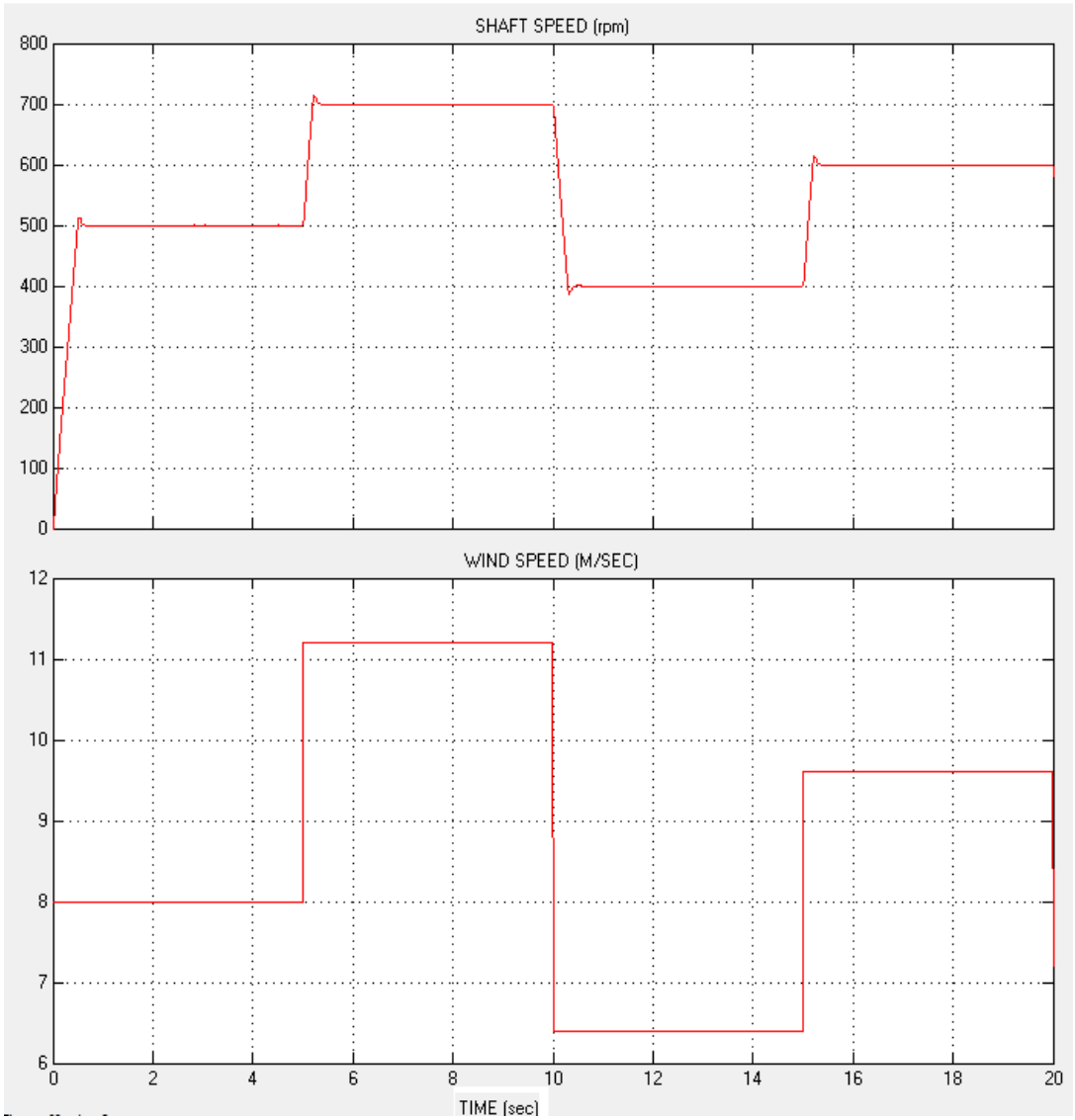

Figure 3.35 Software simulator shaft speed output when a wind speed with step changes has been applied

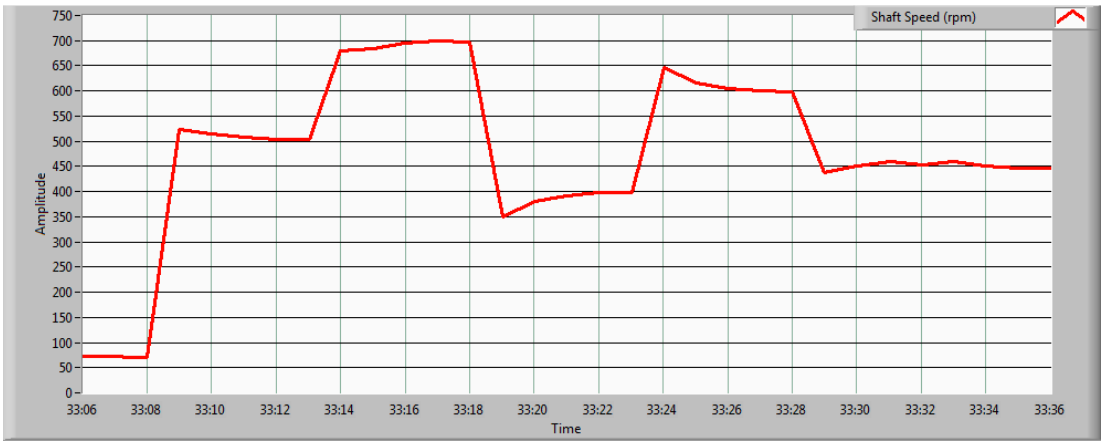

Figure 3.36 HIL emulator shaft speed output when a wind speed with step changes has been applied

3.5.4. Net Output Power of Software Simulator and HIL Emulator

When the wind profile shown in Figure 3.35 is applied again to both platforms, the output powers seen in Figure 3.37 and Figure 3.38 have been obtained. If the graphs and Table 3.3 are examined in detail, it can be said that the output power is almost same except the wind speed of 8 m/s. The performance of the software simulator can be approached to the HIL emulator by increasing the sample number for the training of the neural network. It can be said that neural network mainly shows the characteristics of the HIL emulator converters from the perspective of output power. This result is thought to be enough for the scope of this study.

Table 3.3 Comparison of output powers of software simulator (SS) and HIL emulator

Wind Speed (m/s)	**Output Power in Software Simulator (kW)**	**Output Power in HIL Emulator (kW)**	**Difference between SS and HIL (%)**
6.4	1	0.95	5
8	1.25	1.7	26
9.6	3.02	2.9	3.9
11.2	4.06	4.3	5.5

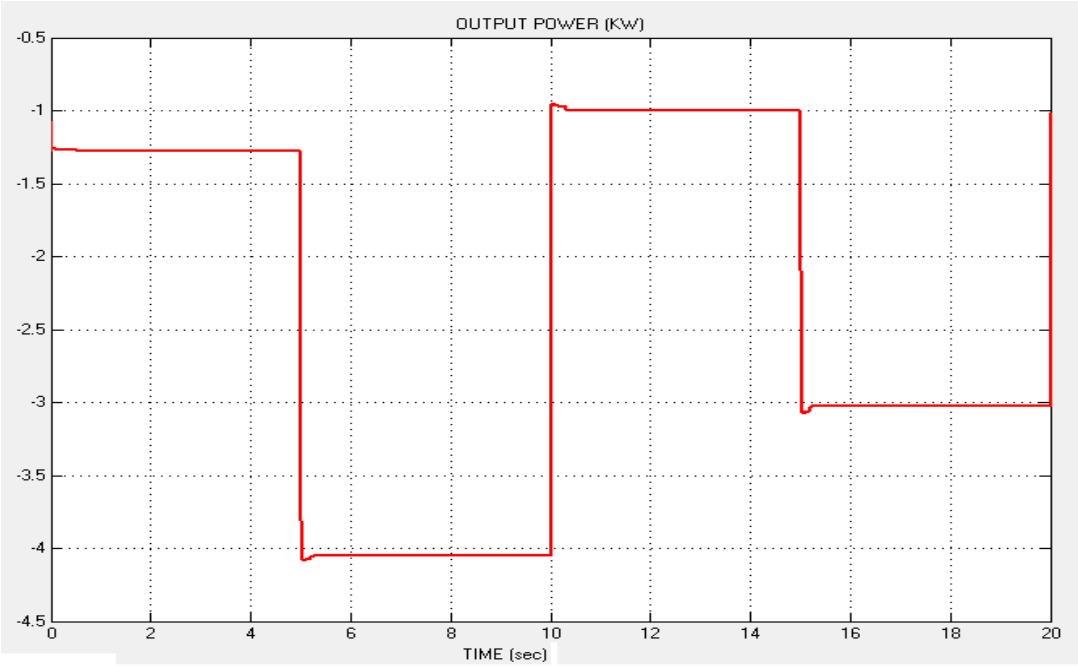

Figure 3.37 Output power at the software simulator according to wind profile in Figure 3.35

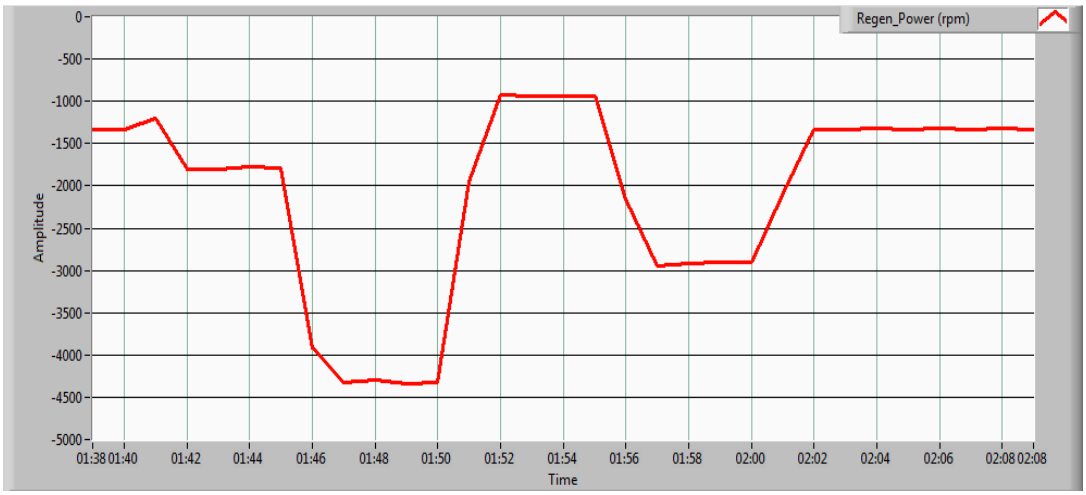

Figure 3.38 Output power at the HIL emulator according to wind profile in Figure 3.35

3.6. Conclusion to the Chapter 3

Hardware-in-the-loop systems can give the results of a wind turbine if the parameters are compatible. Since the HIL setup constitutes from many physical components, the sample times of the controllers, its delay and time constant of the inertias should be taken into consideration to have a consistent software and hardware which emulates wind energy conversion system. The differences between HIL setup and the software simulator can be eliminated with the developments in artificial neural networks; however, there are still some differences due to lack of the neural network including all operation range. To operate software simulator and wind turbine emulator closely, neural networks should be trained more and more data for training, validation and verification should be supplied by the user. In addition, it is seen that the ModBus interface of the software simulator responses slower than expected. The interface can be upgraded at Labview platform or developed in a different platform such as Microsoft Visual, Matlab to approach the results of the software simulator and hardware-in-the-loop emulator.

Table 3.4 Power measurement from the HIL setup and comparison between simulator and the HIL emulator

				Measurements from Test Setup		Measurements from Simulation		Comparison	
Load (% of rated)	PMSG Speed (rpm) (Magtrol)	PMSG Torque (Nm) (Magtrol)	PMSG Input Power (W) (Magtrol)	PMSG Output Power (W) (Hioki 3194)	Regen Drive Output Power (W) (Hioki 3184)	PMSG Output Power (W) (Matlab)	Regen_Neural_Net Output Power (W) (Matlab)	PMSG Error (%)	Regen Error (%)
20	130	33,2	450	410	260	395	245	3,66	3,66
40	130	64,5	880	750	570	710	540	5,33	4,00
60	130	96	1310	1040	790	990	720	4,81	6,73
80	130	125,9	1710	1240	910	1140	830	8,06	6,45
20	300	33,56	1056	980	830	975	825	0,51	0,51
40	300	65,3	2050	1880	1700	1850	1680	1,60	1,06
60	300	96,35	3030	2700	2450	2650	2390	1,85	2,22
80	300	126,3	3970	3450	3120	3330	3050	3,48	2,03
20	500	33,8	1770	1645	1500	1650	1505	-0,30	-0,30
40	500	65,5	3430	3200	3020	3180	2670	0,63	10,94
60	500	96,7	5060	4680	4440	4620	4520	1,28	-1,71
80	500	126	6600	6000	5680	5970	5675	0,50	0,08
20	700	33,93	2489	2320	2170	2300	2400	0,86	-9,91
40	700	65,6	4800	4520	4340	4510	4320	0,22	0,44
60	700	95,05	6970	6480	6230	6500	6240	-0,31	-0,15
80	700	123,7	9070	8350	8030	8370	5950	-0,24	24,91
100	700	150,8	11060	10010	9600	10050	4160	-0,40	54,35

CHAPTER 4

INTEGRATION PROBLEMS OF WIND ENERGY GENERATOR TO THE GRID AND SEAMLESS OPERATION IN ISLANDING MODE

In this chapter, operation of wind turbines when they are disconnected from the grid (islanding operation) has been investigated. Since the seamless operation in islanding mode and reconnection to the grid of the wind turbines is a branch of the smart grid control, the chapter starts with a brief description of smart grid. Distributed generation (DG) which is the integral part of the smart grid systems has been detailed with “pros” and “cons”. The islanding operation which is gaining attention with the increasing employment of the renewables is simulated in the software through a case study. It should be noted that the software simulator is established according to the HIL setup. Results obtained through software simulator are, thus, said to be compatible with the HIL setup. Since the HIL setup is rated at 10kW, the tests conducted on the software simulator are small scale examples of a real-sized wind turbine. The results obtained from the simulator are discussed and the control strategies have been presented for a 10kW wind turbine generation system. Scaling of the simulator to a real-sized turbine is beyond the scope of this study. This will be studied in the future work.

4.1. Smart Grid

Increasing technology and population results in high energy demand. World energy demand has increased 33% between 2000 and 2012 [35]. Although the demand increases, running out of fossil fuels that are the main sources of the energy at the instant with the ratio of 93% leads the people to benefit from renewable energy sources. After 1970s, there is an increasing interest to renewable energy sources, in fact mostly to wind energy. Utilizing renewable energy sources may be the key to solve the ever-increasing demand since these energy sources are naturally replenished. Furthermore, using fossil fuels cause extreme climate changes due to increasing rate of carbon in the atmosphere while renewable energy sources emits no carbon gases or so little amount compared to fossil fuels. In addition, amount of the total fossil energy decreases day-to-day and the future prospect about the lifetime of fossils are declared to end within 55 years. To sum up the topic, renewable energy sources are advantageous due to 1) being replenished naturally, 2) decreased carbon emission, 3) sustainability. Thanks to these benefits, direction of world energy market has been averted to the renewable energy sources.

Renewable energy sources can be utilized within different forms; wind energy, solar, biomass etc. Since these sources have no ownership to any country, all the countries can establish their renewable energy systems. Indeed, all the people can exploit these energy sources. However, such an increase of energy sources creates some problems like grid integration. Many small energy sources can be tied to the national grid; however, they should be limited with the grid codes to ensure the power quality and grid integration. These problems are thought to be solved via smart grid operation in the last years. Simply stated, smart grid can be stated as monitoring the producer and the customer and presenting effective control strategies to improve the efficiency, economics, reliability and sustainability of the production of electricity [36].

Smart grid aims to create a technological electricity network to supply flexibility, accessibility, reliability and economics for both producers and customers. Smart grids assure enhancing power systems by using modern communications and the

control techniques that are more robust, efficient and reliable. There can be a comparison between traditional grid and smart grid to understand better [38].

Table 4.1 Comparison between traditional and smart grid [38]

Traditional Grid	**Smart Grid**
Mostly electromechanical	Digital in nature
One-way communication	Two-way communication
Mostly centralized generation	Distributed generation
Lack of control	Robust control technology
Failures and blackouts	Adaptive and intelligent
Less-energy efficient	Energy efficient
Hard to integrate RE	Possible to integrate large-scale RE

Smart grids can be summarized with three characteristics for the time being: 1) variability, 2) high initial cost and 3) distributed generation.

Since the idea of smart grid is taking attention with the increasing demand to renewable energy, it should control supply and demand for all the time. Wind and solar energy are dependent on an ever-fluctuating resource (the wind and sun, respectively). To ensure the electrical supply, efforts are required to ensure that electricity sources or electricity demands is available that is able to absorb this variability [37].

Smart grid seems to increase the efficiency of the power quality. However, establishing a smart grid is highly expensive when compared to traditional grid. This is noticeably weak point of the smart grid systems. Since the system requires modern technology, high communication techniques/protocols and smart control techniques, cost of the investment is increased. However, it is said to be amortized due to

increased production. Although the statistics prove that smart grid is beneficial for the long term, most investors still keep their position at the traditional grid.

Smart grid can be also said as the consequence of the distributed generation. Since the renewable energy is in use for all the people and countries, it is anticipated that everyone can utilize this energy. In fact, it is thought that everybody will have its energy sources in one day. Due to these reasons distributed generation is estimated to increase with an exponential rate for the future. Thus, smart grid strategies and control techniques should always be developed and updated. In the next section, why distributed generation should be preferred and what are the impacts and lacks of it will be detailed.

4.2. Distributed Generation

Distributed generation can be stated as the generation of electricity from many small energy sources and is located closer to the user, or customer. The purpose of using distributed generation is to improve voltage profile voltage stability and to minimize power losses [39]. The distinction between central and distributed generation can be seen in Figure 4.1. While central generation systems consist of large power stations, distributed generation comprises of many small energy sources such as solar, fuel cell, wind etc. Distributed generation can be thought of a distinct source for the specific user. However, distributed generation is established to connect the grid usually. Thus, it cannot be thought of centrally dispatched for all the time. It is established closer to the user and mainly it power sup the customer on-site and support distribution system by using excess power. Distributed generation is important due to increased awareness with employment of renewable energy sources. Hence, DG should be investigated from all the perspectives: benefits, impacts and problems.

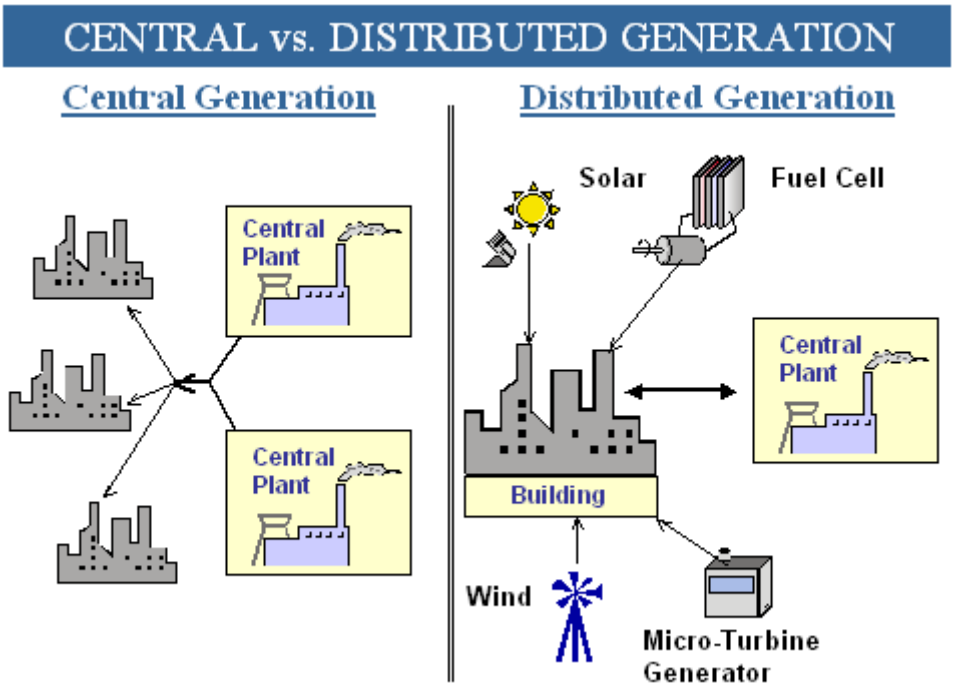

Figure 4.1 Central and distributed generation (source: teachengineering.org)

Distributed generation comes out with several benefits. Firstly, DG makes up the deficiency of large power grid. That is, DG can support emergency power at a moment of shortage. Doing that, power grid flexibility and reliability is increased. Secondly, DGs can be built up without needing power transformers and distribution station. Simply stated, DGs reduce transmission and distribution investment for the investors and so high initial cost is eliminated. Not using transmission system results in decreased line losses and electromagnetic pollution of HV transmission, too. Thirdly, DGs enable power generation with high efficiency reaching up to 95%. It also allows utilizing clean energy and the renewables. For the final benefit, it can be said DGs break the power 'monopoly'. Since the power production and supply is achieved with lower costs, many small investors could participate in the competition. Increasing number of investors can realize the power industry market and so break the monopoly.

Increasing number of distributed generation can also improve the efficiency and economics; however, this will also impact the system from many perspectives. Firstly, there will be an effect on the system voltage. Increased DG capacity at power system will affect the system voltage due to short circuit currents and active and reactive power flows. Secondly, protection of the grid can be weakened. There will be no longer unilaterally current flow. Uncertainty in the power flow results in increased difficulty for power system protection. Thirdly, increased number of DG also propagates number of power electronic devices, capacitors, inductors. For the last, the grid planning may be challenging with large number of DGs. That is, there will be a need to emergence of load forecasting. Since there are many renewables, operation of DGs will be harder and it will also get uncertainty in planning. Smart grid operators are forced to find out optimal network layout.

DGs emerge with some problems. For the first, lack of appropriate laws and regulations can be said. Appropriate technical standards should be set and relevant laws should be established. For the second, lack of previous search can be expressed. That is, since DG is a new topic, there are several subjects that should be investigated. Subjects can be sequenced as protection and control of DG power system, reliability of electronic equipment, structure mode of microgrids (MG) and operation control technologies. Since DGs introduce many research areas, we can manage to solve some issues which are popular for the moment. Islanding is one of the issues for DGs operating at stand-alone. The detailed analysis of islanding operation and its technique will be conducted at the upcoming section.

4.3. Islanding Operation

Islanding operation can be stated as to power up a location even though grid is disconnected from the electric utility (such as wind, solar etc.). Islanding operation can be thought of an operation condition of a microgrid. Normally, as illustrated in "Distributed Generation" chapter, microgrids are usually connected to the grid. However, in some cases, it can be isolated from the grid and forced to power the systems, that is islanding. Islanding is normally accepted as a dangerous operation

due to high surge currents and dangerous conditions for the grid. Thus, there are several techniques developed to stop the production of the power, which is called as anti-islanding.

To start anti-islanding, there are several islanding detection methods to understand whether grid is disconnected or not. Anti-islanding operation is activated to avoid dangerous conditions. Firstly, there are safety concerns for working crews upon the clearance of the fault. Since an island (stand-alone operated microgrid) is formed, there are live wires and crews can meet up with unexpected conditions. Secondly, end-user equipments can experience damages if the islanding operation differs the norm or grid codes. Thirdly, reclosing onto an active island may cause confusion among the inverters and the grid side converters can be damaged. Due to these results, islanding detection methods are a new subject that should be investigated.

For detection of islanding, under/over voltage and frequency are the commonly used techniques. However, these techniques can result in faulty operation. To exemplify, starting of a motor can distort the frequency and voltage at the same time and islanding detection algorithm can result in a wrong situation and disconnect the grid. Different from these, there are also other techniques like rate of change of frequency (ROCOF), voltage phase jump and harmonics detection.

In this thesis, islanding operation has been studied. In the study, a new detection method has been proposed. At the next chapters, this operation will be detailed.

4.4. Case Study: Intentional Islanding

Intentional islanding means to supply power to the local loads even if the generator is disconnected from the grid. This operation is mostly used as a backup power for the systems who sell their excess power to the grid. The usual practice is to stop the wind turbine when there is an interruption in the grid power (anti-islanding). However, in this case, the study here investigates whether the local loads can be provided with

power available in the local generator while preserving power quality and satisfying grid code requirements.

Case study is defined as: A farm house (local load) requiring 10kW peak power is connected to the grid as shown in Figure 4.2. All the required power is supplied from a 10kW turbine and if there is a surplus in the generated power, it is sold to the central grid. While turbine is producing power more than the local loads need, the turbine is isolated from the central grid intentionally. What should have been done to continue operation of power generation without damage to any equipment and the loads?

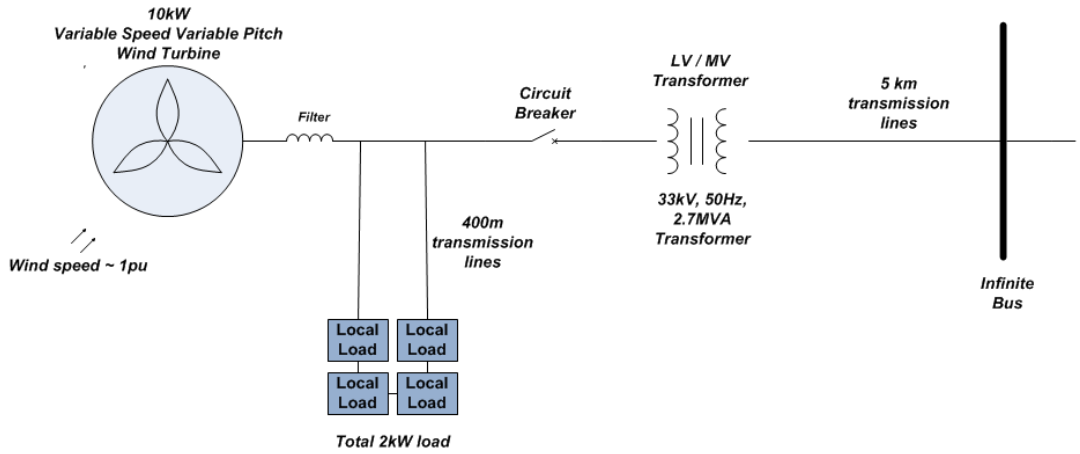

Figure 4.2 Schematic of the case study

In this chapter, this study will be imitated in the software simulator. Setting up the grid connection accordingly with the transmission system (transmission cables, breakers, transformers), the control strategies used in the wind energy conversion systems (braking chopper, MPPT and pitch control) will be compared. While the comparison is made, the load voltage and the frequency will be observed. Torque and speed of the turbine while turbine is operated at islanding mode will be identified and the effects on the load voltage will be shown. Before starting the islanding operation, test system (turbine model, transmission lines, tranformes, loads etc.) is explained in the upcoming section.

4.4.1. Test System

Test system has been set up accordingly with the HIL setup. The test system is included wind turbine emulator, generator, back-to-back converters and grid connection.

The wind turbine model has been explained in section 2.2.2 in detail. This model has been realized in the laboratory by an induction motor via supplying torque to the shaft to emulate the wind turbine. The wind turbine which is emulated in the software simulator is a 11kW wind turbine. It should be noted that the software simulator is set up to imitate the characteristics of both HIL setup and a small scale wind turbine. Thus, the wind turbine is selected to be as 11 kW, which is the rating of the induction machine in the HIL setup. This turbine is included with two controllers: MPPT and pitch controllers. Both pitch and MPPT controllers are detailed in section 2.2.6.1 and 2.2.6.3 respectively.

For the generator, the one which is used in the HIL setup has been utilized as well. Rating of the generator is again 11kW, which is the rating of the test system. The generator has been modeled in synchronous reference frame in section 2.2.3 in detail. However, this model has used many assumptions and ignored dynamic conditions. Thus, the loss of the generator is modeled in section 3.2.2. In addition, drive of the rotor side converter (drive of the generator) has been modeled in neural network to make closer the software simulator to the HIL setup. In the HIL setup, both electrical and mechanical model parameters have been measured with many different tests. Then, the model which is created in Matlab/Simulink has been used to model generator in the HIL setup.

The software simulator also includes back-to-back converters and its filters. For the back-to-back converters, an AC/DC/AC converter has been set up in the simulator. The AC voltage generated in the generator termianls has been rectified to DC voltage. This voltage has been stored to DC link capacitors. The DC link capacitors have been selected as 2 mF, which is the value used in HIL setup as well. The grid

side converter will be detailed in section 4.4.3. Thus, it is not explained here. To filter out harmonics occurred at the PWM frequency has been discarded via LCL filters. The values of the LCL filters have been set accordingly with the HIL setup as well. By this way, results of the HIL setup and software simulator is thought to be similar.

The wind turbine is synchronized to the low voltage system, which is 400 VAC line-to-line voltage. The generated power of the turbine has been transmitted to the national grid by a transformer. Transformer is a step-up transformer which raises 400 VAC to the 33 kVAC, that is the medium level voltage for the national grid. In the case study, it is thought to be farm houses which are powered at the level of low voltage. Thus, the local loads have been connected between the wind turbine and the MV/LV step-up transformer.

Low voltage side is connected as star and the star point has been directly tied to the ground of the turbine [61]. Medium voltage side is connected as delta configuration and the ground reference has been from the star point of the MV/LV. The selected transformer is a 50 Hz, 33 kV, 2.7 MVA delta/wye transformer. The datasheet of the transformer can be seen in [67] as well.

In the application of wind energy conversion systems, the distance between the turbines at the MV central grid changes generally from 400m to 600m. The maximum distance to the high voltage switchyard is said to be 5km [59]. In most applications, the wind turbines are located in a 5km radius of the area of high voltage switchyard. In the medium voltage lines cables are generally used. In recent applications cables which have aluminum conductors are used. Generally, cross-section of 120 mm^2 cables are used for one turbine, 185 mm^2 for more than three turbines and 300 mm^2 for the big wind farms containing more than 10 turbines. Since we model only one turbine, the cable with the cross-sectional are of 120 mm^2 has been used. Transmission line to the infinite bus is modeled to be 5 km. Local loads have been connected with a 400 m cable as well [60]. Line inductances are set accordingly with 120 mm^2 cables which is given in [68].

36kV, 16kA SF_6 gas breakers are used at the feeders of the central of medium voltage. Rarely vacuum breakers are used at those feeders. These breakers are thought to clear the faults at the 300ms, and sometimes at the 100ms as well. In the simulator, SF_6 gas breaker is modeled via 3 breakers considering the breaker resistance and snubber resistances and capacitances for each breaker as seen in Figure 4.3, both simulink and electrical model can be seen. Breaker and snubber resistances are respectively 0.01 Ω and 1 MΩ. However, in this case study, there is no fault scenario. On the other hand, turbine is intentionally isolated from the grid. Thus, effect of the breaker (clearance of the fault) cannot be seen in the simulator.

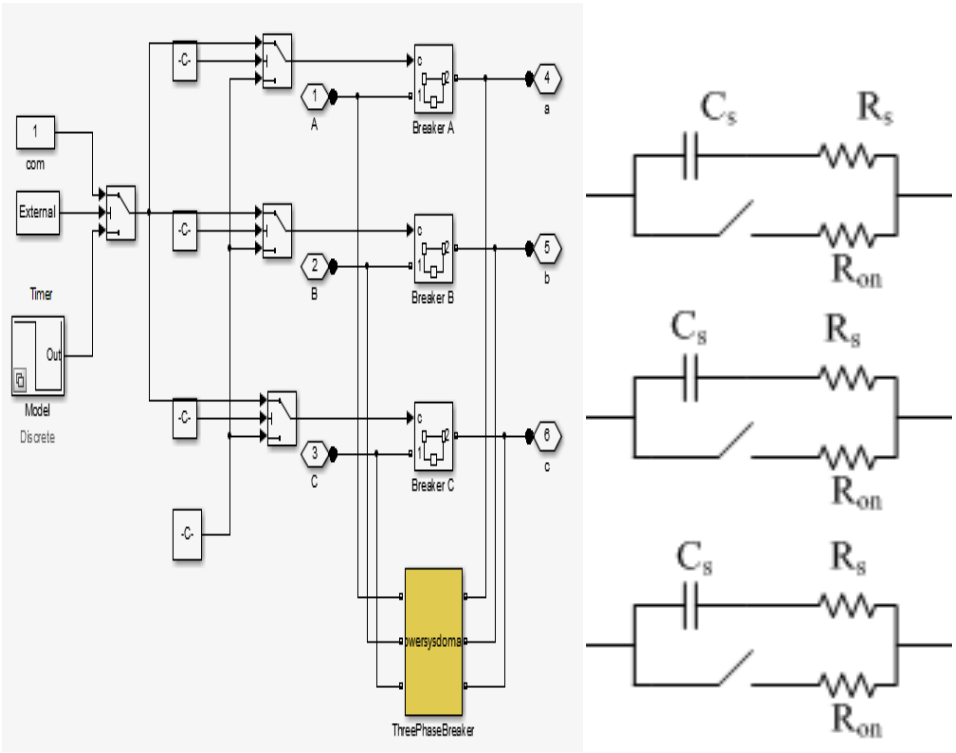

(a) (b)

Figure 4.3 (a) Three-phase breaker model in Simulink, (b) Electrical model of the three phase breaker

Grid connection of the software simulator can be seen in Figure 4.4. All the models used in the software simulator is obtained from Simulink. In Figure 4.4, electrical

model is also given. As seen in electrical model, the wind turbine is grid connected with resistive local loads (which is 1 kW for this case study) at the PCC (rightmost of the electrical model of Figure 4.4). Local loads are connected to the primary side of the transformer with three-phase breakers. These breakers are modeled with on-resistances, breaker resistance and snubbers. The values of the breaker is given at the previous paragraph. For the transformer, a delta/wye transformer is used. The transformer is modeled taking into consideration of phase resistances and inductances of both primary and secondary side and magnetization resistance and inductance. Secondary side of the transformer is wye connected and the star point is grounded. Then, a transmission line which is about to be 5 km has been modeled again in Simulink. Transmission line is modeled by entering self and mutual resistances and inductances. It is a balanced transmission line as seen in Figure 4.4. Transmission line also consists of phase capacitances and ground capacitances. These values are calculated by using positive and zero sequence RLC parameters in the model. Grid connection is ended with an infinite bus, which is medium voltage for this case study. The medium voltage is supplied in the model via three-phase source in Simulink. This supply is a balanced voltage source by including X and R values for the three-phase supply. That is, inductance and resistive values are set in the model.

In the software simulator, turbine is isolated from the grid during 1 seconds and then it is connected to the grid again. In the upcoming section, grid codes that a wind turbine should satisfy will be explained if it is grid connected. Grid codes are searched due to having no regulation for the islanding operation. In this study, it is aimed to satisfy grid codes even if the wind turbine operates disconnected from the grid. By this way, the wind turbine is aimed to satifsy grid codes whether it is grid connected or not. The safety of the grid is thought to be preserved by following this strategy.

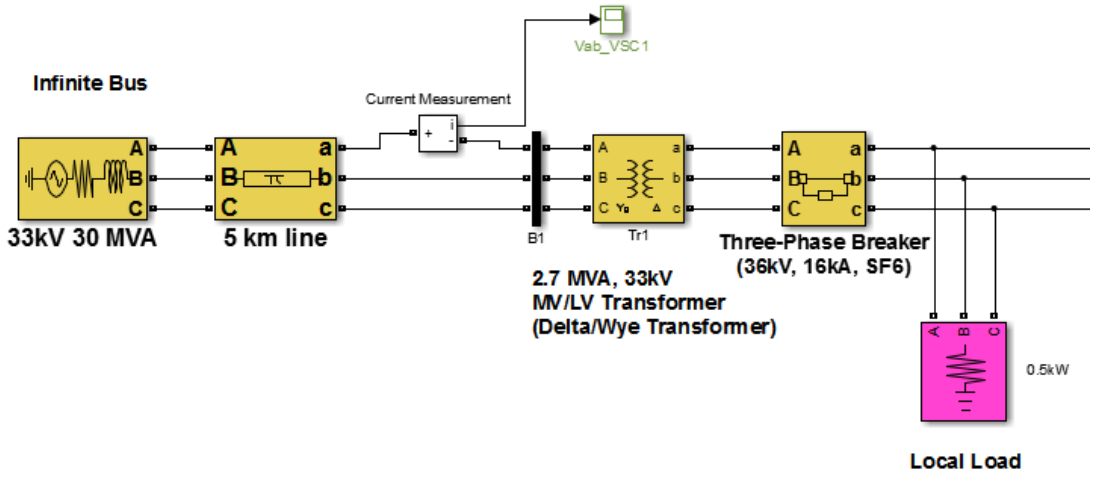

(a)

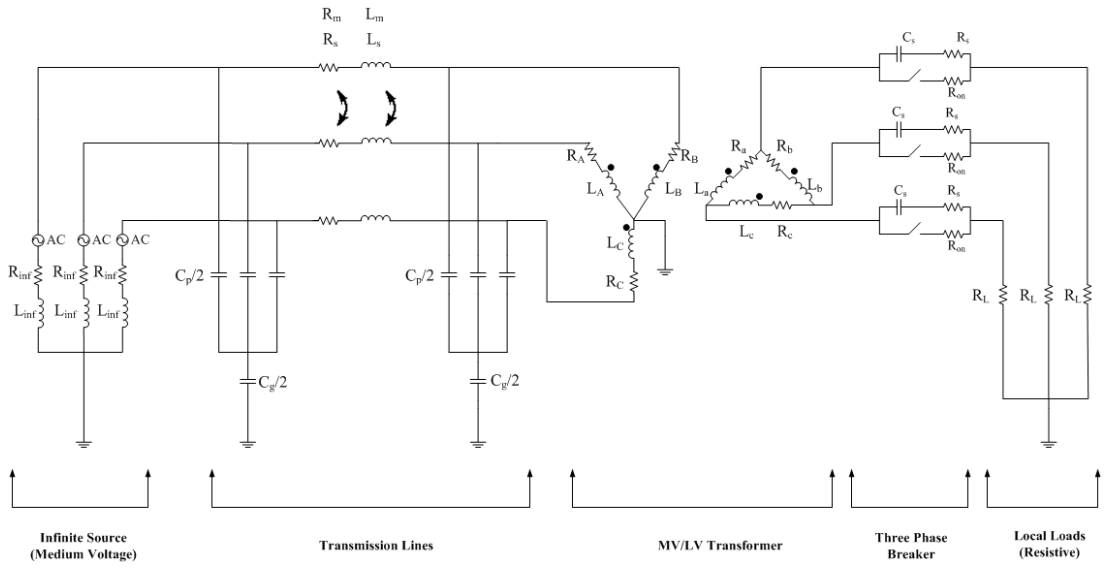

(b)

Figure 4.4 (a) Simulink model of grid connection of the wind turbine, (b) Electrical model of the grid connection

4.4.2. Grid Codes

The increasing demand for the energy makes the customers to lead to new alternative energy sources. Microgrid operation has emerged as a promising option to meet the growing custom needs for electric power with an emphasis on reliability and power quality since it supplements the traditional grid in many aspects. Microgrid creates a flexible operation to the customer since the customer can supply the excess power to the grid when he does not need power such as in the evenings. Moreover, the customer can regulate its power system by providing more stable voltage for the sensitive loads at the microgrid operation [41]. Microgrid operation is essential to increase the utilization of the renewable energy and end the dependence to power of the developing countries.

Microgrid operation can be separated into two modes: grid connected mode and islanding mode. Microgrid owner can either supply power to the grid or disconnect himself from the grid, which is described as islanding, when there is a need for the power. However, passing between the modes causes some control problems. To surpass these problems, the operation of the generators (wind, diesel etc.) were closed when an islanding detection is occurred (islanding detection mechanisms have been clearified at Chapter 4.3) and the power generation has stopped. In 2000s, most grid codes desired to disconnect the generators when there is a fault. However, with the increasing demand and increasing investment, there is no tolerance to stop power generation. Furthermore, the inhabitants located in the vicinity of the generator desire to get power seamlessly. Thus, demand to smart grid has also raised for the smart control of the generators. With the smart grid enterance, microgrids can be directed at the fault conditions. For example, if there is a fault in two of three microgrids which are connected at the same PCC (point of common coupling), the faulty two microgrids can be disconnected from the grid "intentionally" to supply power from the working microgrid to the vicinity of that microgrid. This intentional islanding operation can be stopped at a moment by the smart grid controllers and these three microgrids can be connected to the same PCC again. Due to these connection and

disconnection of the microgrids, the islanding operation should be evaluated. This case study has been conducted due to these issues.

In the case study, the aim is to supply power with a robust frequency and voltage to the end-users whether the microgrid is grid connected or not. Since there is no regulation for the microgrids to obey at the islanding mode, the microgrid should satisfy the requirements of the grid codes of the grid connected mode. With this aim, electric grid regulation of EPDK (Enerji Piyasası Düzenleme Kurulu) [42] has been studied. The requirements of grid regulation are for the wind turbines with installed capacity of 10MW or higher. Eventhough we study for the 10kW wind turbine generator in this case study, we aim to obey the rules. The rules consist of low-voltage fault-ride-through regulations, active power control, frequency response, reactive power capacity and support of reactive power to the grid regulations. In the upcoming subsections, the grid codes which are related to wind turbine conversion systems are explained.

4.4.2.1. Reactive Power Support

In the regulation [42] , voltage fluctuations between ±10% (0.9pu – 1.1 pu) at the PCC are allowable operating conditions and wind energy conversion systems supply reactive power to the grid with the limitations stated in the regulation. Value of the droop is set by TEİAŞ, which is set between 2% and 7%. Droop can be defined as rate of change of reactive power to obtain maximum reactive power excessively excited from 0 to rate of change of voltage from the set value. Figure 4.5 explains "droop" such that there is an allowable range for the grid voltage while reactive power is supplied to the other power stations. While wind turbine systems generate maximum reactive power (Q_{max} and $-Q_{max}$), both the voltage fluctuations should be stay in a range of ±10% and droop value should be stay in the range of TEİAŞ dictates (generally 2% and 7%).

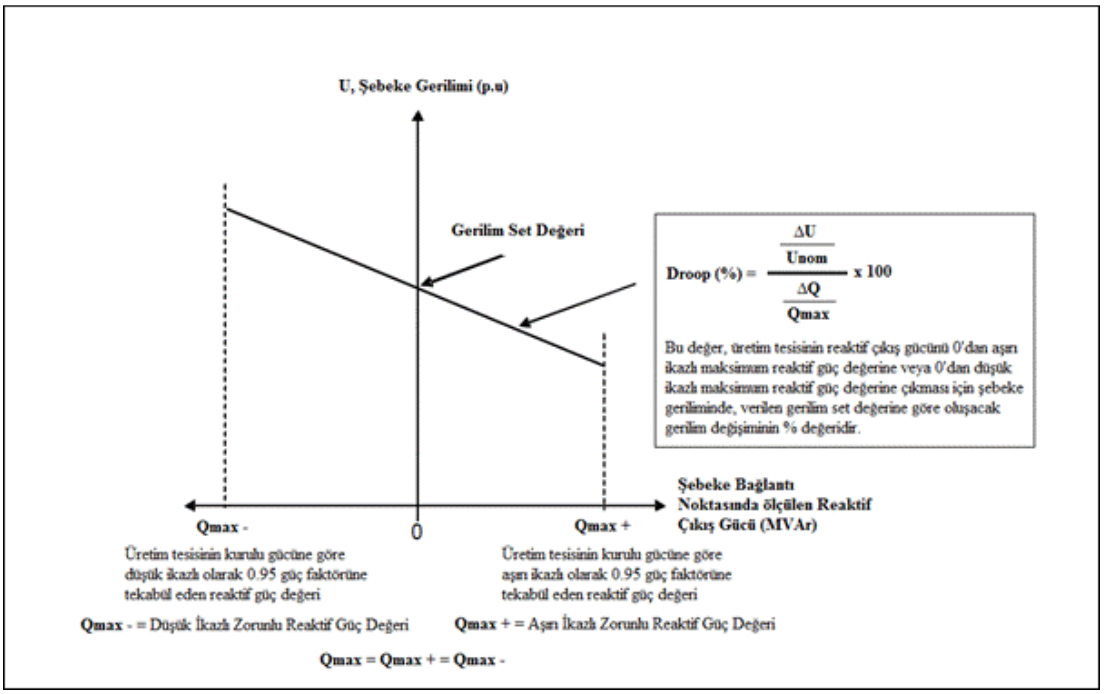

Figure 4.5 Reactive power supply trajectory, which is given to the system by the WECS [42]

4.4.2.2. Frequency Response

In the regulation, wind energy conversion system is desired to give complete available power if the frequency is in the range of 47.5 and 50.3 Hz. If the frequency is above 50.3 Hz, wind station should start to decrease its power generation. If there is an increasing frequency regime at the grid voltage, it means that there is an imbalance on demand-supply chain of electricity. In other words, electricity supply is higher than the demand. Thus, conversion system is controlled according to Figure 4.6. Turbine decreases its power generation with the slope of given in Figure 4.6. Beyond the frequency of 51.5 Hz, wind station should be disconnected not to damage components connected to the grid.

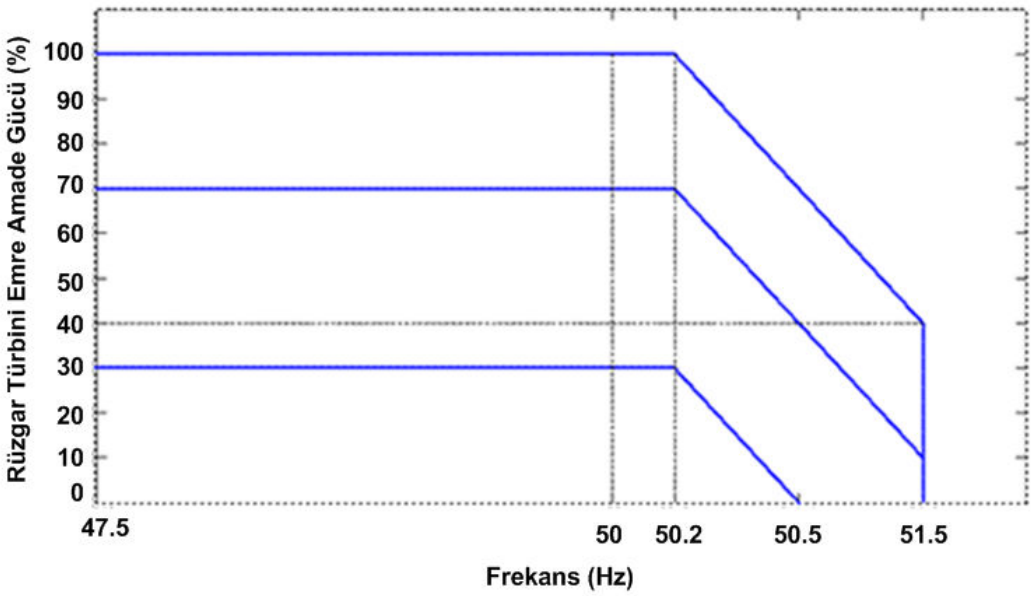

Figure 4.6 Wind turbine power-frequency trajectory [42]

4.4.2.3. Reactive Power Capacity

For the active power control, there is a limitation of 5% to load up for the station with installed capacity of less than 100MW. This regulation applies to us if the HIL setup is grid connected since the system is rated at 10kW. For the reactive power control, there is a trajectory of reactive power versus active power for different power factors as seen in Figure 4.7. If turbine generates power more than 0.1pu, it should support reactive power in case of a grid fault by following the trajectories in Figure 4.7. Trajectories are decided considering power factor of the system (e.g. lower limit for power factor is 0.835). There is no need to supply reactive power if the generated power is below 0.1pu and the power factor is lower than 0.835. In this study, however, the setup is disconnected from the grid. Thus, there is no need to satisfy reactive power capacity requirement for the islanding mode.

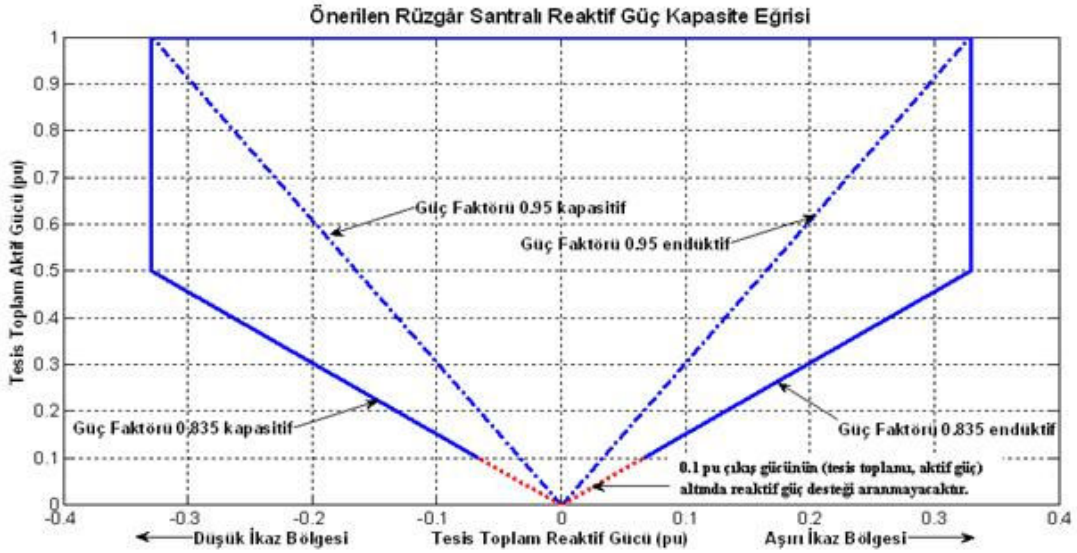

Figure 4.7 Wind station reactive power trajectory [42]

4.4.2.4. Total Harmonic Distortion

Total harmonic distortion in the grid voltage is limited to 8%. There are also some limitations for different numbered harmonics as seen in Table 4.2.

Table 4.2 Harmonic Voltage Compatibility Limit Values for distribution systems below 154kV [42]

Tek Harmonikler (3'ün katı olmayan)		Tek Harmonikler (3'ün katı olan)		Çift Harmonikler	
Harmonik No. "h"	Harmonik Gerilim (%)	Harmonik No. "h"	Harmonik Gerilim (%)	Harmonik No. "h"	Harmonik Gerilim (%)
5 7 11 ≥13	5,0 4,0 3,0 2,5	3 9 15 21	3,0 1,3 0,5 0,5	2 4 ≥6	1,9 1,0 0,5
THB_V:% 8					

Low-voltage fault ride through regulations are not addressed here since there is no operation related to it. When fault-ride through ability of the inverters is searched, this grid code will be analyzed as well.

Grid-side converter should supply voltage with the requirements listed above. However, in the islanding operation, there is no need to supply reactive power support to the grid since it is already disconnected. In the islanding operation, it should be paid attention to voltage fluctuation (0.9pu-1.1pu), frequency reaction and total harmonic distortion not to damage the equipments at the load side. The case study is focused on so that grid-side converter should generate to the grid with the limitations declared above. Thus, before starting the study, control strategy of the HIL system and simulator should be explained to clearify how grid safety and power control will be achieved in the stand alone mode.

4.4.3. Control Strategy of the HIL System & Simulator

For variable speed wind turbine applications, back-to-back converters have been used as explained in Chapter 2. For now, grid side converter of the back-to-back converter is the interest area to control the load side AC voltage at the islanding mode. Grid side converter aims 1) to control DC link, 2) power quality. Grid side converter is mainly established with 1) bridge circuit (two, three or multilevel converter), 2) controller (PWM generator), 3) filters (LC or LCL filter, EMI filter) as seen in Figure 4.8. In Figure 4.8, DC link capacitors decouple the generator side from the grid. The voltage stored in DC link is used by the grid side bridge switches to invert the DC voltage to AC voltage. The control of the switches is established by the main controller. Controller is explained in the next paragraph. In the simulator, controller and switches are selected to be same with the AC regenerative drive used in the HIL setup. The details of the grid side converter can be seen in [54] as well.

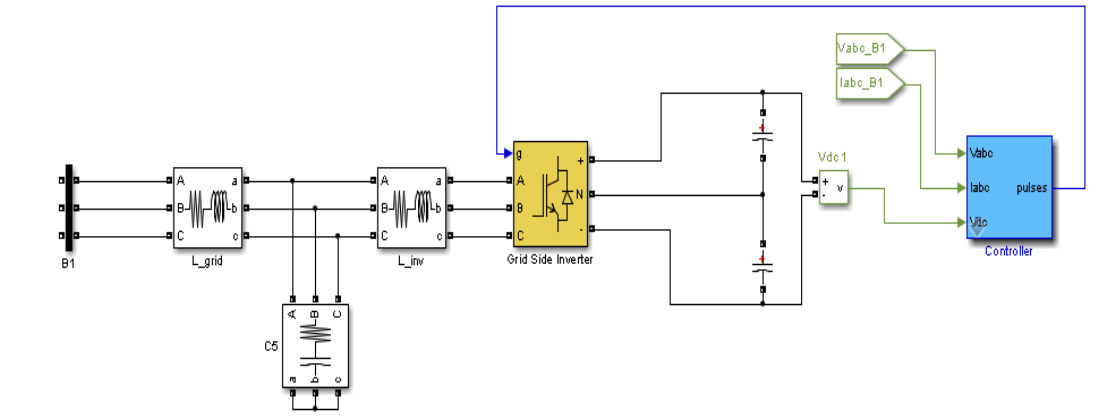

(a)

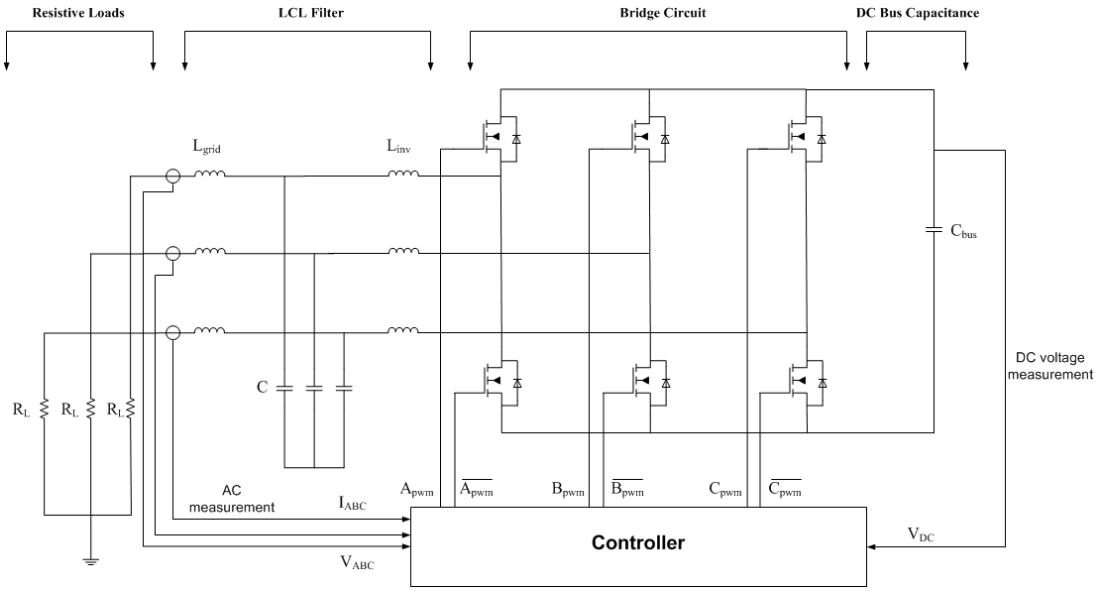

(b)

Figure 4.8 (a) Simulink model of grid side converter, (b) electrical model of the grid side converter

In the simulator, six-pulse IGBT block has been used as bridge element. LCL filter is selected as in HIL setup, that is explained in Chapter 3. Thus, it is not explained here again. The controller of the grid side converter is emphasized in this chapter.

The main issue on the grid side converter is the “controller”. Controller gets voltage and current measurements of the three phase output of the inverter with DC link voltage. Using grid voltage and current values, both synchronization and the power control is achieved. DC link voltage is used to control I_d current and stabilize DC voltage.

Controller mainly consists of three blocks; 1) PLL, 2) current regulator, 3) DC voltage regulator as seen in Figure 4.10. The overall strategy of the controller can be seen in Figure 4.9 as well. In the next sections, three main subblocks of the controller will be explained in detail. The parameters of the subblocks will be given. It should be noted that the software simulator of this controller is established according to HIL setup. Thus, the results are expected to be similar with the HIL setup.

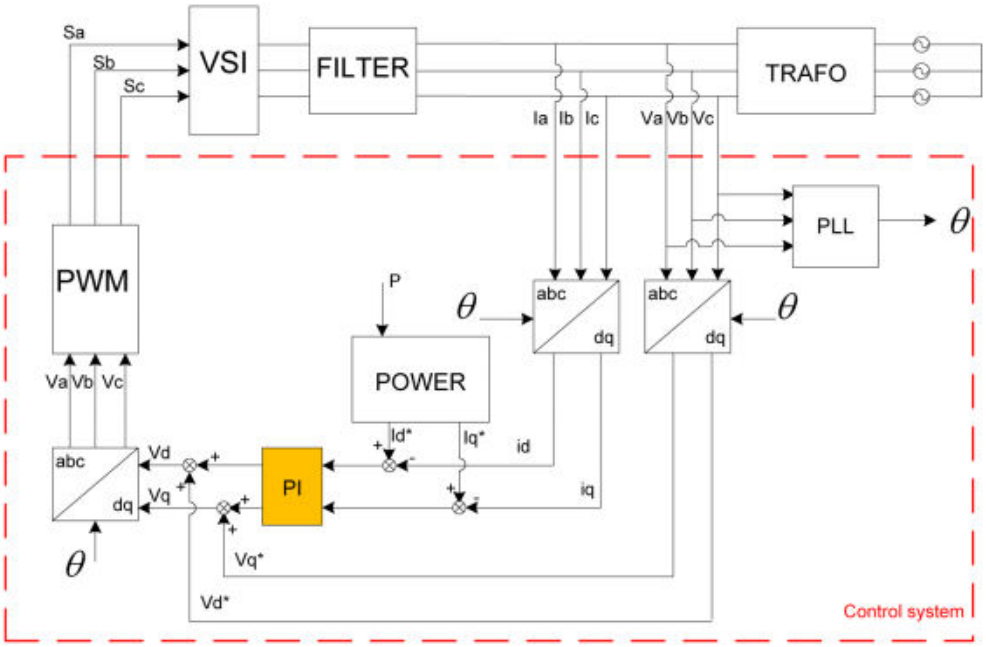

Figure 4.9 Control scheme for the synchronous reference frame controller [43]

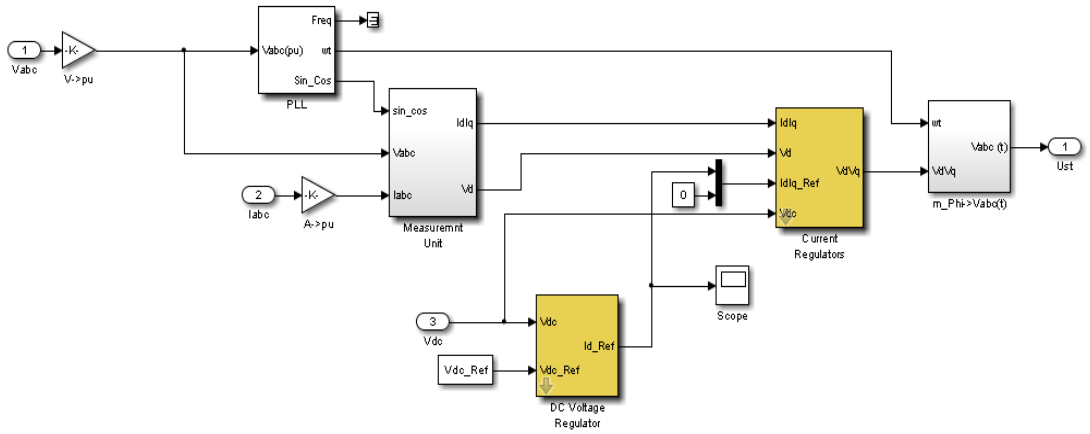

Figure 4.10 Controller of grid side converter realized in Simulink

4.4.3.1. Phase Locked Loop (PLL)

PLL is used to synchronize the wind energy system to national grid system, which is a sinusoidal source at a frequency of 50 Hz. PLL block of the controller generates phase angle of the voltage and frequency of the system. Using phase angle of the grid voltage, both grid voltage and current has been transformed into synchronous reference *dq* frame. Converting to *dq* frame is due to get constant control variables. In PLL block, three phase voltage (abc) has been transformed to dq0 rotating reference frame using Park transformation. To eliminate changes in the grid voltage, automatic gain controller is also used in the PLL block to supply constant phase angle even if the grid voltage changes slightly. PLL block supplies output as frequency and phase angle to transform voltage and current values to dq rotating reference frame.

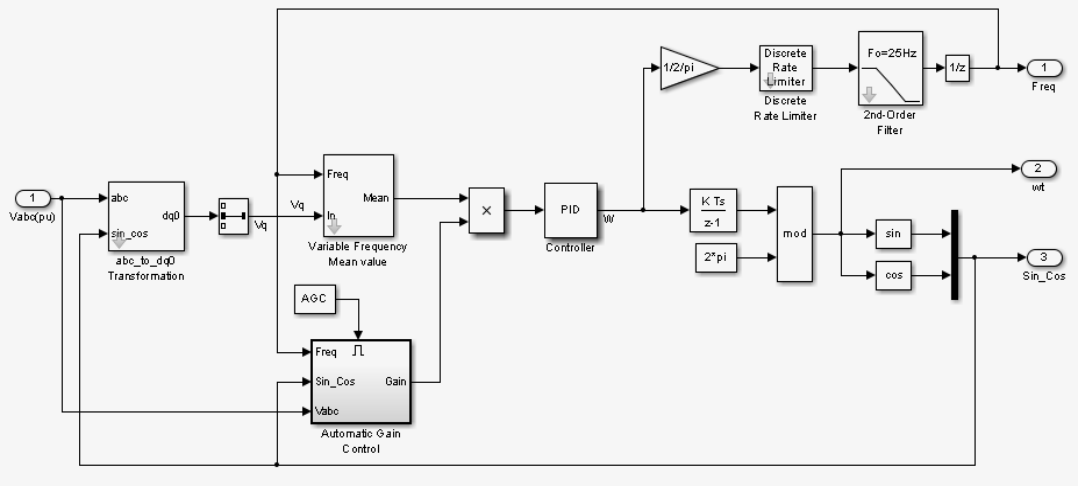

Figure 4.11 PLL block of the controller of the grid side converter

4.4.3.2. DC Voltage Regulator

After converting voltage and currents, DC voltage regulator creates I_d reference to define how much active power should be supplied to the grid to fix DC bus level to the reference value. Active power is controlled directly by means of generator torque and pitch control; however, indirectly through DC link voltage. Keeping the DC link voltage at a constant level assures that the total available active power is transferred to the grid. In the DC voltage regulator block, reference I_d current is determined and sent to the current controller. To summarize, dc voltage regulator determines how much active power should be drawn or delivered to stabilize DC link voltage at the reference value.

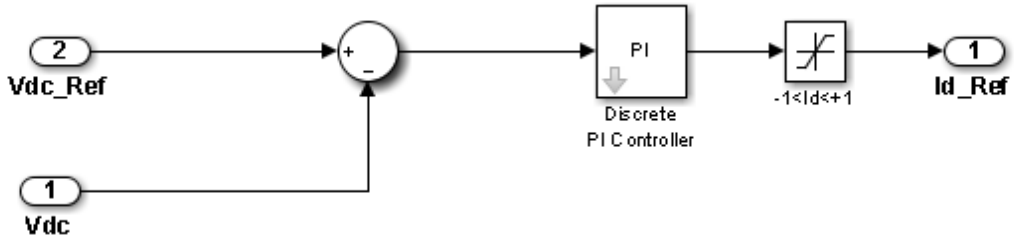

Figure 4.12 DC voltage regulator block of the controller of the grid side converter

4.4.3.3. Current Regulator

Since the DC link completely decouples the reactive power of the generator from the reactive power injected to the grid, the reactive power injected to the grid can be controlled by the grid side converter [17]. For the unity power factor (no reactive power), I_q is set to 0 in the controller. This is due to relation of direct axis and quadrature axis currents. As seen in Equation (4.1) and (4.2), I_d is directly related to active power and I_q is directly related to reactive power. If quadrature axis is set to 0, the reactive power is minimized and the unity power factor is achieved. To summarize, current regulator is used to satisfy unity power factor requirement and supply V_d, V_q references for the PWM switching block.

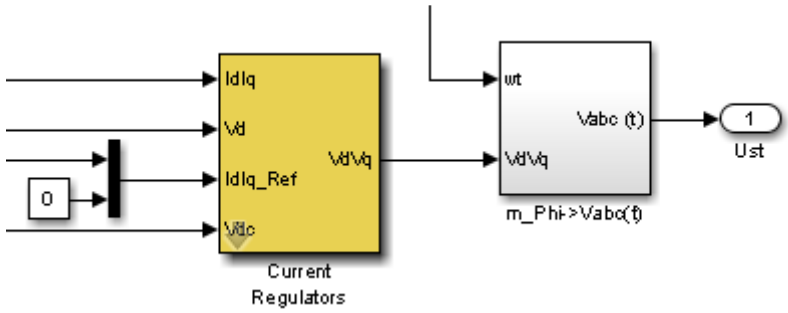

(a)

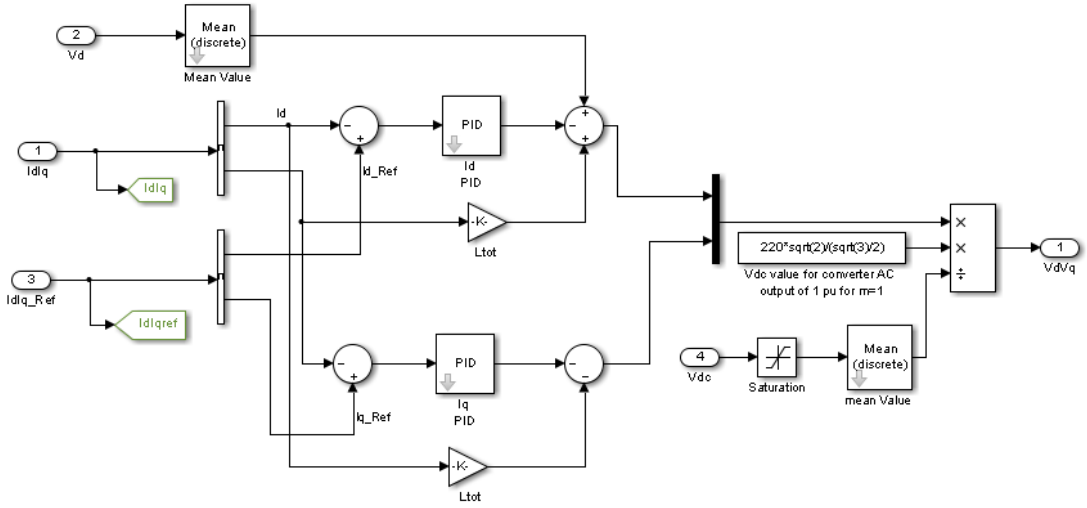

(b)

Figure 4.13 (a) Current regular block, (b) detailed view of the current regulator

Lastly, I_d, I_q and $V_{d,}V_{dc}$ values are used and V_d^*, V_q^* references have been generated as seen in Figure 4.13. These references are converted to three phase square wave switch signals and sent to the switches (IGBT in this case) as gate signals. The overall logic of the controller can be seen in Figure 4.9

$$P = \frac{3}{2}\left(v_d * i_d + v_q * i_q\right) \tag{4.1}$$

$$Q = \frac{3}{2}\left(v_d * i_q + v_q * i_d\right) \tag{4.2}$$

The controller has been realized in MATLAB/Simulink environment. The controller aims to keep DC bus voltage at 600V. The carrier frequency is selected accordingly with the HIL setup. In the HIL setup, switching carrier frequency is selected at 3 kHz firstly. However, in the simulation, it is shown that 3 kHz switching frequency can cause problems at the islanding operation (this is shown in the upcoming section). Thus, switching frequency has been changed to 6 kHz for all the modes (grid connected and microgrid). It should be noted that switching frequency selection is done accordingly with the HIL setup. Control parameters (K_p, K_i) are set again accordingly with the HIL setup (DC voltage regulator K_p = 0.015, K_i = 2.5, current regulator K_p = 0.3, K_i = 5). Thus, it can be said that the software simulator can imitate the characteristics of the grid side converter used in the HIL setup. With this aim, the islanding operation can be simulated in Simulink and the control techniques can be compared. After founding the appropriate control strategy, it will be tested on the HIL setup and efficiency of the strategy will be determined.

4.4.4. Microgrid Operation

Grid connected wind turbine is separated in this case study at a moment. The separation of the microgrid from the grid may be from a fault happened in other microgrids. The case study is started with the conditions of:

- There is a wind flow to the blades with a speed of 9.6 m/s. Wind is constant in this case. Tower shadow and the wind shear effects have been ignored.

- The turbine is connected to 400 V, 50 Hz AC system. In addition, turbine is established in a vicinity of the farm house which needs 1 kW for the moment islanding happened.
- The wind energy conversion system is operating at the steady state conditions. That is, there is no changes in the grid voltage and frequency.
- Turbine has two power controllers and both of them are active. The MPPT controller is following the maximum power by controlling the current of the generator, that is electromagnetic torque. Pitch controller controls whether the generated power is above the limit or not (These controllers will be modified after some observartions have been conducted, thus they are repeated again).
- Braking resistor is active. It checks DC link voltage and chopper is activated at 750VDC or deactivated at 550V with a frequency of 1kHz (selection of this frequency comes from the HIL setup). In the HIL setup, switching of the chopper of AC drives has been fixed by the producer. Although the switching frequency has been set between 300 and 500 kHz for commercial wind turbines, this condition is overwritten for this study).
- The generator side converter is current controlled and the grid side converter is voltage controlled (Control of the converters have been emphasized in this point since the control schematics will be changed at some control strategies)

4.4.4.1. Disconnection of the WECS from the Grid

With the conditions above, wind energy conversion system has been disconnected at 1.6 second. At the moment of disconnection, there is no islanding detection method and no control strategy to keep connection has been applied. Only the variables at the

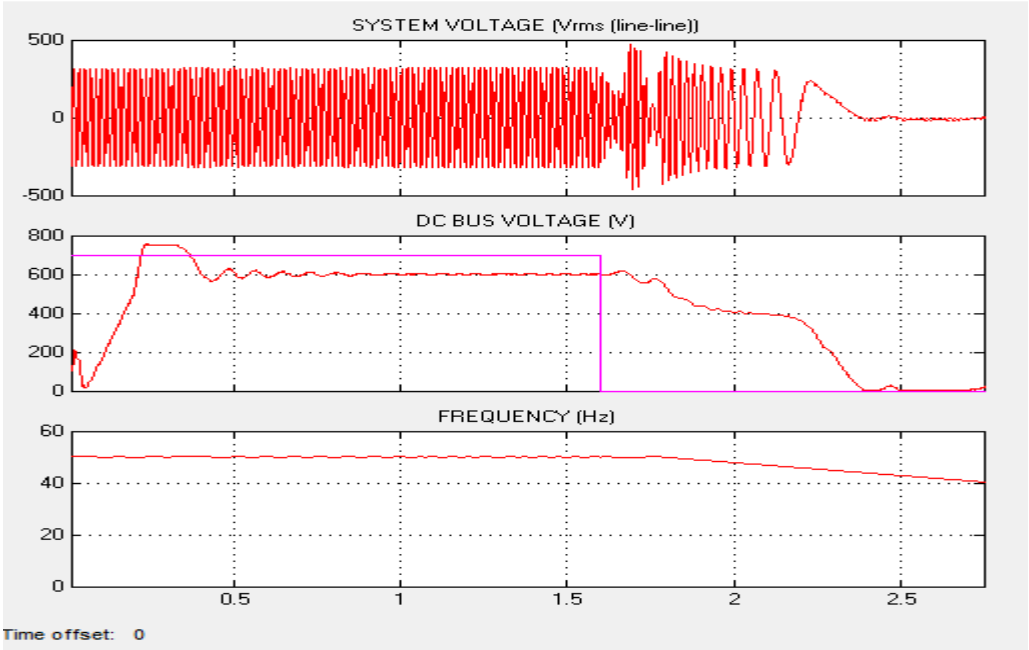

Figure 4.14 System voltage, DC link voltage and frequency at islanding operation (no control strategy is applied and disconnection moment (t=1.6 seconds) can be observed in pink trajectory at DC Bus Voltage graph)

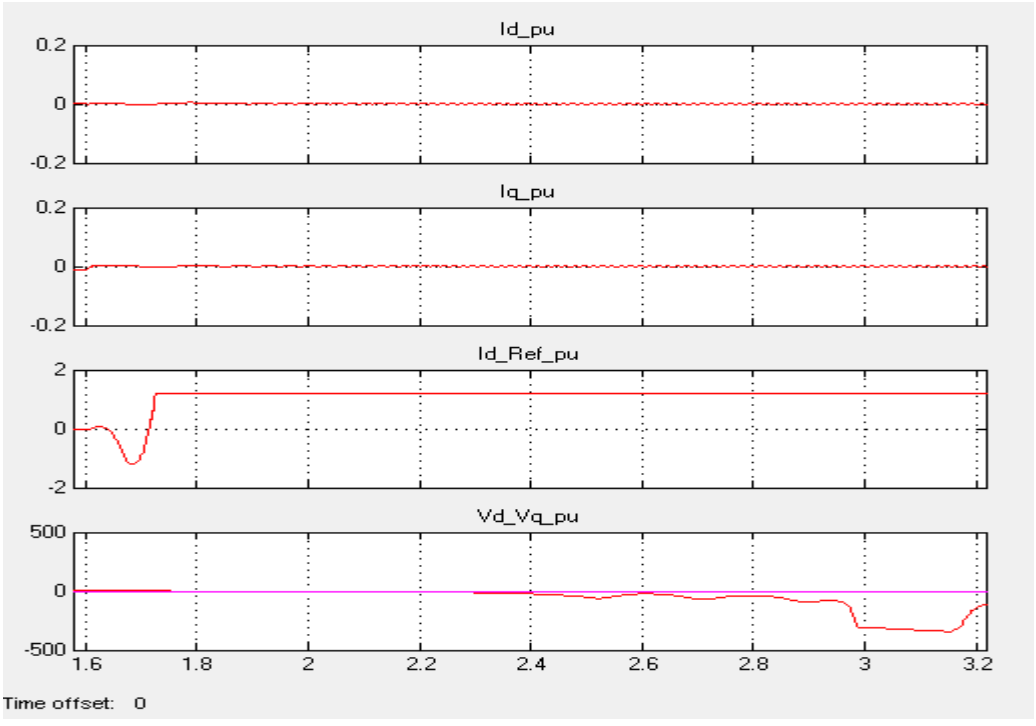

Figure 4.15 Direct and quadrature axis current, direct axis reference current and direct and quadrature axis voltages (values are pu based)

system has been observed. As seen in Figure 4.14, the grid voltage collapses. The grid voltage should be understood as the voltage supplied to the load when the microgrid is disconnected. Change in the grid voltage is in variables, voltage and frequency. Voltage starts to decrease after an oscillation at 1.7s. Moreover, the frequency of the supply voltage starts to increase (e.g. frequency at 2.1 seconds is 56Hz). If this microgrid is connected to the national grid, SCADA system at TEİAŞ force the wind turbine to drop from the grid since high limit of the frequency, which is 51.5 Hz, is surpassed. In addition, the DC bus voltage starts to decrease due to wrong references generated at the current controller and DC voltage regulator. Wrong references are generated due to absence of the PLL. Since the synchronization with the grid is lost, theta and frequency are generated in a wrong pattern and thus currents and voltages cannot be transformed to *dq* frame. As a result, almost zero currents in the *dq* frame have been generated as seen in Figure 4.15. Since there is a high power in the generator system, dc voltage regulator desires to sent it to the grid by increasing I_d reference as seen in Figure 4.15. Increase in the I_d reference current results in high voltage references (V_d and V_q) at the output current controller as seen in Figure 4.16. This increase in the reference voltages forces the PWM modulation index to the limit, which is 1 as seen in Figure 4.17.

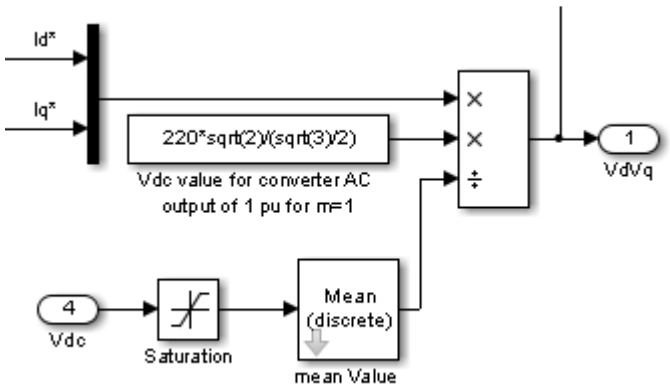

Figure 4.16 Direct and quadrature voltage references (VdVq) generated at the current controller and sent to the PWM block

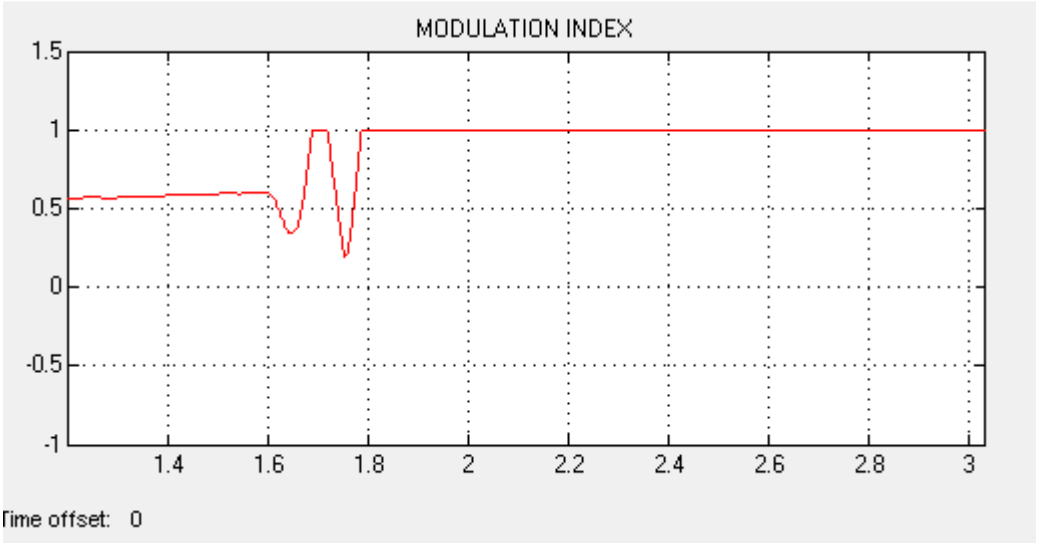

Figure 4.17 Modulation index at the islanding condition

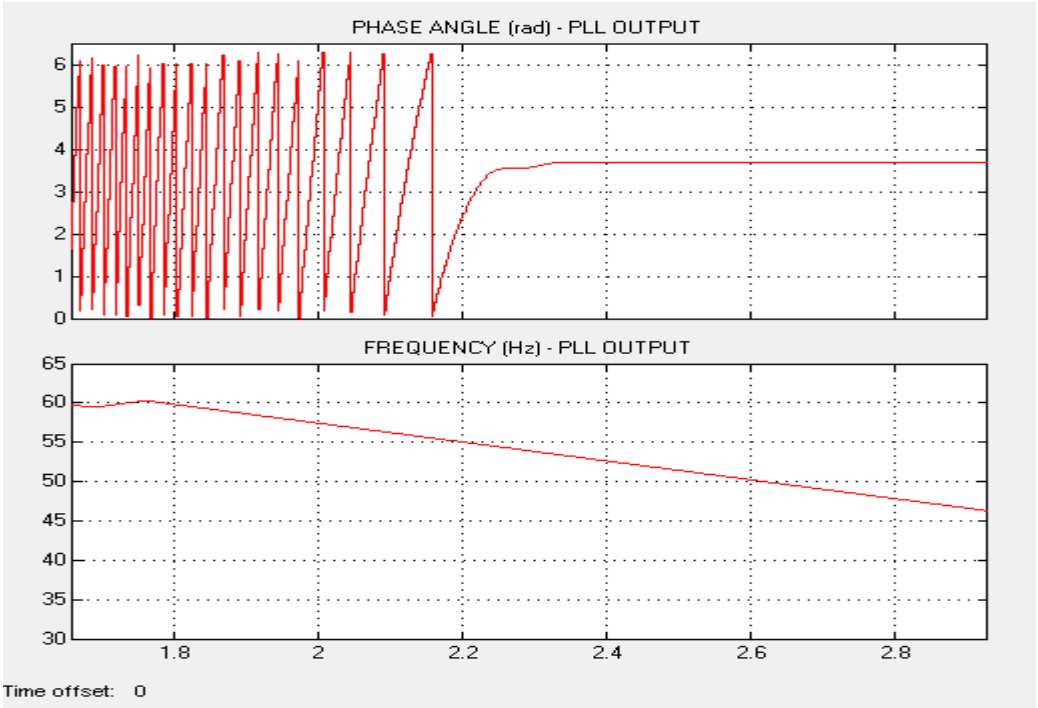

Figure 4.18 PLL outputs – upper graph shows the phase angle output, lower graph shows the frequency output

When modulation index is set to “1”, magnitude of switching signal which is applied to the PWM block increases and results in high current absorption from the DC link capacitors. Meanwhile, the phase angle continues to distort as seen in Figure 4.18 due to loss of grid synchronization. Both increasing modulation index and distortion of the phase angle leads a distorted switching pattern as seen in Figure 4.19. Switching of the IGBTs has been stopped at 2.2 seconds. Beyond this point, grid side converter cannot produce any voltages at its output as seen in Figure 4.14. DC bus voltage keeps decreasing. Since DC link is not constant, current controlled generator cannot draw enough current to draw MPPT of the turbine. This leads to decrease in the electromagnetic torque of the generator and shaft of turbine starts to increase. With the start of increasing speed at the shaft, system is now in positive feedback mode. While shaft of the speed is increasing, operating point of the turbine comes to a worse point and generated power is decreased and the DC link continues to fall. Falling DC bus voltage cause lower electromagnetic torque and it goes on and on. Until the wind turbine stops itself due to high speed (stopping can be done yawing the nacelle of the turbine), this loop continues as seen in Figure 4.20. At 3 seconds, there is no more energy to transport to the grid and if this system is realized in a site, we would have to stop the turbine.

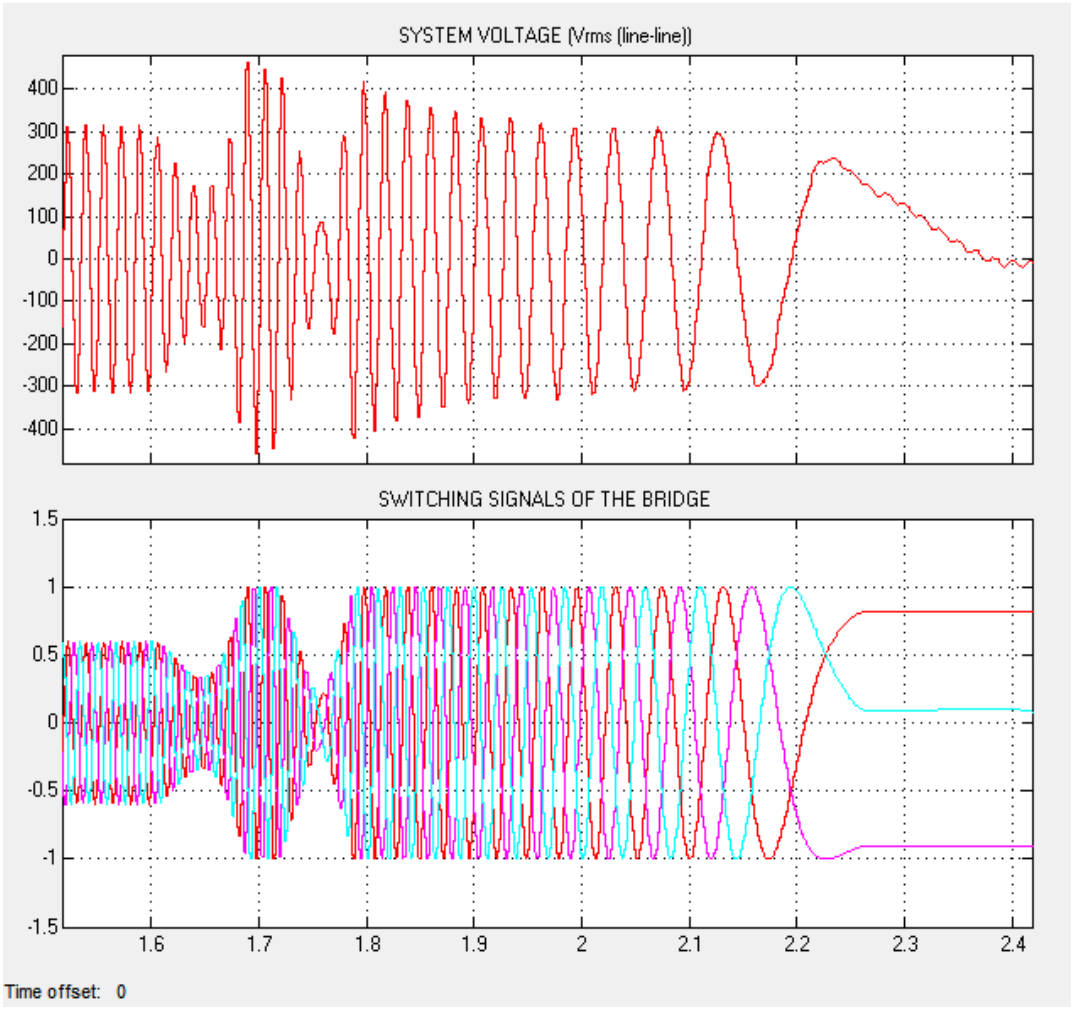

Figure 4.19 Switching pattern sent to the PWM block

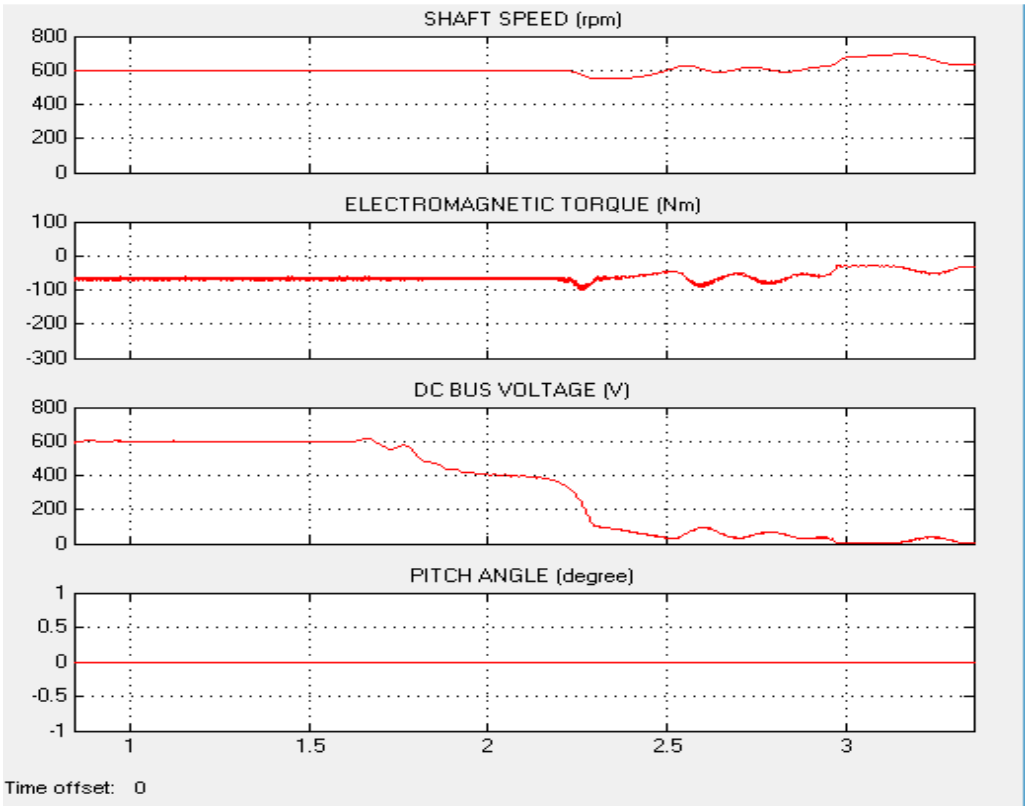

Figure 4.20 Shaft speed, electromagnetic torque of the generator, DC link voltage and the pitch angle at islanding operation (no control strategy is applied)

4.4.4.2. Results of Disconnection of the WECS from the Grid

The simulation results showed at the upper paragraphs conclude that generation of the electricity at the grid side converter is interrupted with the loss of grid synchronization. It is necessary to maintain the frequency stability in islanding mode to prevent interruption of service and continue to feed the local loads with available power from the local distributed generation [44]. To achieve this goal islanding detection algorithm should detect the grid disconnection and it should trigger the internal frequency reference to maintain fixed and stable frequency. That is, inverters should be designed to include internal sinusoidal 50 Hz reference signals to generate phase angle, which is used at the *dq* transformation. Thus, the inverter is modified to

have internal reference signals that are activated at the stand alone operation as seen in Figure 4.21. If the islanding is detected, the internal reference has been activated and the frequency of the overall grid can be stabilized in a few cycle.

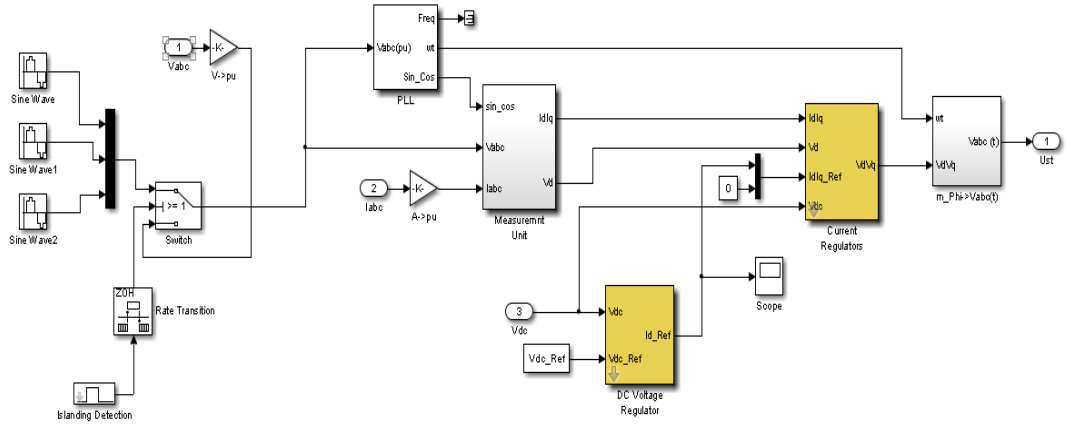

Figure 4.21 Controller of the grid side converter: an internal reference (3 sine waves have been added)

For the grid detection method, there are numerous options which are stated in "Islanding Operation" section. However, in this study, we used a new detection method and utilized it through all control techniques (braking, pitch and MPPT control). As seen in Figure 4.22, DC link voltage rises if system voltage is achieved to keep constant. Thus, we aim to use DC link voltage as the islanding detection for this study. When DC link increases beyond 600V, it is understood that microgrid is operated as stand-alone. At the next paragraph, islanding operation is started; but this time braking resistor is used as the control parameter.

4.4.4.3. Braking Resistor Controlled Microgrid Operation

Before starting microgrid operation, the internal PLL sources have been added to the grid side converter. If islanding operation is detected, the internal sources will

operate. Thus, with the addition of the reference signals, we will achieve to stabilize grid voltage.

Three phase breaker is again opened at t=0.8 s for this time. Since there is an excess power at the WECS, DC link capacitors started to increase as seen in Figure 4.22. When the voltage level reaches to 750V, braking resistor is activated and the excess power is dissipated in the chopper. However, with the start of the islanding operation, harmonic distortion at the load voltage increases as seen in Figure 4.22. This is due to change of the value of filter resonant frequency with the absence of the transformer.

Grid connection of the grid side converter has been completed with 1) LCL filter and 2) MV/LV transformer. That is, both LCL filter and primary side of transformer define the value of cut-off frequency of the grid side converter. While the carrier frequency of the grid side converter is 3 kHz, there is almost no harmonic in the grid voltage for the grid connected mode. However, with the grid disconnection, transformer is separated from the microgrid. Thus, value of cut-off frequency is determined only by LCL filter in this situation. While carrier frequency is kept at 3 kHz and the grid is disconnected, it is seen that harmonic distortion increased as seen in Figure 4.23 (THD increases from 0.57% to 7.7%). Such a condition has been estimated while doing the simulation. After seeing the problem, the carrier frequency of the inverter is set to 6 kHz. When the islanding operation is repeated with the same conditions, the harmonic distortion was almost same as the grid connected mode as seen in Figure 4.24. This shows that filtering the grid side converter is another engineering issue. Thus, while setting up a system which can be used at stand-alone, transformers and line impedance should be taken into consideration as well.

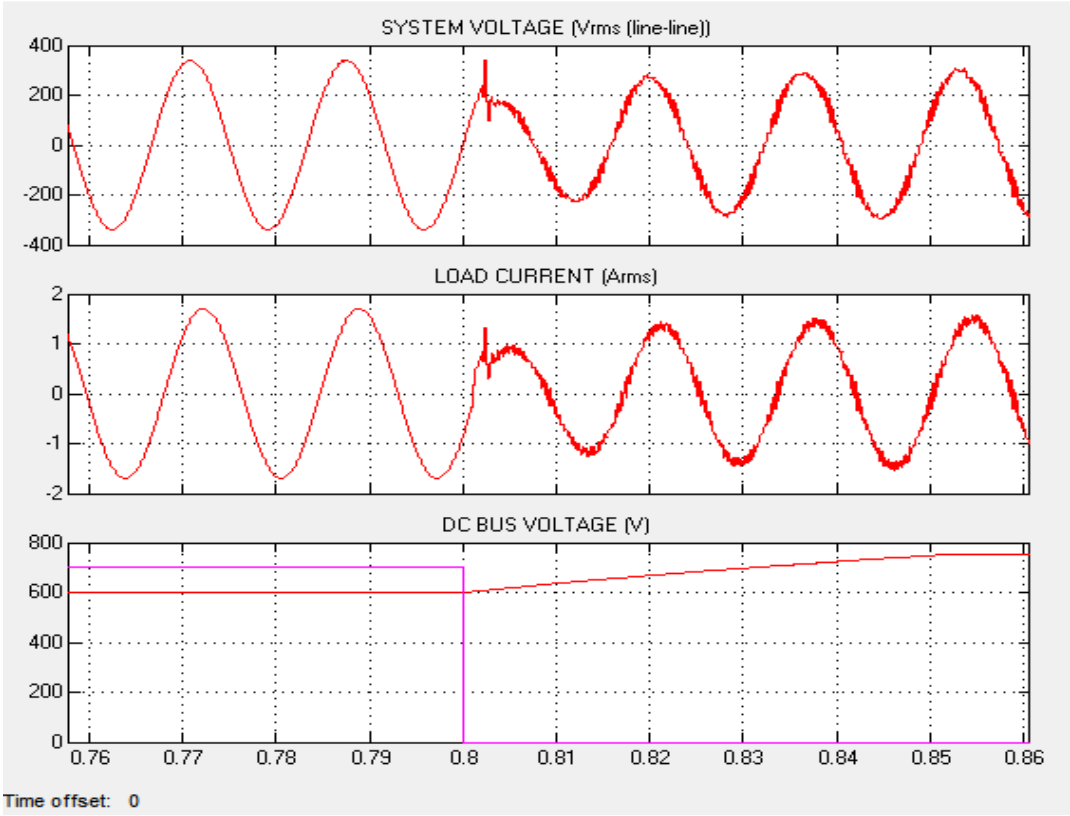

Figure 4.22 System voltage after the grid is disconnected. Grid side converter is modified to have internal reference signals. Carrier frequency of the converter is 3 kHz for this operation. Disconnection moment is shown in pink trajectory at DC Bus voltage graph

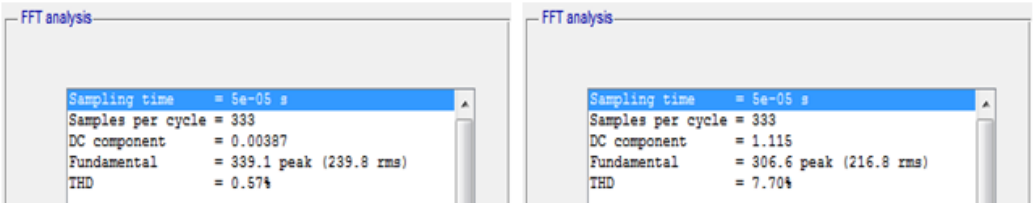

Figure 4.23 THD of system voltage before grid is disconnected (left graph) and after grid is disconnected at t=0.8 seconds

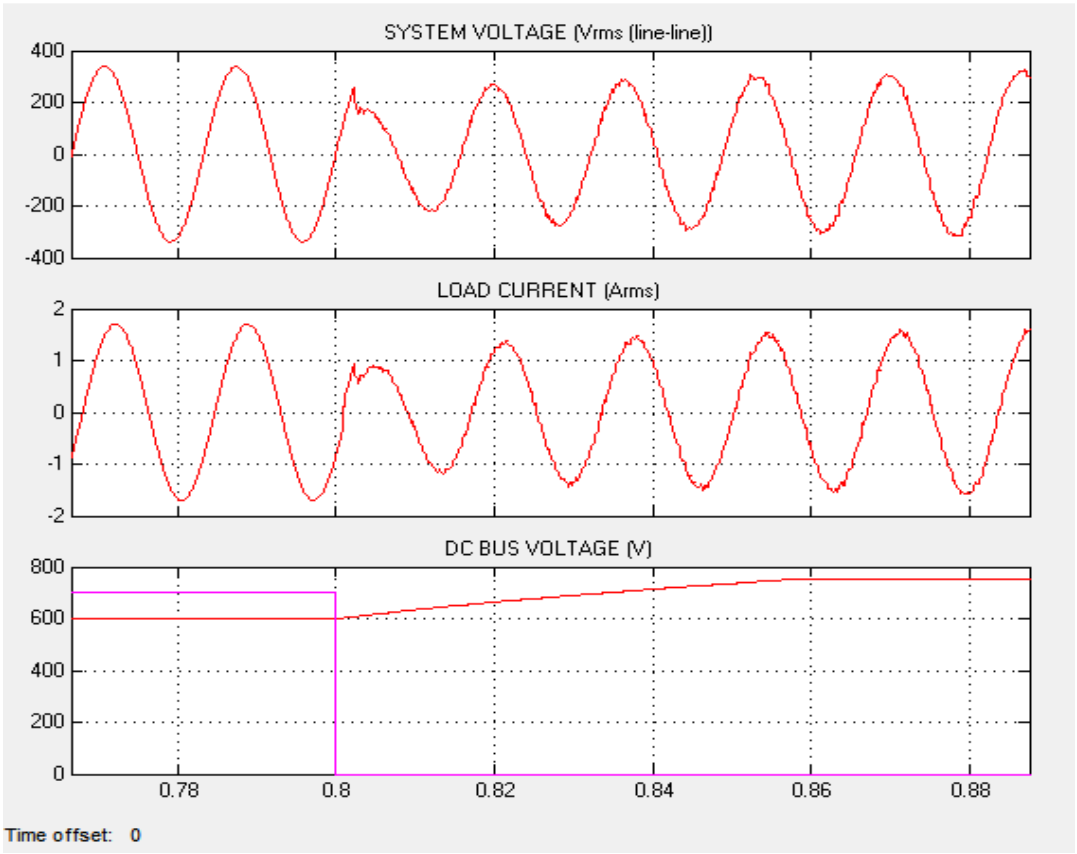

Figure 4.24 System voltage after the grid is disconnected. Grid side converter is modified to have internal reference signals. Carrier frequency of the converter is 6 kHz for this operation.

If the grid is disconnected and the converter continue to work in power control mode, the voltage at the converter terminals can become unregulated and trying to continue feeding constant power after grid disconnection leading to over voltage. If the DC voltage is not stabilized at a point, inverter may have to decrease its modulation index. However, for excess power, DC link continues to increase and it can affect the grid voltage, too. Thus, to improve the microgrid reliability and maintain continuous service, the converter control mode must be automatically configured to voltage control mode when islanding is detected to regulate the voltage and continue feeding the local load. The reconfiguration to voltage mode can be triggered by the trip signal of the islanding detection algorithm. Control strategies of the grid side converter can

be seen in Figure 4.26 and Figure 4.27. In braking resistor controlled microgrid operation, this strategy has been applied. When the islanding is detected, voltage control mode has been activated. Only observing frequency and the voltage (that can be named as V/f control), the load side AC voltage is supplied.

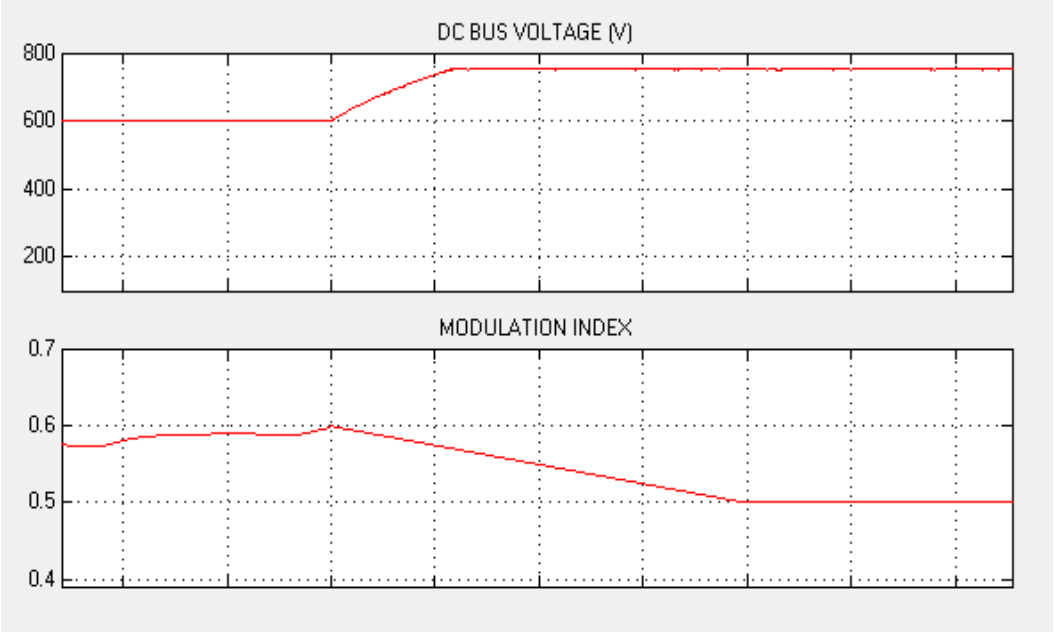

Figure 4.25 Change of control mode and modulation index accordingly

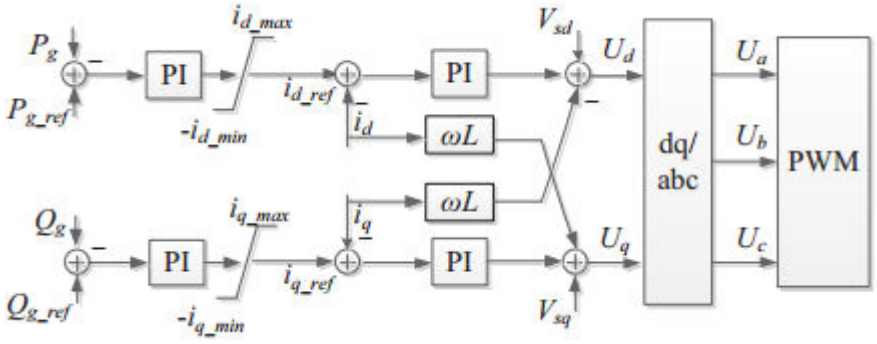

Figure 4.26 Control block diagram of microgrid at the grid connected mode [45]

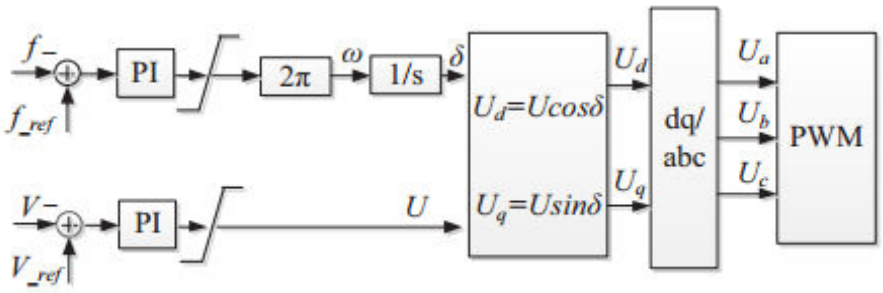

Figure 4.27 Control block diagram of microgrid at the islanding mode [45]

However changing the mode while passing from standalone to grid connected can cause some bad results. In the simulation, three phase breaker at the MV side has been closed again at t=1.8s. With the synchronization of the grid, the control has been changed to power control mode again. At this moment, it is seen that there are high currents flowing at the switches. This is due to being short circuit of the switches while the control mode is changed. These high currents cause to decrease DC link voltage. As seen in Figure 4.28, DC bus voltage decreases up to 350V. Such a drastic change in the DC link creates distortion in the electromagnetic torque as seen in Figure 4.29. Ripples in the torque are due to insufficient current source at the DC link capacitors. Thus, shaft speed also experiences an oscillation. This situation cause high mechanical stress on the shaft. Furthermore, using braking resistor creates high magnitude currents on a resistor and a switch. Flowing highly impulsive currents in the chopper can cause to derate the materials and decrease the life-time. Due to these bad effects, utilizing braking resistor and transitioning between the modes does not present a good solution. To see the efficiency of the control method, measured parameters for especially grid stabilization have been tabulated as seen in Table 4.3 for braking resistor control strategy. Since the braking resistor control is not effective enough, the operating point of the turbine is changed at the next section to decrease the absorbed power from the system.

Table 4.3 Grid and DC link parameters at the transition of islanding for braking resistor control

Change in system voltage	drops by 28% at the disconnection moment
Variation in frequency	increases 2% (maximum 51Hz): in limits
Recovery of grid voltage	7 cycles
Change of THD (%)	0.19⟶11.89 at3kHz / 0.19⟶3.22 at 6 kHz
Maximum DC link voltage	750V
Minimum DC link voltage	350V

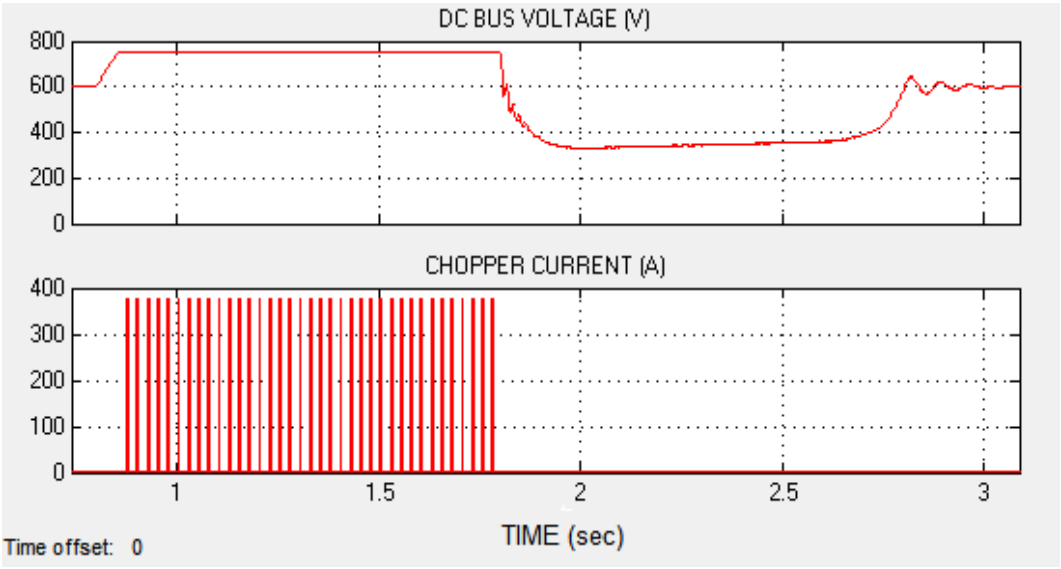

Figure 4.28 Passing from stand-alone operation to grid connected operation

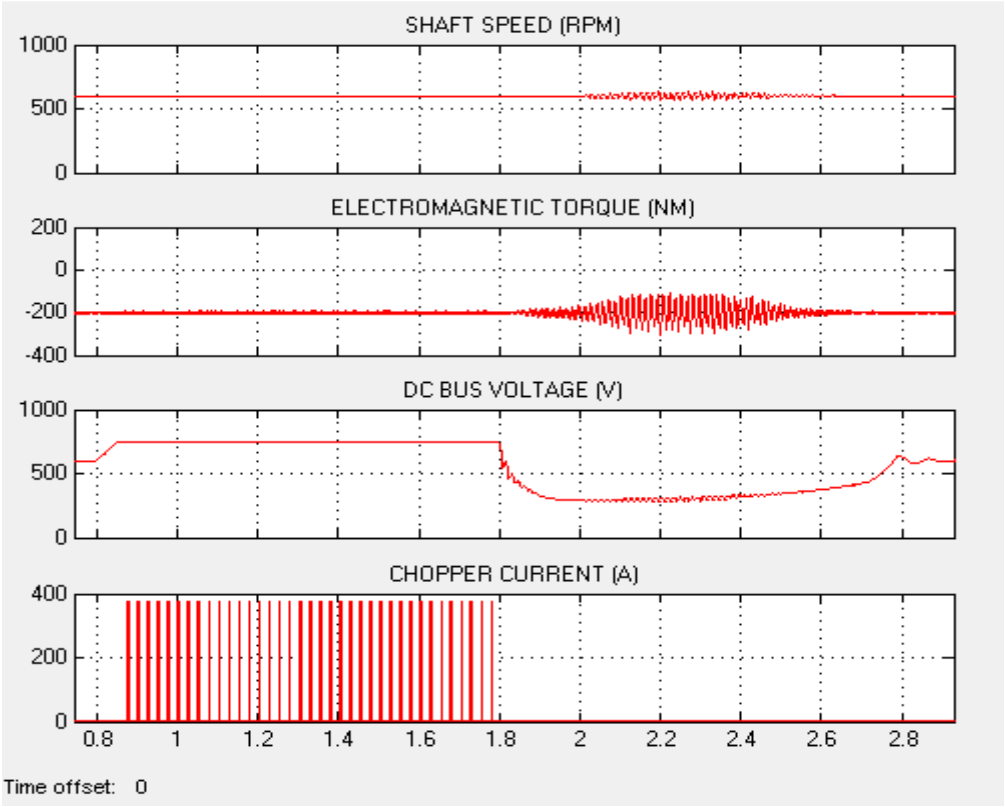

Figure 4.29 Shaft speed, electromagnetic torque of the generator, dc link voltage and the chopper current at the grid connected mode and islanded mode

4.4.4.4. Operating Point Controlled Microgrid Operation

The case study is implemented again by presenting operating point control strategy for this time. Since we know that the excess power causes DC link increase, it can be a solution to control DC link. Thus, MPPT control strategy has been modified.

MPPT strategy is applied to get the maximum power for a specific wind speed. Thus, the MPPT controller in the simulator has been established accordingly. However, this control strategy can also be applied to the islanding operation even if the MPPT is catched at that moment. If the operating point is modified so that speed of wind turbine is either decreased or increased to reduce the extracted power, we can achieve not to increase DC link voltage excessively. That is, if we move away from

the MPP curve as seen in Figure 4.30, the extracted excees power can be minimized and demand-supply of power generation can be reached.

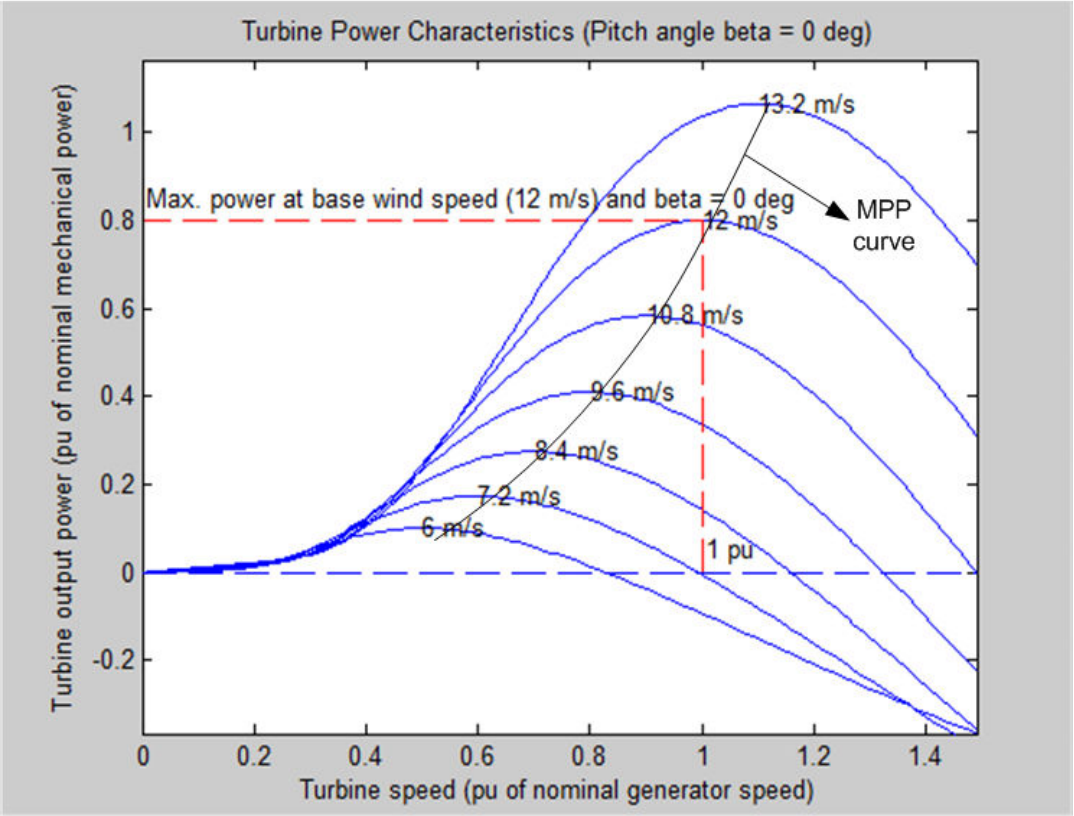

Figure 4.30 MPP curve of the turbine

Eliminating of the excess power can facilitate the islanding operation. Firstly, utilization of the braking resistor is decreased or stopped. Secondly, we cannot change the control mode of the grid side converter. If the MPPT control strategy is modified such that DC link is kept constant at the reference value (which is 600V for our system), power mode controlled grid side converter can also be used at the islanding operation. Since we also eliminate change of control modes, we can get rid of low level DC link voltages and high stresses on the shaft. To start the operation of the MPPT control, the sequence listed below has been generated.

1. Observe the DC link to detect islanding operation. If DC link is not set to 600V, start to control speed of the generator with MPPT.
2. At the islanding moment, stop current controller and keep VdVq value of the PWM block constant same (fix the modulation index)
3. MPPT control should aim to get DC link voltage to 600V to keep grid voltage and frequency stable (since the fixed modulation index is according to 600V)
4. Continue until DC link is kept constant if MPPT can.
5. If the grid side converter is grid connected again, stop looking DC link voltage and go back to old strategy, follow maximum power point, turn on current controllers.

The flow of the MPPT has been explained above between 1 and 5. Why we don't want to use changing control mode and modify inverter type is due to using the industrial inverters in the laboratory. The grid side converter in the laboratory has been designed so that it trips when the grid synchronization is lost. However, there are some ways to keep working of these converters. If the converter in the HIL setup is powered with 24VDC, it continues to work. While the converter is working, "fixed boost mode" can be set to the modulation index which the stable operation creates. However, this fixed modulation index will desire a constant DC voltage. Hence, generator should be controlled to keep DC link voltage. The idea that we want to develop here comes from the utilization of the industrial AC drives even if grid is disconnected.

The simulation has been started again and three-phase breaker has been opened at t=0.8s. When islanding operation is detected, MPPT control strategy is taken into action. As seen in Figure 4.31, changing the rotor speed to either direction (increase or decrease) causes to decrease output power. It can be thought that decreasing speed can be advantageous due to being exposed to compulsive air forces in a decreased level. However; decreasing the speed of the generator causes to have higher electromagnetic torque. That is, rotor side converter should draw more current and it should be rated higher than the full scale since at the highest wind speed there may

be need for the MPPT controller, too. However, increasing the shaft speed is easier than the other strategy. By reducing electromagnetic torque, shaft is accelerated and we do not need any higher rated converter. Increasing the shaft speed can be disadvantageous for higher wind speeds. At high wind speed, aerodynamic force components can damage to the rotor. It should be also taken into consideration.

With the start of islanding at t=0.8s, shaft speed started to increase. In the duration of 0.8s and 1.8s, shaft speed has been changed continuously and the DC link also changed with it as seen in Figure 4.32. In other words, shaft speed is increased to decrease extracted power when DC link voltage is beyond 600V and speed is decreased when DC link voltage drops below 600V. However, we can see that stabilizing DC link voltage is almost impossible for the operating point control strategy. This is due to high inertia of the system. System inertia is too high such that rate of change of shaft speed cannot be faster than increase in DC link voltage. Furthermore, increase in shaft speed cannot control DC link voltage itself. Operating point control strategy is not enough so chopper resistor is put in use at t=1.7 as well. DC bus voltage experiences high transients and this is a cause of high mechanical stress.

One another aspect of this strategy is the grid side. Since we fix the modulation index and switching scheme of the inverter, the grid side AC voltages are directly dependent to the DC link voltage. As seen in Figure 4.33, the grid side voltages experiences high transients, high frequency shift and excess harmonics. The parameters can be seen in Table 4.4. Since the voltage change is high above ±10% and the frequency is beyond 51.5 Hz, this microgrid should be turned off not to damage the equipments.

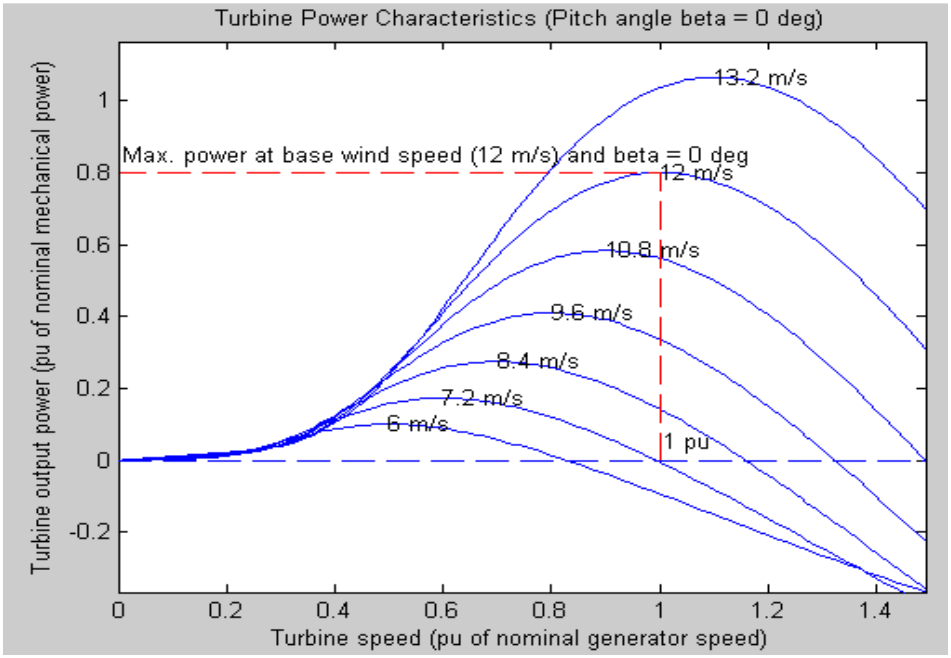

Figure 4.31 Power vs. turbine speed for different wind speeds

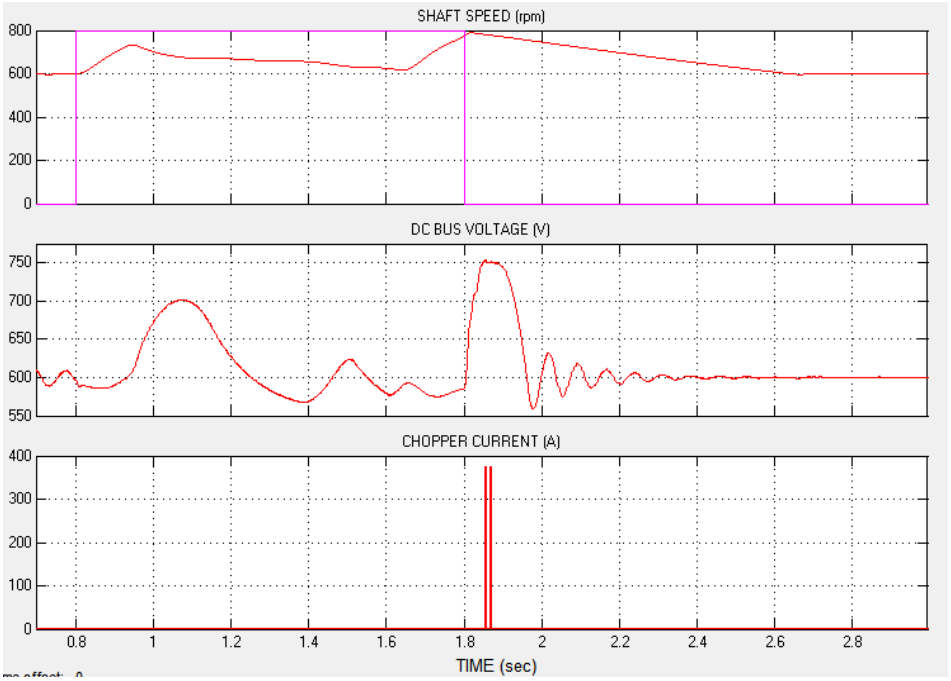

Figure 4.32 Shaft speed, dc link voltage and the chopper current when MPPT strategy has been activated in the islanding mode

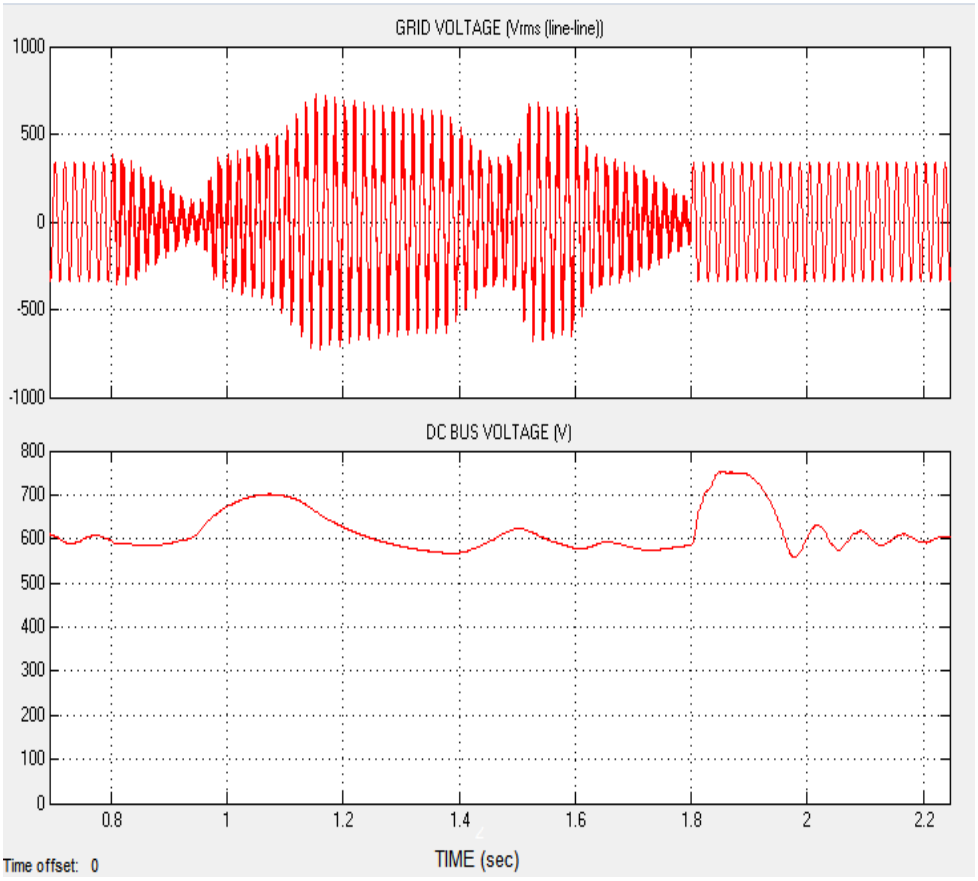

Figure 4.33 System voltage and DC link voltage at the islanding duration

Table 4.4 Grid and DC link parameters at the transition of islanding for MPPT control

Change in system voltage	drops by 65% at the disconnection moment
Variation in frequency	increases 10% (max. 55Hz): beyond limits
Recovery of grid voltage	-
Change of THD (%)	0.19 → 23.71
Maximum DC link voltage	750V
Minimum DC link voltage	560V

4.4.4.5. Pitch Controlled Microgrid Operation

The case study is implemented again by using pitch control method. In the previous technique, shaft speed is changed to lower the extracted power from the wind turbine. This time a similar strategy will also be applied. When DC link changes from the set value 600V, pitch controller starts to increase angle of the blades. Effect of increasing pitch angle can be seen in Figure 4.34.

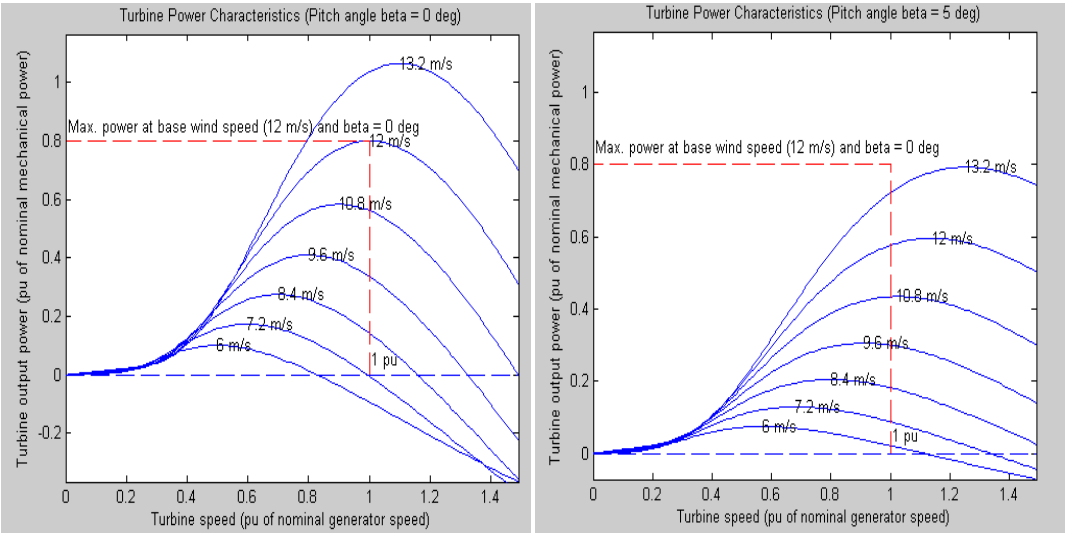

Figure 4.34 Change of power of wind turbine with increasing blade angle

Pitch controller is modified to be active even if the extracted power is below the rated power. If the islanding is detected, pitch controller is activated. Pitch controller is a slow control since there is a time delay (time constant) of the hydraulics used inside the blades. However, it can also supply the required decrease in the output power. Thus, pitch controller is modified to work at the islanding operation. If the turbine is operated at the grid connected mode, configuration of the Figure 2.40 has been applied. Otherwise, the configuration which is shown in Figure 4.35 is implemented. Simulink realization of the pitch controller can also be seen in Figure 4.36.

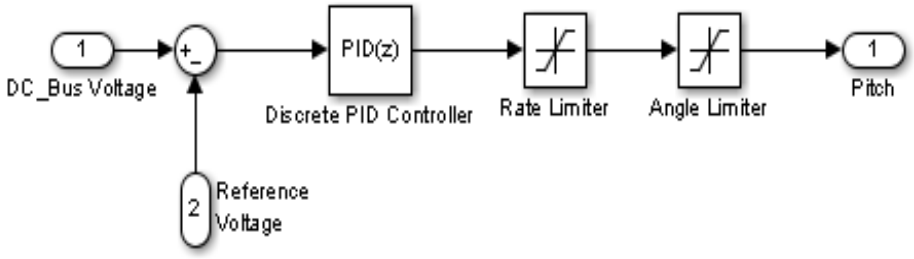

Figure 4.35 Pitch controller realized in Simulink for standalone operation

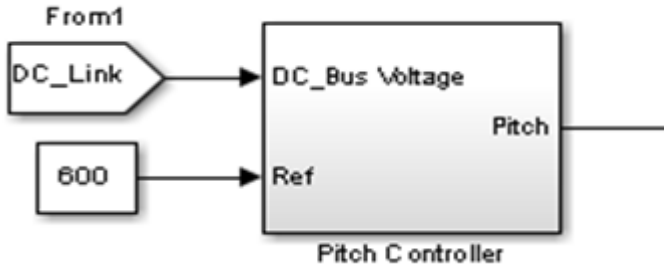

Figure 4.36 Simulink realization of pitch controller

When the three-phase breaker is opened at t=0.8s, it is shown that angle is increased to limit the power. As seen in the Figure 4.37, pitch angle is activated when the islanding detection has occurred. Pitch angle is both rate limited and angle limited. That is, rate limiter is used for the time constant of the system while the angle limiter is used to limit the rate of change of the blade angle. For large wind turbines, the change of the blades are almost 10^0/s [34]. Since we use a 10kW wind turbine in the study, we used a change of 20^0/s due to having smaller inertia compared to MW rated turbines. Time constant has been set as t=0,1 seconds. PID controller is tuned with trial-and-error method. Parameters of controller is found as Kp = 1,4, K_i = 0.2 and K_d = -0.8. With the application of the pitch angle, DC link is kept almost constant at the vicinity of 600V. This is desired to have a small distorted voltage and frequency at the customer side. In addition, small changes in the DC link increases

the system integrity due to lowered mechanic stress and torque changes. If Figure 4.37 is examined, it can be seen that there is no change at the shaft speed. This is the most important specification of the pitch controller, which is also emphasized at the Chapter 2. For the turbine side, it can be said that pitch angle is effective at the islanding operation. We must also examine the grid side before taking a decision.

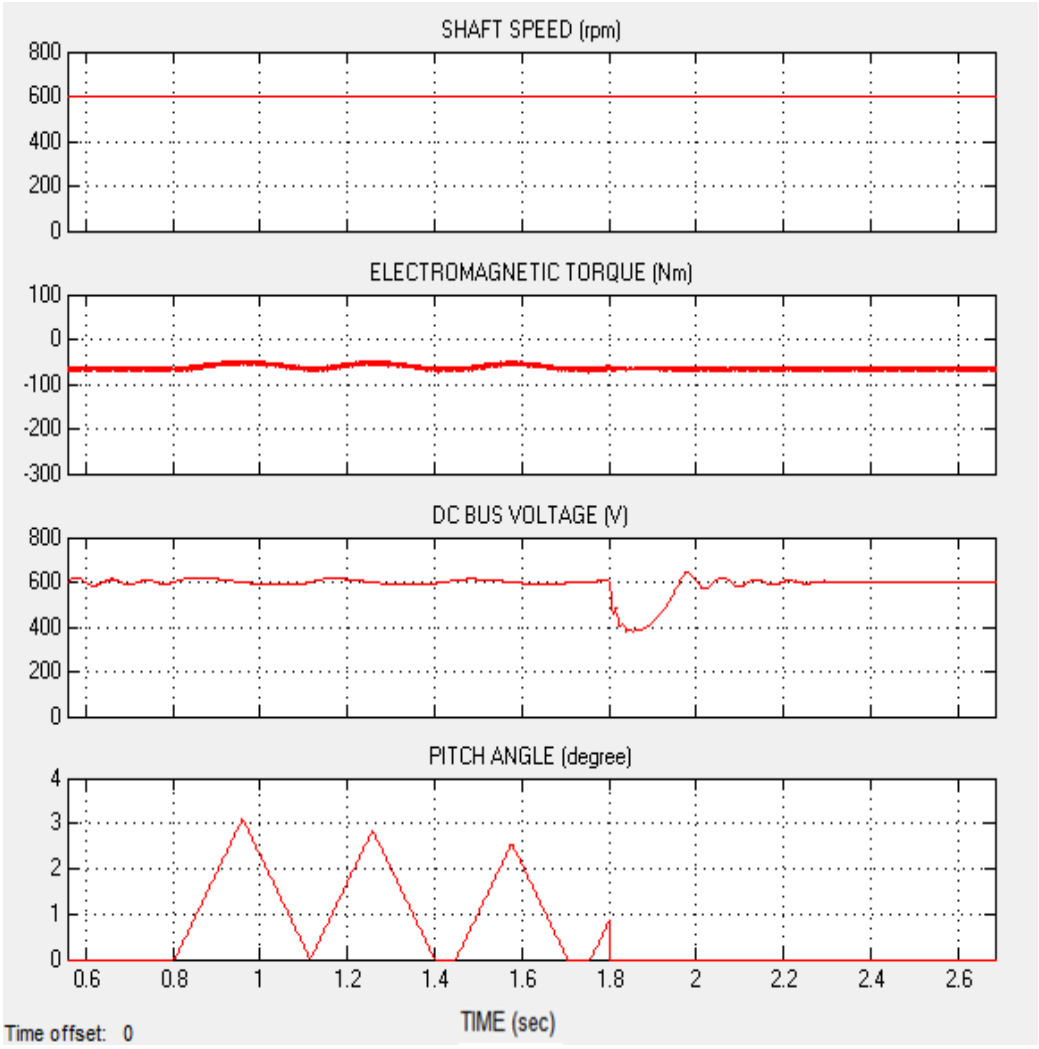

Figure 4.37 Shaft speed, electromagnetic torque of the PMSG, DC link voltage and pitch angle are shown when the modified pitch controller is used at the islanding operation

For the grid side results, Figure 4.38 can be investigated. Since there is a small change in the DC link voltage, load voltage has some fluctuations. Grid voltage is recovering itself for the normal operation in 8 cycles. After 8 cycles, there are still some fluctuations, which are maximum 5% above the rated voltage (220V). Since the grid codes dictate to be in the range of ±10%, this grid voltage quality is acceptable. Voltage droop is not calculated for this system since there is no reactive power control for the grid side converter. For the frequency limitation, the grid codes dictate to be between 47.5-50.3 Hz. If the grid frequency passes out 50.3, power station should start to decrease power generation. Until 51.5 Hz, the station is allowed to power the customers but with a drop in the supply. The maximum frequency at the islanding operation is 51 Hz and it is just seen at the recovery time t=1.8 seconds. Then, there is a grid voltage at 50 Hz. Since we feed only one load in this study, supply limitation is not required. However, if there are several loads, we would have to cut the supply. There is also a limitation for the total harmonic distortion. THD for the islanding operation is measured to be 5.3 with the FFT tool of the "powergui" of the Simulink. Since maximum 8% of THD is acceptable, it can be said that pitch control satisfied the harmonics limits with 5.3%.

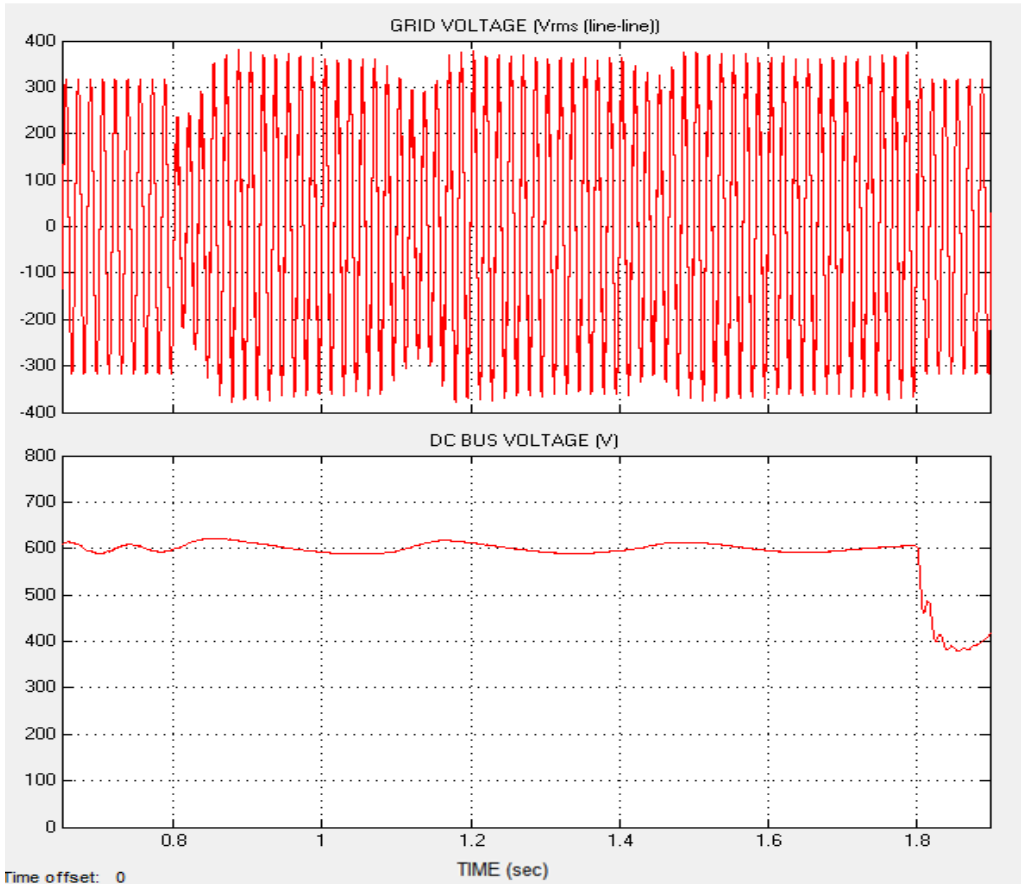

Figure 4.38 Load voltage and DC link voltage at the islanding duration for pitch controller

Table 4.5 Grid and DC link parameters at the transition of islanding for pitch control

Change in system voltage	drops by %5 during islanding operation at max.
Variation in frequency	increases 2% (max. 51Hz): in limits
Recovery of grid voltage	8 cycle
Change of THD (%)	0.19 → 5.3
Maximum DC link voltage	620V
Minimum DC link voltage	390V

4.5. Conclusion to the Chapter 4

Islanding operation of the wind turbines is a popular topic due to increasing entrance of the distributed generation. Thus, the control techniques and the application of these techniques to the industrial converters are the arising topics. In the case study, a new islanding detection method and islanding operation has been proposed. For the islanding detection method, DC link can be utilized. For the islanding operation, the controller should be modified for assuring the quality of the energy provided to the user. What should be done can be summarized as follows: adding internal reference signals for PLL, run the system using the reference signal produced by the conversion system to maintain voltage and magnitude and frequency as desired, maintain DC bus voltage level with changing load conditions by utilizing one of 3 methods; i.e. control of pitch angle, braking resistor and operating point control.

CHAPTER 5

CONCLUSION AND FUTURE WORKS

In this novel study, we designed a hardware-in-the-loop emulator which can be used for the research and development of wind energy conversion systems. The emulator consists of software, an induction machine which imitates the characteristics of the turbine shaft, a generator and necessary electronics to connect the system to the grid or facility which operates at islanding mode. While the turbine and its drive train have been simulated in the software, the generator and the converters have been set up physically in the laboratory. The test platform gives the chance to the users to test control algorithms with generation of the electricity at a realized platform and test electronic components, generator, grid connection and protection behavior under adverse wind conditions without harm to the physical system.

A software simulator has been developed as well. The software simulator is designed to imitate the characteristics of the HIL setup. By doing that, the user can experiment with designed control ideas without risk of harming the physical system and identify approaches which present advantage. These approaches can then be safely implemented on the HIL system to study behavior of the physical system. The contribution of this study in modeling the HIL system with software is especially in the area of modeling converters which are highly nonlinear. The indefinite regions at the HIL setup (the internal structure of the AC drives) have been modeled using artificial neural networks. In addition, loss of the permanent magnet synchronous generator has been modeled to give solutions compatible with the HIL setup. The results of the HIL setup and the software simulator have been compared and the efficiency of the applied networks and loss models has been pointed out. Although software simulator gives similar results, it cannot replace the HIL setup. Software and hardware is compatible for the steady state conditions. However, for dynamic

situations, it is observed that software cannot totally imitate the HIL setup due to time constant of the components, sample time of controllers and propagation delay of the system.

Software simulator and HIL emulator setup have been used to focus on the grid problems. With the increasing energy demand, it is seen that distributed generation and microgrid operation gained attention. Their control at the grid-connected or stand-alone operation comes up with several problems. The software simulator is established to observe the effect of stand-alone operation (islanding) of the microgrids. The control techniques used for the power control has been investigated at the islanding mode and efficiency and drawbacks of the strategies have been examined. A new islanding detection method and control strategy for the grid side converter has been proposed.

Satisfying the HIL setup and observing the grid problems for islanding operation, we are planning in the future to implement a normal sized wind turbine at the HIL setup. The techniques of scaling of a real-sized wind turbines will be investigated and the optimal technique will be applied at the HIL setup. In addition, the islanding control techniques are planning to be developed at the HIL setup. The strategies created at the software simulator will be tried out and the efficiency of the software simulator and the HIL setup will be observed again.

REFERENCES

[1] A. Rolan, A. Luna, G. Vazquez, D. Aguilar, and G. Azevedo, "Modeling of a variable speed wind turbine with a Permanent Magnet Synchronous Generator," *2009 IEEE Int. Symp. Ind. Electron.*, no. ISlE, pp. 734–739, 2009.

[2] A. D. Hansen, F. Iov, F. Blaabjerg, and L. H. Hansen, "Review of Contemporary Wind Turbine Concepts and their Market Penetration," *Wind Eng.*, vol. 28, pp. 247–263, 2009.

[3] M. Uyar, M. Tunay Gençoğlu, and S. Yildirim, "Değişken Hızlı Rüzgar Türbinleri İçin Generatör Sistemleri," YEKSEM 2005, III. Yenilenebilir Enerji Kaynakları Sempozyumu,Sh.173-178.

[4] The impact of variable speed concepts on wind power. [Online]. Available: http://www.renewableenergyfocus.com/view/32093/the-impact-of-variable-speed-concepts-on-wind-power/ (last accessed on 9 February 2015)

[5] A. D. Hansen and L. H. Hansen, "Market penetration of wind turbine concepts over the years," *EWEA*, 2007.

[6] A. Gupta, D. K. Jain, and S. Dahiya, "Some Investigations on Recent Advances in Wind Energy Conversion Systems," vol. 28, pp. 47–52, 2012.

[7] Navigant Research (2014) World Market Update 2013. [online]. Available: http://www.navigantresearch.com/research/world-market-update-2013 (last accessed on 9 February 2015)

[8] K. E. Okedu, "Effects of Drive Train Model Parameters on a Variable Speed Wind Turbine," vol. 2, no. 1, pp. 17–19, 2012.

[9] P. R. Andronov, M. Z. Dosaev, G. Y. Dynnikova, Y. D. Selyutskii, and S. D. Strekalov, "Wind Turbine Modeling," *Power*, vol. 38, pp. 383–387, 2009.

[10] D. McSwiggan, T. Littler, D. J. Morrow, and J. Kennedy, "A study of tower shadow effect on fixed-speed wind turbines," *Proc. Univ. Power Eng. Conf.*, no. 1, 2008.

[11] W. H. W. Hu, Y. W. Y. Wang, X. S. X. Song, and Z. W. Z. Wang, "Development of wind turbine simulator for wind energy conversion systems based on permanent magnet synchronous motor," *2008 Int. Conf. Electr. Mach. Syst.*, pp. 2322–2326, 2008.

[12] B. Neammanee, S. Sirisumrannukul, and S. Chatratana, “Development of a wind turbine simulator for wind generator testing,” *Int. Energy J.*, vol. 8, pp. 21–28, 2007.

[13] C. N. Bhende, S. Mishra, and S. G. Malla, “Permanent magnet synchronous generator-based standalone wind energy supply system,” *IEEE Trans. Sustain. Energy*, vol. 2, no. 4, pp. 361–373, 2011.

[14] H. Li, Z. Chen, “Overview of Different Wind Generator Systems and Their Comparisons,” IET Renewable Power Generation, vol. 2, no. 2, pp. 123–138, June 2008.

[15] K. W. E. Cheng, J. K. Lin, Y. J. Bao, and X. D. Xue, “Review of the wind energy generating system,” *8th Int. Conf. Adv. Power Syst. Control. Oper. Manag. (APSCOM 2009)* , pp. 1–7, 2009.

[16] Characterizing and Validating a Permanent Magnet Synchronous Motor Model. [online]. Available: http://www.mathworks.com/company/events/conferences/automotive-conference-michigan/2012/proceedings/parameterizing-and-verifying-a-permanent-magnet-synchronous-motor-model.pdf (last accessed on 9 February 2015)

[17] T. Hadjina, M. Baotic, N. Peric, M. Baoti, and N. Peri, “Control of the grid side converter in a wind turbine,” pp. 925–930, 2013.

[18] F. Iov, R. Teodorescu, F. Blaabjerg, B. Andresen, J. Birk, and J. Miranda, “Grid code compliance of grid-side converter in wind turbine systems,” *PESC Rec. - IEEE Annu. Power Electron. Spec. Conf.*, 2006.

[19] A. D. Hansen and G. Michalke, “Multi-pole permanent magnet synchronous generator wind turbines’ grid support capability in uninterrupted operation during grid faults,” *IET Renew. Power Gener.*, vol. 3, no. November 2008, p. 333, 2009.

[20] E. F. Camacho, T. Samad, M. Garcia-Sanz, and I. Hiskens, “Control for Renewable Energy and Smart Grids,” *Impact Control Technol.*, 2011.

[21] Wind Turbine Control Methods. [online]. Available: http://www.ni.com/white-paper/8189/en/ (last accessed on 9 February 2015)

[22] Pitch-regulated and Stall-regulated Wind Turbine. [online]. Available: http://www.bindichen.co.uk/post/Fundamentals/Pitch-regulated-and-Stall-regulated-Wind-Turbine.html (last accessed on 9 February 2015)

[23] H. Polinder, D. Bang, R. P. J. O. M. Van Rooij, a. S. McDonald, and M. a. Mueller, “10 MW wind turbine direct-drive generator design with pitch or

active speed stall control," *Proc. IEEE Int. Electr. Mach. Drives Conf. IEMDC 2007*, vol. 2, pp. 1390–1395, 2007.

[24] D. Bang and H. Polinder, "New active speed stall control compared to pitch control for a direct-drive wind turbine," *EWEC*, 2007.

[25] M. Örs, "Maximum Power Point Tracking for Small Scale Wind Turbine With Self-Excited Induction Generator," *Control Eng. Appl. Informatics*, vol. 11, no. 2, pp. 30–34, 2009.

[26] Q. W. Q. Wang and L. C. L. Chang, "An intelligent maximum power extraction algorithm for inverter-based variable speed wind turbine systems," *IEEE Trans. Power Electron.*, vol. 19, no. 5, pp. 1242–1249, 2004.

[27] Thongam, Jogendra Singh, and Mohand Ouhrouche, "MPPT control methods in wind energy conversion systems," INTECH Open Access Publisher, 2011.

[28] Mahdi,A.J., Tang, W. H., Wu, Q. H. , "Novel Perturbation and Observation Algorithms for Variable-Speed Wind Turbine Generator Systems," *PES, 2012.*

[29] D. Petreuş, T. Pâtârâu, S. Dârâban, C. Morel, and B. Morley, "A novel maximum power point tracker based on analog and digital control loops," *Sol. Energy*, vol. 85, pp. 588–600, 2011.

[30] A. Mesemanolis, C. Mademlis, and I. Kioskeridis, "Maximum Efficiency of a Wind Energy Conversion System with a PM Synchronous Generator," 7th Mediterranean Conf. And Exh. on Power Gen., November, pp. 1–9, 2010.

[31] J. Conroy and R. Watson, "Aggregate modelling of wind farms containing full-converter wind turbine generators with permanent magnet synchronous machines: Transient stability studies," Renewable Power Generat. IET, vol. 3, no. 1, pp. 39–52, Mar. 2009.

[32] J. Benjanarasut and B. Neammanee, "The d-, q- axis control technique of single phase grid connected converter for wind turbines with MPPT and anti-islanding protection," *ECTI-CON 2011 - 8th Electr. Eng. Electron. Comput. Telecommun. Inf. Technol. Assoc. Thail. - Conf. 2011*, pp. 649–652, 2011.

[33] L. Dusonchet, F. Massaro, and E. Telaretti, "Transient stability simulation of a fixed speed wind turbine by Matlab / Simulink," vol. 1, no. 3, pp. 651–655, 2007.

[34] M. De Prada Gil, A. Sumper, and O. Gomis-Bellmunt, "Modeling and control of a pitch-controlled variable-speed wind turbine driven by a DFIG with frequency control support in PSS/E," *PEMWA 2012 - 2012 IEEE Power Electron. Mach. Wind Appl.*, 2012.

[35] International Energy Outlook. [online]. Available: http://www.eia.gov/forecasts/ieo/ (last accessed on 9 February 2015)

[36] Smart Grid. [online]. Available: http://en.wikipedia.org/wiki/Smart_grid (last accessed on 9 February 2015)

[37] IRENA, November 2013. Smart Grid and Renewables. [online]. Available: http://www.irena.org/DocumentDownloads/Publications/smart_grids.pdf (last accessed on 9 February 2015)

[38] Swedish Coordination Council for Smart Grids, "Smart Grid for a Sustainable Energy Society," vol. 2013, no. February, pp. 23–34, 2013.

[39] Yadav, Alka, and Laxmi Srivastava. "Optimal placement of distributed generation: An overview and key issues." Power Signals Control and Computations (EPSCICON), 2014 International Conference on. IEEE, 2014.

[40] H. Kuang, S. Li, and Z. Wu, "Discussion on advantages and disadvantages of distributed generation connected to the grid," *2011 Int. Conf. Electr. Control Eng. ICECE 2011 - Proc.*, pp. 170–173, 2011.

[41] H. Sun, M. Han, C. Luo, "Voltage Stability Study of Micro-grid with Asynchronous Wind Turbine in Islanding Mode", Industrial Electronics, pp. 2180-2185, 2014.

[42] TEİAŞ. (2014, May) . Elektrik Şebeke Yönetmeliği. [online]. Available: http://www.epdk.gov.tr/index.php/elektrik-piyasasi/mevzuat?id=89 (last accessed on 9 February 2015)

[43] G.Pla, A. Matias, "Control of Grid Side Inverter for Wind Turbine", Master Thesis, Institute of Energy Technology, Aalborg University, 2010.

[44] T. A. Youssef and O. Mohammed, "Adaptive SRF-PLL with reconfigurable controller for Microgrid in grid-connected and stand-alone modes," *IEEE Power Energy Soc. Gen. Meet.*, pp. 1–5, 2013.

[45] Y. Liao, X. Shi, C. Fu, and J. Meng, "Hardware In-the-Loop Simulation System Based on NI-PXI for Operation and Control of Microgrid," IEEE 9th Industrial Electronics and Applications, pp. 1366–1370, 2014.

[46] N. Muntean, L. Tutelea, D. Petrila, and O. Pelan, "Hardware in the loop wind turbine emulator," *Int. Aegean Conf. Electr. Mach. Power Electron. ACEMP 2011 Electromotion 2011 Jt. Conf.*, no. September, pp. 53–58, 2013.

[47] J. Chen, J. Chen, C. Gong, and H. Wang, "Design and Analysis of Dynamic Wind Turbine Simulator for Wind Energy Conversion System TL TD," IECON

2012-38th Annual Conference on IEEE Industrial Electronics, pp. 971–977, 2012.

[48] Y. J. Y. Jia, Z. W. Z. Wang, and Z. Y. Z. Yang, "Experimental Study of Control Strategy for Wind Generation System," *2007 IEEE Power Electron. Spec. Conf.*, pp. 1202–1207, 2007.

[49] S. Kumsup and C. Tarasantisuk, "Real-time wind turbine emulator for testing wind energy conversion systems," *2010 IEEE Int. Energy Conf. Exhib. EnergyCon 2010*, no. 4, pp. 7–9, 2010.

[50] Yun, D., B. Han, and N. Choi. "Hardware simulator for PMSG wind power system with matrix converter." Telecommunications Energy Conference, 2009. INTELEC 2009. 31st International. IEEE, 2009.

[51] B. Han, H. Lee, and D. Yoon, "Hardware simulator development for PMSG wind power system," *2009 IEEE Power & Amp; Energy Soc. Gen. Meet. (PES), 26-30 July 2009*, p. 6 pp., 2009.

[52] N. Karakasis, A. Mesemanolis, and C. Mademlis, "Wind Turbine Simulator for Laboratory Testing of a Wind Energy Conversion Drive Train," , 8th Mediterranean Conference, vol. 624, pp. 1–6, 2012.

[53] W. Hu,Y. Wang, X. Song, and Z. Wang, "Development of wind turbine simulator for wind energy conversion systems based on permanent magnet synchronous motor," *2008 Int. Conf. Electr. Mach. Syst.*, pp. 2322–2326, 2008.

[54] Control Techniques, "UniDrive SP Advanced User Guide", datasheet, 2004.

[55] C. Huynh, L. Zheng, and D. Acharya, "Losses in High Speed Permanent Magnet Machines Used in Microturbine Applications," *J. Eng. Gas Turbines Power*, vol. 131, no. March 2009, p. 022301, 2009.

[56] Y. Ying, Z. Jianguo, and G. Youguang, "A Permanent Magnet Synchronous Motor Model with Core Loss," *Japanese Soc. Appl. Electromagn. Mech.*, vol. 15, pp. 147–150, 2007.

[57] MATLAB, "Neural Network Toolbox User Guide", datasheet, 2014.

[58] TÜREB. (2015, January). Türkiye Rüzgar Enerjisi İstatistik Raporu. [online]. Available: http://www.tureb.com.tr/attachments/article/420/T%C3%BCrkiye%20R%C3%BCzgar%20Enerjisi%20%C4%B0statistik%20Raporu_Ocak%202015.pdf (last accessed on 9 February 2015)

[59] S. Dutta and T. J. Overbye, "Optimal wind farm collector system topology design considering total trenching length," *IEEE Trans. Sustain. Energy*, vol. 3, no. 3, pp. 339–348, 2012.

[60] E. H. Camm, M. R. Behnke, O. Bolado, M. Bollen, M. Bradt, C. Brooks, W. Dilling, M. Edds, W. J. Hejdak, D. Houseman, S. Klein, F. Li, J. Li, P. Maibach, T. Nicolai, J. Patino, S. V. Pasupulati, N. Samaan, S. Saylors, T. Siebert, T. Smith, M. Starke, and R. Walling, "Wind power plant collector system design considerations," *IEEE Power Energy Soc. Gen. Meet.*, pp. 1–7, 2009.

[61] E. H. Camm, M. R. Behnke, O. Bolado, M. Bollen, M. Bradt, C. Brooks, W. Dilling, M. Edds, W. J. Hejdak, D. Houseman, S. Klein, F. Li, J. Li, P. Maibach, T. Nicolai, J. Patino, S. V. Pasupulati, N. Samaan, S. Saylors, T. Siebert, T. Smith, M. Starke, and R. Walling, "Wind power plant collector system design considerations" *2009 IEEE Power Energy Soc. Gen. Meet.*, pp. 1–7, 2009.

[62] F. González-Longatt, P. Regulski, H. Novanda, and V. Terzija, "Effect of the shaft stiffness on the inertial response of the fixed speed wind turbines and its contribution to the system inertia," *APAP 2011 - Proc. 2011 Int. Conf. Adv. Power Syst. Autom. Prot.*, vol. 2, pp. 1170–1175, 2011.

[63] R. G. Ferraz, L. U. Iurinic, a. D. Filomena, and a. S. Bretas, "Park's transformation analitycal approach of transient signal analysis for power systems," *2012 North Am. Power Symp. NAPS 2012*, no. 1, pp. 2–7, 2012.

[64] H. Karmaker, "Report on IEEE standard working group P1812 on guide for testing permanent magnet machines," in *2012 IEEE Energy Conversion Congress and Exposition, ECCE 2012*, 2012, pp. 2326–2333.

[65] PM Synchronous Motor Drive. [online]. Available: http://www.mathworks.com/help/physmod/sps/powersys/ref/pmsynchronousmotordrive.html (last accessed on 9 February 2015)

[66] AC/DC Three-Level PWM Converter. [online]. Available: http://www.mathworks.com/help/physmod/sps/examples/ac-dc-three-level-pwm-converter.html (last accessed on 9 February 2015)

[67] Geafol Cast-Resin Distribution Transformers. "4GB6475-3DA," datasheet, last accessed on 9 February 2015

[68] Hes Cables, "20.8/36 kV XLPE Insulated, Lontudinally Sealed, Single Core Cables with Aluminum Conductor," datasheet, last accessed on 9 February 2015

[69] Leroy Somer 3-phase TEFV Induction Motors, "LS180L," datasheet, last accessed on 9 February 2015

[70] LSRPM Permanent Magnet Synchronous Motors, “LSRPM160LR,” datasheet, last accessed on 9 February 2015